



QUANTUMNESS OF THE PHOTONIC BLOCKADE EFFECT

Santiago Bermúdez Feijóo

Advisor: Herbert Vinck Posada

Master Thesis

Dissertation presented for the degree of

Master in Science

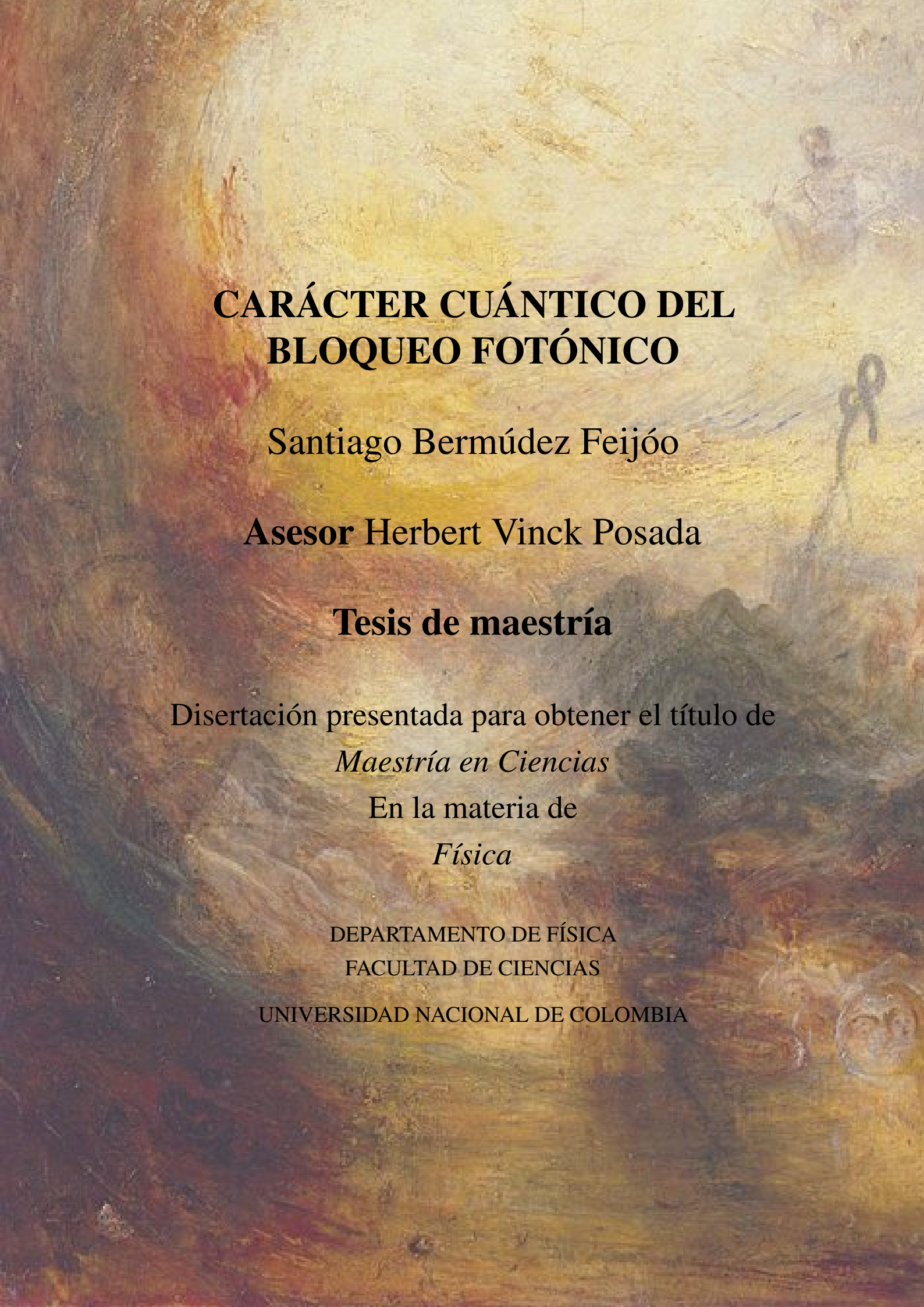
In the subject of

Physics

DEPARTAMENTO DE FÍSICA

FACULTAD DE CIENCIAS

UNIVERSIDAD NACIONAL DE COLOMBIA



CARÁCTER CUÁNTICO DEL BLOQUEO FOTÓNICO

Santiago Bermúdez Feijóo

Asesor Herbert Vinck Posada

Tesis de maestría

Disertación presentada para obtener el título de

Maestría en Ciencias

En la materia de

Física

DEPARTAMENTO DE FÍSICA

FACULTAD DE CIENCIAS

UNIVERSIDAD NACIONAL DE COLOMBIA

COVER PICTURE: "*Light and Colour (Goethe's Theory) – The Morning after the Deluge – Moses Writing the Book of Genesis*", BY JOSEPH MALLORD WILLIAM TURNER

*To my family,
Olga Lucía, German and Lucianna,
for their constant support and faith.*

*To **Alejandra**, for her eternal trust
and unconditional love.*

Acknowledgements

I would like to start by thanking my advisor, **Herbert Vinck Posada**, for his continuous support and trust. From his hand, I was able to start thinking more deeply about Physics, and thanks to that, I developed a great passion for Quantum Optics. I also thank him for always supporting me in my projects to be able to present them at international conferences, which led me to have countless experiences and meet magnificent people.

To my parents, **Olga Lucía** and **German**, who accepted without question my choice to study physics, and to whom I owe all the support, love and confidence they gave me throughout my academic formation. To my sister, **Luci**, for always being there for me. Without her constant company, this would not have been possible. I will forever remain grateful for making me laugh and bringing me serenity even in my darkest moments.

To **Aleja**, whom I do not have enough words to thank. You know more than anyone the difficulties that arose in developing this thesis. Without your unconditional love and support, I would have quit long ago. I thank you for supporting my dreams, and for being my pillar and my compass. I cannot wait to spend my life with you, and I will forever spend my days trying to give back everything you have done for me.

To **Juan Camilo Lopez**, who, without any duty, answered an email I sent in 2020 without waiting for a reply, and extended his hand to me to start a project. From him, I have indirectly learned what it is to be a true researcher. He has my deepest admiration and my sincere gratefulness for his patience while I obtained the results.

To the brothers that life has given me, **Juanse**, **Cales**, **Zulu** and **Tabo**, for taking my head of my concerns and helping me bring balance and joy to my life. I also want to take my time to thank **Cales** for opening the road for starting a path that I will otherwise never have considered, which has brought uncountable blessings to my life.

I also thank **Miguel**, **Stiven**, **Juliana**, **Camila** and **Juan Carlos**, for their friendship and the wonderful shared experiences through my formation as a physicist. Finally, I want to thank my colleagues at GOIC, **Andres U**, **Juan Pablo R**, **Carlos J**, **Vladimir V**, **Nicolas P**, **Jhon Edison M** and **Erik N** for the useful discussions that help me understand more deeply the field of quantum optics.

Abstract

The present thesis aims to investigate the photon blockade effect, understood as a phenomenon in which the presence of a single photon inhibits further photons, effectively transforming a system into one that emits one photon at a time. This effect can be classified into two categories: The conventional photon blockade, which relies on the nonlinearities of a system, and the unconventional photon blockade, which employs quantum interference between two paths to cancel the probability to access a particular state.

In order to investigate the underlying physical mechanisms of these two forms of blockades, this thesis employs numerical solutions of master equations, complemented by the application of analytical techniques for determining optimal conditions for each type of blockade. Specifically, the study finds that the driven dissipative Jaynes-Cummings model represents an ideal scheme in which both mechanisms are exhibited simultaneously. This enables the analysis of the photon blockade mechanism in a unique and experimentally feasible setup, such as a cavity-QED scheme composed of a semiconductor quantum dot grown inside a micropillar. Additionally, intrinsic differences between both blockade mechanisms are uncovered through the utilization of the theory of frequency-filtered correlations and the integration of dissipative mechanisms such as phonon-mediated coupling. Furthermore, new criteria for the theoretical classification based on the study of higher-order correlation functions are employed to analyze the numerical solutions of the model, determining if the systems can act as single photon sources. Moreover, the research applies the aforementioned tools to study a system that consists of an elliptical microcavity with an embedded quantum dot, subject to external excitation by a laser and a magnetic field. The optimal conditions for generating conventional photon blockade in this system were identified, constituting it to act as a single photon polarization switch.

This thesis, therefore, provides a comprehensive examination of the photon blockade effect, which could be used in the future for developing high-quality single photon sources, helping for the implementation of quantum technologies.

Keywords: Conventional photon blockade, Unconventional photon blockade, Driven Dissipative Jaynes Cummings, Single photon polarization switch, Single photon sources.

Abstract

La presente tesis tiene como objetivo investigar el efecto de bloqueo de fotones, entendido como un fenómeno en el cual la presencia de un solo fotón inhibe la emisión de más fotones, transformando efectivamente un sistema en uno que emite un fotón a la vez. Este efecto se puede clasificar en dos categorías: el bloqueo de fotones convencional, que se basa en las no linealidades de un sistema, y el bloqueo de fotones no convencional, que emplea la interferencia cuántica entre dos trayectorias para cancelar la probabilidad de acceder a un estado particular.

Con el fin de investigar los mecanismos físicos subyacentes de estas dos formas de bloqueo, esta tesis utiliza soluciones numéricas de ecuaciones maestras, complementadas con la aplicación de técnicas analíticas para determinar las condiciones óptimas para cada tipo de bloqueo. Específicamente, el estudio encuentra que el modelo de Jaynes-Cummings bombeado y disipativo representa un esquema ideal en el que ambos mecanismos se exhiben simultáneamente. Esto permite el análisis del mecanismo de bloqueo de fotones en una configuración única y experimentalmente factible, como un esquema de cavidad-QED compuesto por un punto cuántico semiconductor crecido dentro de un micro-pilar. Se descubren a su vez diferencias intrínsecas entre ambos mecanismos de bloqueo a través de la utilización de la teoría de correlaciones filtradas por frecuencia y la integración de mecanismos disipativos como el acoplamiento mediado por fonones. Además, se emplean nuevos criterios para la clasificación teórica basada en el estudio de funciones de correlación de orden superior para analizar las soluciones numéricas del modelo, determinando si los sistemas pueden actuar como fuentes de un solo fotón. Complementario a ello, la investigación aplica las herramientas mencionadas para estudiar un sistema que consiste en una microcavidad elíptica con un punto cuántico incrustado, sujeto a excitación externa por un láser y un campo magnético. Se identificaron las condiciones óptimas para generar un bloqueo de fotones convencional en este sistema, lo que lo convierte en un interruptor de polarización de un solo fotón.

Esta tesis, por lo tanto, proporciona un examen exhaustivo del efecto de bloqueo de fotones, que podría en el futuro servir para desarrollar fuentes de fotones individuales de alta calidad, que ayuden a la implementación de tecnologías cuánticas.

Palabras clave: Bloqueo de fotones convencional, Bloqueo de fotones no convencional, Jaynes-Cummings bombeado y disipativo, Interruptor de polarización de un solo fotón, Fuentes de un solo fotón.

Contents

List of Figures	xiii
1 Backgrounds	1
1.1 State of the art	1
1.2 The emergence of Quantum Optics	5
1.3 Current Advancements in solid state Cavity-QED	6
1.3.1 Microcavities	6
1.3.2 Quantum Dots (QD)	9
1.3.3 Single Photon Sources	10
1.4 Scope of this thesis	12
2 Theoretical framework	15
2.1 Formalisms of Quantum Mechanics	16
2.1.1 Laser rotating frame transformation	16
2.1.2 Gaussian states in Quantum Mechanics	18
2.1.3 Two level systems	27
2.2 Light – Matter interaction	30
2.2.1 Semiclassical theory of light-matter interaction	30
2.2.2 Quantization of the Electromagnetic Field	32
2.2.3 Quantum theory of light-matter interaction	34
2.3 Quantum Correlation Functions	35
2.4 Frequency filtered quantum correlation functions	40
2.4.1 Sensor method	41
2.4.2 Cascaded formalism	43
2.4.3 Experimental measurement of frequency filtered correlations	45
2.5 Interference of quantum states	46
2.5.1 Interference of a classical source and a quantum source	48

2.6	Theoretical criteria for single photon sources	50
3	Results	53
3.1	Unconventional photon blockade	53
3.1.1	Original proposal	53
3.1.2	Modifications to the original model	62
3.2	Simultaneous Photon Blockade	64
3.2.1	Driven-dissipative Jaynes Cummings model	64
3.2.2	Experimental realizations	74
3.2.3	Effects of frequency filtered correlations on photon blockade	75
3.2.4	The role of phonon mediated coupling in photon blockade	78
3.2.5	Photon blockade beyond the strong coupling regime	80
3.3	Single photon polarization switch via photon blockade	81
4	Conclusions and perspectives	91
A	Appendix Open Quantum systems	93
	Bibliography	103

List of Figures

1.1	Theoretical proposal for the photon blockade effect by Imamoglu <i>et al.</i> [1], and first experimental observation of PB by Birnbaum <i>et al.</i> [3].	2
1.2	Theoretical model and explanations for the unconventional photon blockade effect.	3
1.3	Experimental scheme used by Vaneph <i>et. al</i> [9] to measure UPB in the microwave regime. The image of the left corresponds to the coupled Nb resonators, while the image of the right displays the complete scheme to detect UPB.	4
1.4	Whispering gallery cavity modes. Original idea and semiconductor microstructures.	7
1.5	Photonic crystals microcavities. Representation of periodical structures and applications on biological systems.	8
1.6	Example of semiconductor micropillars.	9
1.7	QD formation from the Stranski-Krastanov method and current applications	10
2.1	Wigner's function for the Fock states	20
2.2	Wigner's function of the coherent state.	21
2.3	Wigner's function of the vacuum squeezed state	27
2.4	Two level system population in resonance as a function of coherent driving strength and rate of incoherent pumping.	29
2.5	Solutions for the semiclassical model of light matter interaction	32
2.6	Scheme of a Hanbury Brown set up for measuring frequency correlations, by using two filters before the detectors.	41
2.7	Sensor method as proposed by del Valle <i>et. al</i> [58]	41
2.8	Example of the sensor method for the incoherently driven Jaynes Cummings model	42
2.9	Schematics of the cascaded coupling based on the input-output formalism.	43
2.10	a.) Transitions of the Two level system in the Mollow triplet, b.) Second order correlation function and c.) Violation of the Cauchy-Schwarz inequality.	45
2.11	Results from experimental measurements of the frequency filtered correlations in the Mollow triplet by Peiris <i>et al.</i> [63].	46
2.12	Possibilities for measuring higher-order correlation functions.	51
3.1	$g^{(2)}(0)$ for Optimally Squeezed Gaussian states.	57

3.2	Optimally Squeezed Gaussian states $g^{(2)}(0)$ for small deviations of α , r , and Wigner function for a Squeezed Coherent state $ \xi, \alpha\rangle$	57
3.3	Comparison of the Wigner function of the displaced squeezed vacuum for the conditions that generate antibunching and bunching	58
3.4	Mean photon number and second order correlation function of the two coupled quantum modes model, as reproduced from [4, 5]	59
3.5	$g^{(2)}$ incoherent decomposition for the two coupled quantum modes model.	60
3.6	Higher order correlation functions vs cavity frequency and Kerr nonlinearity for the two coupled quantum modes model	61
3.7	Higher order correlation function analysis of the two interacting cavities model	62
3.8	Reproduction and new classification for the UPB model used in [71]	63
3.9	Mean photon number and Second order correlation function of the Jaynes cummings model as a function of $\tilde{\omega}_i$	69
3.10	$g^{(2)}$ decomposition of the Jaynes Cumming model for the red cut in Figure (3.9)	70
3.11	Higher order correlation function analysis for the Jaynes Cummings model as a function of emitter and cavity detunings $\tilde{\omega}_i$	71
3.12	UPB conditions to minimize $g^{(2)}$ for different rates of cavity and 2LS driving.	73
3.13	Effect of the coherent driving to the 2LS in the Jaynes Cummings statistics	74
3.14	a.) Micropillar cavity of AlAs/GaAs DBR with an embedded InAs quantum dot that has been grown by molecular beam epitaxy that acts as an SPS b) Hanbury-Brown Twiss setup for measuring $g^{(2)}$	75
3.15	Frequency resolved correlations for the JC model with conditions of CPB and UPB	77
3.16	Cut in the frequency-resolved correlation function	78
3.17	Effects of phonon mediated coupling dissipative terms γ_θ, P_θ on each mechanism of the photon blockade.	79
3.18	Effect of the simultaneous phonon mediated coupling rate ξ_θ on the mechanisms of photon blockade.	79
3.19	Eigenenergies of the total Hamiltonian as a function of the magnetic field	85
3.20	Cavity photon occupation for each mode and polarization factor as a function of the magnetic field and laser detuning.	85
3.21	Mean photon number (a) and second order correlation function (b) as a function of laser detuning for a fixed magnetic field.	87
3.22	Incoherent decomposition of second order correlation function of the y-polarization mode as a function of laser detuning for a fixed magnetic field.	87
3.23	Higher order correlation functions of the elliptical microcavity with an embedded quantum dot for a fixed magnetic field.	88
3.24	Analytical mapping of the second order correlation function for the x and y polarization modes.	89

Backgrounds

1.1 State of the art

The improvement over the control in light-matter experiments has allowed scientists to build high-quality optical cavities with embedded active media, where strong orders of interaction are possible. By strengthening the interaction (g), the way in which light and matter respond to one another transforms from a simple perturbative correction to a reversible exchange of energy. This allows the creation of a new type of quasiparticles, which are understood as a superposition of matter and light wavefunctions: the *polaritons*.

The fundamental property of this quasiparticle is that the energy gap between same manifold polaritons scales proportionally to \sqrt{n} , as one climbs up the energy ladder. This characteristic opens up the possibility for generating *Photon Blockade* (PB), because if the system is resonantly driven at a frequency of one of the polaritons manifold, then the possibility of accessing further states is blocked due to the non-resonant distribution of the energy ladder. The term *Photon Blockade* was introduced in the seminal paper by Imamoglu *et al.* (1997) [1], where they proposed a scheme with a nonlinear cavity that had an embedded Kerr media, which was able to realize strong and deterministic antibunching. The term was coined after the effect observed for mesoscopic systems, the *Coulomb blockade*, where electrons create a strong repulsion that enhances the position of one electron while preventing the flow from others [2]. The first experimental proof of photon blockade was performed by Birnbaum *et al.* (2005) [3], when they first proposed a setup for measuring the photon blockade effect, by using the anharmonicity of the eigenstates of a system for suppressing non-resonant transitions. Their results were the first experimental proof for photon blockade, finding values of $g^{(2)}(0) = 0.13 \pm 0.11$ as well as $g^{(2)}(0) < g^{(2)}(\tau)$, finding not only antibunching but as well a Subpoissonian property of the distribution.

Although the excellent result by Birnbaum was a fundamental step in the consolidation of the Photon Blockade, scientists wanted to push forward the investigation on proposing schemes that could achieve the desired suppression of the second order correlation function. In that sense, studies divided into two alternatives: Accessing Photon Blockade via the anharmonicity of the eigenstate of a system, which was named as *Conventional Photon Blockade* (CPB), or by the use of quantum interference, which was referred as *Unconventional Photon Blockade* (UPB) [4] (2010). The proposal of Liew and Savona for UPB resembled the original idea from Imamoglu, using a driven cavity with a nonlinear Kerr media inside. The difference in the proposal was that they employed not one, but two cavities with these characteristics, allowing also an interchange of photons

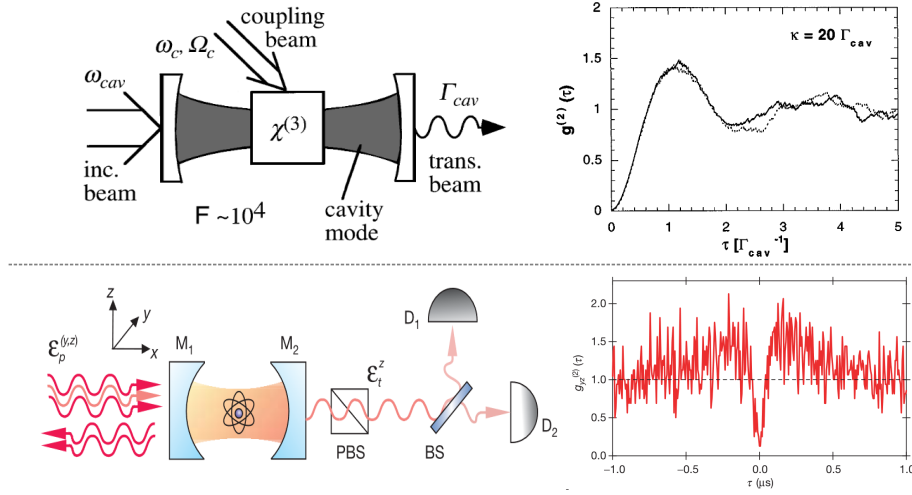


Figure 1.1 (Top row) Theoretical proposal for the photon blockade effect by Imamoglu *et al.* [1]. The picture on the left illustrates the system that was studied, which consisted of a driven optical cavity that possesses a nonlinear Kerr media, while the image on the right displays the results demonstrating antibunching in the second-order correlation function. **(Bottom row)** Experimental confirmation of the photon blockade effect by Birnbaum *et al.* [3]. The image on the left shows the experimental setup, which consisted of Cesium atoms that were trapped in a Fabry-Perot cavity. The right image shows the experimental results for $g^{(2)}(0) = 0.13 \pm 0.11$, confirming the existence of PB.

due to the proximity between the cavities. The simulation for such a theoretical scheme indicated that photon blockade could also be generated without the necessity of achieving strong interactions between light and matter, and rather, was obtained by the use of small values of the Kerr nonlinearity U , which in principle was easier to achieve experimentally. The first explanation of the UPB was performed by Bamba *et al.* (2011) [5], where they identified that the origin of the photon blockade was due to subtle interferences that occur between different paths to access a particular state, namely, the state with two photons in the cavity. If the interference process could happen, the only states allowed were those with one photon (in the weak driving condition), thus transforming the incident coherent radiation into a single photon turnstile.

An alternative explanation to the UPB phenomenon was proposed by Lemonde *et al.* (2014), where they proved that the general aspect of the minimization of the second order correlation function was because the steady state of the two interacting cavities model corresponded to a particular optimization of *Gaussian states*, which they referred to as *optimally squeezed Gaussian states*. The particularity of these states was that there were optimal relationships between the displacement in phase space, quantified by the coherent state amplitude α , and the squeezing factor r , which would lead to a minimization of the $g^{(2)}(0)$.

Although this explanation provided a more general framework for UPB, since the displaced squeezed states that sustained the $g^{(2)}$ minimization could be obtained by an interference process between a coherent ($|\alpha\rangle$) and a squeezed ($|\xi\rangle$) state, the objectives around UPB in later years consisted in proposing various schemes, mainly systems of *Cavity QED*, *Hybrid Optomechanics*, among others, that used the framework of quantum interference of Bamba to obtain small values in the second order correlation function.

Despite those numerous theoretical proposals for the UPB, attempts to generate the experimental realiza-

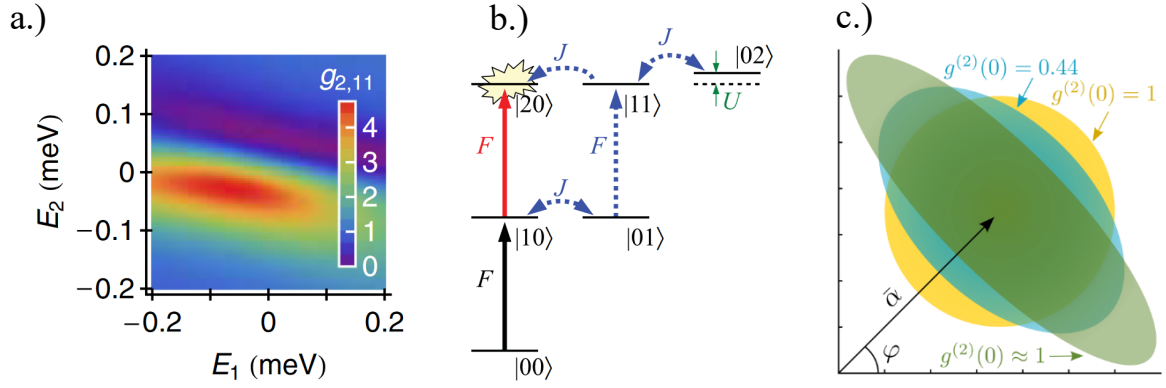


Figure 1.2 Two interacting cavity model that resulted in the birth of Unconventional photon blockade. **a.)** Theoretical results of the second order correlation function with varying laser rotating frame energies of the cavities E_i , as modeled by Liew and Savona [4] for a Kerr nonlinearity of $U = 0.0428\gamma$. **b.)** Quantum interference process to obtain UPB in the two interacting cavities model, as proposed by Bamba *et al.* [5]. **c.)** Explanation of the UPB as a particular realization of an optimally squeezed Gaussian state, as formulated by Lemonde *et al.* [6].

tion of UPB were hindered by a lack of suitable platforms, as explained by Radulaski [7]. It was not until 2018 that two separate groups were able to experimentally demonstrate this effect.

The group of Snijders *et al.* [8] used a single quantum dot that was simultaneously coupled to two orthogonally polarized cavity modes, and by tuning the input and output state of the polarization, they were able to observe UPB. The setup consisted of a self-assembled InAs/GaAs quantum dot embedded in a micropillar cavity. This quantum dot presented a fine structure splitting, which allowed it to interact with different polarization modes of the cavity. Their focus consisted of carefully studying the dependence between the excitation angle of the cavity modes and the output polarization angle, finding that UPB is possible when both cavity modes are excited. They were able to measure values as low as 0.005 in the $g^{(2)}(0)$ with their scheme.

On the other hand, Vaneph *et al.* [9] had a different approach than the experimental setup from Snijders. They used a scheme of two coupled superconducting resonators (Nb), one being linear and the other weakly nonlinear, which allowed them to find Unconventional Photon Blockade in the microwave region. The weakly nonlinear resonator was achieved by coupling the end of the resonator to a SQUID. The relevant parameters of the system, such as nonlinear strength U and coupling, J were tuned by means of the SQUID flux ϕ_0 . The parameters they found were $\omega_a = \omega_b = 2\pi \times 5.878\text{GHz}$, $J = 2\pi \times 25\text{MHz}$, $U = 2\pi \times 0.3\text{MHz}$ and $\gamma = 2\pi \times 8\text{MHz}$. They were specifically chosen so that U fulfilled the optimal conditions proposed by Bamba *et al.*, given by Equations (3.10). Which such a setup, Vaneph *et al.* were able to confirm the Gaussian nature of the state, and to minimize the $g^{(2)}(0)$. The best results showed a minimal value of $g^{(2)} \approx 0.4$ for a population of 10^{-2} microwave photons.

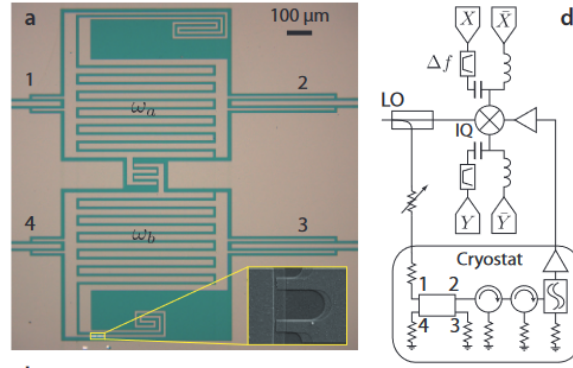


Figure 1.3 Experimental scheme used by Vaneph *et. al* [9] to measure UPB in the microwave regime. The image of the left corresponds to the coupled Nb resonators, while the image of the right displays the complete scheme to detect UPB.

Another seminal contribution to the field of photon blockade came in 2020 when Zubizarrieta *et al.* [10] showed that the light emission characteristics of different systems associated specifically with conventional or unconventional blockade mechanisms could be explained from the unified framework of interference between quantum states and classical components. The theoretical aspects of this formalism, called *Interference of quantum states*, will be a crucial component for analyzing the results of photon blockade through the second order correlation function. For that reason, a complete derivation of the process will be explained in section 2.5.

The view introduced by Zubizarrieta established a more general explanation of the methods to be employed to create single photon sources from the photon blockade effect, indicating that, since both conventional and unconventional features are understood from the same framework, a single system could be capable of generating both types of blockades, simply by properly tuning its parameters. This represented a major contribution because attention could now be centered in creating feasible experimental designs that exhibit both types of blockades. As will be later shown, a semiconductor cavity system strongly interacting with a self-assembled quantum dot is capable of generating *both* CPB and UPB, which, due to the excellent experimental control that is currently available for this type of system, makes it a promising candidate for implementation as a single photon source. Furthermore, this type of setup can be built in such a way as to take advantage of some of their properties, such as intentionally including asymmetries in the microcavities which are directly related to the polarization properties of the light. This allows the inclusion of more relevant contributions to the dynamics that can be used as a parameter of control for tuning photon statistics, and therefore expanding the possibilities for building stable single photon sources. This aspect will be exhaustively explored in section 3.3.

1.2 The emergence of Quantum Optics

Light is a phenomenon that has inevitably inspired and aided in human evolution in countless ways. Some vital applications of light range from its usefulness as a power source passed throughout the development of agriculture by using light to grow crops, continuing through the establishment of communication systems such as the telegraph and Internet, and finally, serving even for artistic and cultural expressions, came from ancient rituals with fires to the modern stage lighting in theater.

The earlier formal study of the properties of light could be traced back to the ancient Greeks, where some treatises by Aristotle regarding the nature of light and shadows could be found. Afterward, the development of the scientific method in the 17th century inspired the work of scientists such as Robert Hooke and Isaac Newton in order to try to find mathematical models that could describe the nature of light. Particularly, the contributions of Newton in his renowned work *Hypothesis of light* gave the light a *corpuscular* nature, which was emitted in all directions from the source. He used his vision to explain a wide range of phenomena, such as the behavior of light when it passes through a prism. On the other hand, the opposing theory was proposed by the Dutch mathematician Christiaan Huygens. He developed a theory in 1690 that postulated light as a *wave* that propagates through an invisible medium, called luminiferous ether, which was later proven to be nonexistent by the famous Michelson-Morley experiment. Among the main explanations of the wave theory of light, the most prominently supported effects were the correct description of interference and diffraction, as supported by the experiments performed by Thomas Young in the 1800s. The debate came to an “end” in 1850 when Leon Foucault was able to find a way to measure the speed of light, discovering that light would travel slowly in a denser medium, contrary to the claims of Newton’s corpuscular theory that it would travel faster, and for that reason, wave theory was constituted as the correct depiction of the nature of light.

The modern view of light began with the blooming of experiments on electricity and magnetism, such as the ones performed by Michael Faraday and Ampère. Nevertheless, it was the Scottish mathematician James Clerk Maxwell who envisioned light as a new form of a wave, the so-called electromagnetic wave. He proposed a set of four equations that explained and related the oscillation of electric and magnetic fields, which could be derived from a pair of wave equations for these fields that correctly propagated at a velocity $c = 1/\sqrt{\epsilon_0\mu_0}$. Shortly after, the German physicist Heinrich Hertz developed an experiment that generated radio waves, which behaved just as predicted by Maxwell’s electromagnetism theory.

Although Maxwell’s electromagnetism theory was regarded as one of the most solid theories ever developed, there were some phenomena that could not be correctly described by this formulation. Specifically, the experiments on Black Body radiation were irreconcilable with classical electromagnetism, which led to the renowned ultraviolet catastrophe. This problem was solved at the dawn of the 20th century by Max Planck (1918 🏆), suggesting that although the light was a wave, electromagnetic radiation could only be emitted or absorbed in discrete energy packages which he called *quanta*, later widely known as *photons*. In 1905, Albert Einstein (1921 🏆) used this interpretation to correctly explain the Photoelectric Effect, and later on, Niels Bohr (1922 🏆) would apply it to his model of the hydrogen atom. All these models joined with the mathematical tools from Erwin Schrödinger (1933 🏆), Paul Dirac (1933 🏆), Wolfgang Pauli (1945 🏆), Werner Heisenberg (1932 🏆), Louis De Broglie (1929 🏆), among others, gave rise to the field of *Quantum Mechanics*, which aimed to provide an explanation of matter phenomena at the subatomic scale.

Due to this theory, the modern perception of light emerged, in which light is neither a particle nor a wave, but actually, it is described by both behaviors, establishing the famous *wave-particle duality* of light, proposed by Louis De Broglie. This was corroborated by multiple experiments, such as the notorious double slit experiment, which proved not only useful in the description of how light and matter behaves but actually opened the debate over the multiple interpretations of quantum mechanics, such as the Copenhagen or Many Worlds interpretations.

Continuous studies from quantum mechanics led to fundamental technological developments in the mid-1950s, such as the creation of the Maser by Townes (1964 🏆), and afterward the laser by Maiman in the 1960s. Furthermore, the contributions from the American physicist Roy Glauber (2005 🏆), such as the development of a *theory of quantum coherence* [11], which led to the creation of photon statistics and a complete theory of the role that *coherent states* have regarding the quantum properties of light. These discoveries were the framework that gave rise to the field of *Quantum Optics*, which aims to explain how photons interact with matter at the nanoscale level. The seminal paper of Kimble, Dagenais, and Mandel [12] on *Photon antibunching in resonance fluorescence* gave the first experimental confirmation that light was composed of photons. Even more, the experimental confirmation by Slusher *et al.* [13] that quadratures of light could be reduced further than the uncertainty of coherent states, i.e., *squeezed states* of light, set up the field of quantum optics as one of the most thrilling fields for future developments in communication, computing, and metrology, which applications that nowadays range from the discovery of gravitational waves at LIGO [14], to the claim of Google to have reached Quantum supremacy [15].

1.3 Current Advancements in solid state Cavity-QED

In this section, we will briefly review the state of the art of Microcavities, Quantum Dots, and Single Photon Sources. Each one of them is fundamental for the advancement of quantum technologies and will be a crucial concept for the development of this thesis.

1.3.1 Microcavities

Optical resonators, or *Optical cavities*, are devices that use the principle of interference to confine light. The most simple device that acts as an optical cavity is known as a Fabry Perot cavity, which is composed of two mirrors facing each other, where light can reflect multiple times, generating constructive and destructive interference that leads to a set of standing waves known as resonating modes. Meanwhile, *Optical microcavities* (Henceforth microcavities) correspond to resonators that have dimensions that are close to the wavelength of the confined light, generally of the size of a few microns ($\mu m = 10^{-6}m$).

There are multiple realizations for microcavities, each one having its own characteristics. A common property among all of them that measures its quality of confinement is known as the *quality factor* (Q factor). It is built as the ratio of the resonant frequency and the bandwidth of the resonance

$$Q = \frac{\omega_c}{\delta\omega_c}, \quad (1.1)$$

and is also understood as a measure of the decaying energy of a system, where Q^{-1} corresponds to the loss of energy in the microcavity after one round-trip (Kavokin, 2017, pg. 3 [16]). Nowadays, current techniques allow the construction of microcavities that exhibit high-quality factors, with designs that vary substantially. In

particular, we will refer in this thesis to *semiconductor microcavities*, which are microcavities that are built using semiconductor materials such as gallium (Ga), arsenide (As), or silicon (Si). The different realizations of semiconductor microcavities can be mostly classified into three categories: *Whispering gallery mode cavities*, *Photonic crystals*, and *Fabry-Perot cavities*. Each one will be briefly introduced.

Whispering gallery mode cavities (WGM)

The effect of the principle of use for this type of microcavities was initially discovered in the field of acoustics, specifically at St. Paul's Cathedral in London, England, where Lord Rayleigh (1904) found that when people spoke sideways over the curved dome in the church, they could clearly hear one another, even if they were separated by a great distance [17]. In the context of semiconductor physics, these microcavities are formed by a closed optical path, on which light can travel around multiple times. Although the shape of these structures can vary, from triangles, squares, and even hexagons, the usually employed geometry is for circular structures, where it could be made for disks (2D) or spheres (3D). For these geometries, ultrahigh quality factors, of the order of 10^8 and, 10^9 have been obtained for microtoroid resonators [18] and microsphere resonators, respectively [19]. One problem with WGM microcavities is that they have low coupling efficiency, meaning that it is difficult to transfer light into and out of the resonator. For a review of the current methods for WGM coupling, see [20]. However, they are suitable for applications for sensing and the study of nonlinear optics.

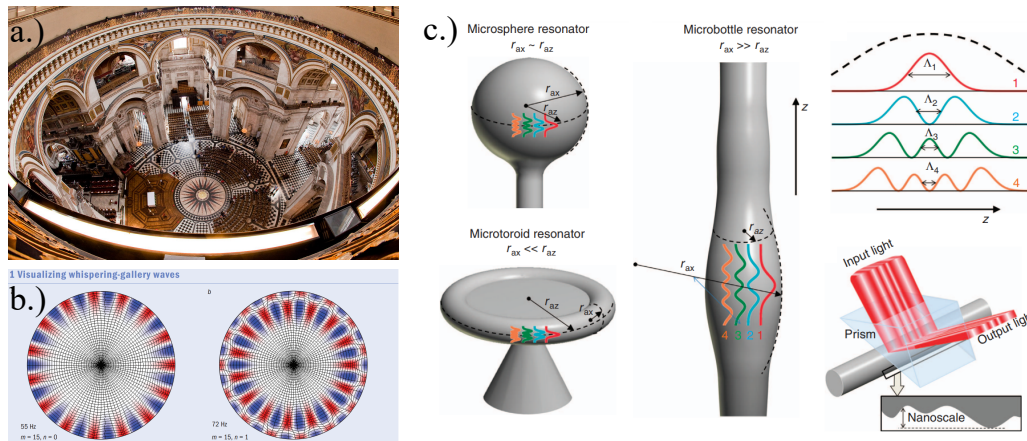


Figure 1.4 a.) Whispering Gallery of St. Paul's Cathedral, London, England. b.) Snapshot of whispering gallery modes. Image is taken from [21]. c.) Design for several Whispery Gallery Modes microcavities, showing Microspheres, Microtoroids and micro bottles. Image taken from [22].

Photonic crystals (PhC)

Photonic crystals are optical structures on the nanometric scale, which are formed from a periodic arrangement of dielectric materials, such as semiconductors, that generate a bandgap within the structure. This forbids the transmission of frequencies of light that reside inside this photonic bandgap. Furthermore, by deliberately introducing a defect in the periodicity of the structure, light can be confined over a specific region. Although previously these structures presented quality factors of the order of $Q = 10^3$ [23], current technologies have found methods for obtaining ultrahigh photonic crystal cavities, with reported values of $Q = 8 \times 10^5$ [24]. One crucial application of the theory of photonic crystals resides in the fact that these structures unexpectedly arise

in biological systems, such as in the wings of some butterflies (The Colombian *Greta Oto* species, also as *Glasswing butterfly*), and in some bugs, such as the Colombian *Jewel beetle*. Photonic crystals on these animals allow the generation of iridescence, which is responsible for their vibrant colors.

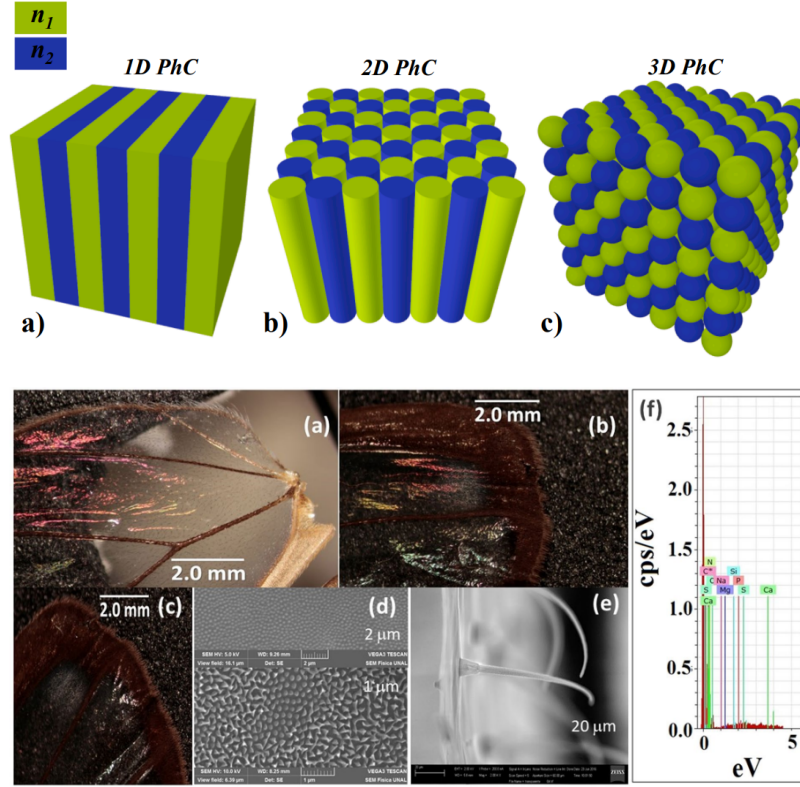


Figure 1.5 (Top row) Pictorial representation of different dimensions for photonic crystals, image taken from [25]. (Bottom row) Photographs of the Colombian *Glasswing butterfly*. Electron microscope images reveal the periodic structure responsible for iridescence. Image is taken from [26].

Fabry-Perot cavities (FPC)

As mentioned earlier, Fabry Perot microcavities are structures that use two mirrors that allow multiple reflections of light, creating resonating modes. The reflections on these microcavities can be achieved by employing mirrors composed of single (usually metallic) materials (Kavokin, 2017, pg. 8 [16]), or by using alternating layers of materials with different refractive indexes. The latter is commonly known as *Distributed Bragg Resonators* (DBR). An adequate design of the thickness of each layer, and a correct selection of the refractive indexes, can cause the DBR to confine light from a specific range of wavelengths (Kavokin, 2017, pg. 9 [16]). These results essential for the development of high-quality factor microcavities.

The semiconductor microcavity that will be of most interest in this thesis consists of the so-called *pillar microcavities*. They are structures that employ DBRs on the top and the bottom in order to confine light in the vertical direction, while light in lateral directions is normally confined by total internal reflection. They are multiple techniques in order to grow these pillars. *Molecular beam epitaxy* (MBE) is one of the most commonly used techniques. It consists of a process in which atoms are directed onto a substrate, where they deposit to

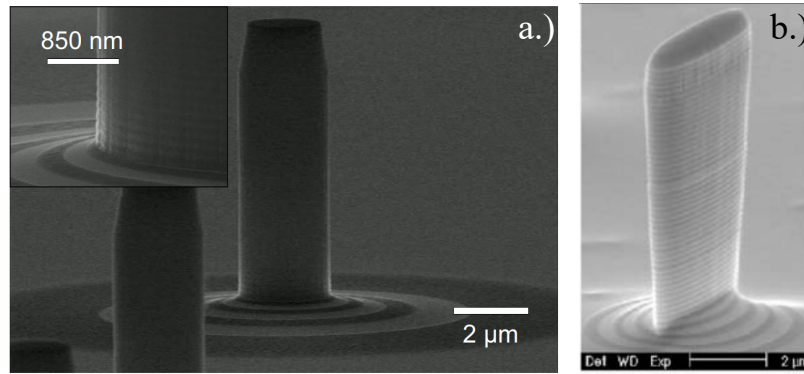


Figure 1.6 a.) An AlAs/GaAs micropillar that exhibited ultrahigh quality factors, image taken from [27]. b.) Example of a micropillar with an elliptical geometry, image taken from [28].

form a thin film. the exact dimension of the films can be controlled with the properties of the source, such as the temperature, pressure, flux, etc. Also, the ultra-high vacuum conditions that are normal for these setups account for the precise growth of the thin semiconductor layers. This method also allows growing active media, such as quantum dots and quantum wells inside the microcavity, facilitating the creation of setups that are ideal for the study of light-matter interactions. It is important to note that the thin film growth method employed in MBE for the DBR corresponds to a *Frank Van der Mewe* (FM) method, also known as the *layer by layer* method. It is one of the *three* techniques of thin film growth, which occurs when *adatoms* attach preferentially to the surface. The term adatom stems from *adsorption-atom*, which corresponds to the effect where atoms adhere to one another (Adsorption is thus very different from absorption and should not be confused). The other two methods will be mentioned in the next subsection.

On the other hand, they are also several techniques for controlling the geometry of the microcavities, such as electron beam lithography or focused ion beams. The quality factor for these microcavities ranges between 6.000-20.000, however, ultrahigh quality factors exceeding $Q = 250.000$, have been already demonstrated in micropillars that used 36(32) AlAs/GaAs layer pairs in the top (bottom) DBR [27].

1.3.2 Quantum Dots (QD)

The continuous comprehension of semiconductor physics led to experiments where a constraint in one of the directions of motion resulted in a reduced dimensionality, due to quantum confinement. This is only possible when dimensions of such confinement become comparable to the De Broglie scales of the carriers in the semiconductors. From this idea, the concept of solids was translated to *quantum wells* (2D), continuing to *quantum wires* (1D), and finally getting to *quantum dots* (0D). The complete reduction of the dimensionality in Quantum Dots led to the discretization of their energy levels, exhibiting thus the same quantized energy structure of real atoms. For this reason, they are also referred to as *artificial atoms*. They have dimensions of a few nanometers and their characteristics can be controlled by varying the growth conditions, such as the temperature and time of the process. There are various types of quantum dots, including semiconductor, metallic, and superconducting QDs.

In this thesis, we will focus on semiconductor QDs that are grown by the method of molecular beam epitaxy, the same one that was used to build Fabry Perot microcavities that employ DBRs. As was mentioned in the

discussion of these types of microcavities (1.3.1), the MBE method that was used to grow the thin film layers was known as the Frank Van der Mewe (FM) method. Here, although the same MBE process can be used to grow the QDs, the thin film growth method is different from the aforementioned method. Specifically, for the growth of QDs by means of molecular beam epitaxy, the Stranski-Krastanov (SK) method is employed, also known as the *layer plus island* method.

The steps of the SK method can be understood as follows: First, a thin film of a semiconductor is deposited over a substrate. The thickness of this film continues to grow by MBE deposition until it reaches a critical thickness. When this happens, the *strain energy* overcomes the *surface energy*, leading to the formation of islands, which are later covered with other semiconductor materials in order to protect them, or grow further heterostructures. The value of the critical thickness depends on the *lattice mismatch* between the semiconductor and the substrate. A common confusion arises from the fact that *epitaxy* refers to the growth of a film over a substrate with the characteristic that they both share the same crystal structure. However, there could still be a mismatch in the lattice constants. This can happen due to different compositions of the film semiconductor and the substrate, even though, as required, the crystal structure remains the same. This can be observed, for example, by doping the same material that was used as a substrate and depositing a thin film. A good experimental demonstration of SK QDs was made by Yamaguchi *et al.* [29]. Semiconductor quantum dots can be constituted inside pillar microcavities by the MBE technique, where common materials are InAs or InGa QDs, which are sandwiched between AlGaAs/GaAs heterostructures [30–32].

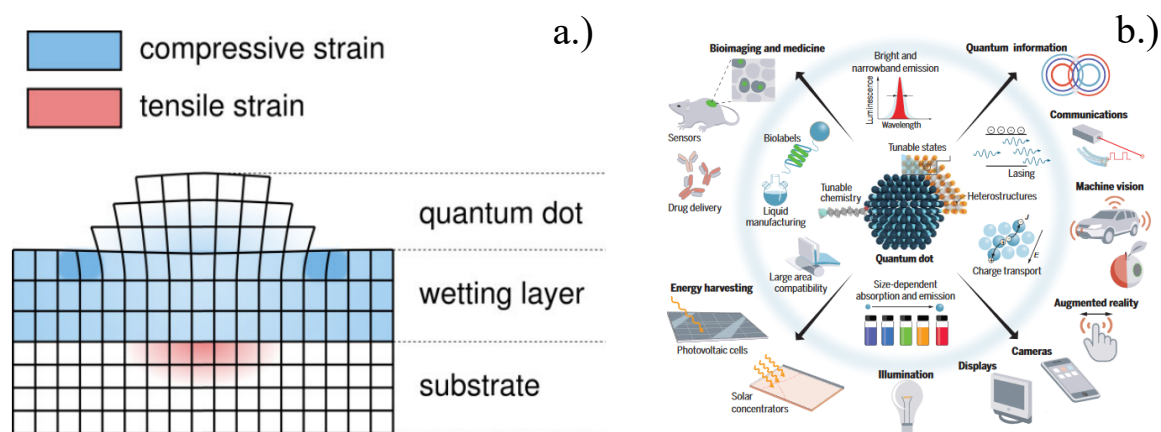


Figure 1.7 a.) Schematics of QD formation via the Stranski-Krastanov method, image taken from [33]. b.) Current applications of semiconductor quantum dots, Image taken from [34]

Semiconductor quantum dots have a wide range of applications, from developing quantum technologies such as single photon sources to everyday technologies like cameras and displays, and even in biological systems for accurate tracking and drug delivery. For an in-depth revision of current progresses and future challenges, refer to the excellent review by F. Pelayo Garcia de Arquer *et al.* [34].

1.3.3 Single Photon Sources

The last relevant quantum technology that will be reviewed is the *single photon sources* (SPS). SPS are devices capable of producing streams of single photons, making them crucial for fields such as quantum computing,

quantum communications, and testing intrinsic quantum mechanical properties in quantum optics setups. These applications are based on the ability to control the production of single photons, which allows for the creation of photonic qubits. In these qubits, information is encoded in the properties of the photon, such as its polarization or momentum, making them ideal for fast and efficient transmission over long distances [35].

Some key concepts that surround SPS are the *brightness* and the *purity* of the emitted photons. The first one corresponds to the number of single photons that can be emitted per unit of time, while the latter accounts for the degree of indistinguishability of the emitted photons. While the single-photon nature of an SPS can be studied by means of a Hanbury Brown Twiss setup, which consists of an interferometric scheme used to measure the second-order correlation function (The experiment will be later clarified when we introduce the notion of quantum correlation functions in section 2.3). On the other hand, the purity of the photons can be quantified by using a Hong Ou Mandel setup [36], which consists of an interferometer that interferes single photons on a beam splitter and measures the probability of detecting photons at the same port. If they are indistinguishable, the probability of detection to observe each photon at different ports is nullified by a quantum interference process (*Gerry-Knight, 2004, pg. 141* [37]). Current challenges in the field correspond to the production of high-purity and brightness single photon sources.

Single photon sources (SPS) can be divided into two main categories: probabilistic and on-demand. Probabilistic SPS emit photons randomly with a specific probability, while on-demand SPS emit photons after excitation of the system, whether by optical or electrical pulses, resulting in a controlled and deterministic emission rate. The most famous schemes of probabilistic SPS rely on the effects of *spontaneous parametric down conversion* (SPDC) or *four-wave mixing* (FWM). While on-demand sources are based on schemes such as single photon emitters or NV color centers. A noteworthy remark was made by Eisaman *et al.* [35] in which they clarify that although the classification of SPS is feasible in theory, real applications lead to a blur in the distinction, because there are several processes that can turn a deterministic emission into a probabilistic one, such as losses in the system.

Spontaneous Parametric Down Conversion (SPDC)

Spontaneous parametric down conversion refers to the nonlinear effect on which a high energy photon (pump), after interacting with a nonlinear media, can decay into two lower energy photons, known as signal and idler photons. This process can be achieved by means of interaction with nonlinear crystals such as Beta Barium Borate (BBO) or Potassium Titanyl Phosphate (KTP) crystals. This decay process accounts for a physical process that conserves energy and momentum, known as phase matching conditions:

$$\omega_p = \omega_s + \omega_i \quad (1.2a)$$

$$\mathbf{k}_p = \mathbf{k}_s + \mathbf{k}_i. \quad (1.2b)$$

Furthermore, the relationship among the polarization states between the pump and the idler and signal photons differentiates the type of SPDC that is achieved. Type 0 SPDC is obtained when the polarization of the incident beam is equal to both polarization states of the signal and idler photon. On the other hand, for type I, once again both signal and idler share the same polarization state, but they are orthogonal to the incident beam. Finally, in type II, the signal and idler photons have an orthogonal polarization state. This allows the generation of pairs of entangled photons, and furthermore, since the photons are correlated, the detection of one photon *heralds* the presence of another, effectively establishing a *heralded single photon source*. However, these sources may not

be adequate for implementation in scalable quantum technologies, since the down conversion rate happens for a few photons over millions of incident photons.

Quantum dots SPS

Quantum dots single photon sources are one of the most prominent schemes for producing on-demand single photons. The level of control of the design of the quantum dots, such as for epitaxially grown QDs, and the enhanced capabilities of confinement in optical resonators, account for the high versatility of these systems to act as single photon sources. One great advantage of this system is that the wavelength of the emitted light can be tailored depending on the employed semiconductor compounds for the quantum dots and microcavities, and also, can be built to perform in increasing temperatures, reaching values close to even 100K [38], although with the drawback of the introduction of non-desired effects such as broadening due to phonons [39]. For this reason, most of the experimental demonstrations are performed using cryogenic cooling (4K). Furthermore, the development of techniques such as the fluorescence imaging method allows to precisely determine the position of the self-assembled quantum dots, with an uncertainty of 20nm, which allows growing SPS based on positioned quantum dot exhibiting high brightness and purity [40].

The properties of these schemes provide single photon emission with high indistinguishability and efficiency, and that could be generated deterministically. For a complete review of the progress of quantum dot-based SPS, we encourage the reader to refer to the work of Arakawa and Holmes [39].

In the following sections, we will discuss how the *photon blockade effect* can further improve single photon sources based on semiconductor quantum dot-microcavity systems [41], due to its distinctive characteristic of suppressing multiphoton events, improving the quality of these SPS and making them more suitable for quantum applications.

1.4 Scope of this thesis

Having understood the framework on which the phenomenon of Photon Blockade Effect relies, as well as the current advancements on the technologies employed for its generation, we proceed to properly define the general and specific objectives of this thesis.

General objective:

To study the differences and similarities between conventional photonic blockade effect (CPB) and the unconventional photonic blockade (UPB), reviewing whether the current criteria used for the classification of such systems as single-photon sources are adequate.

Specific objectives:

- *Conduct an in-depth literature review related to previous studies on photonic blockade.*
- *To pose and solve the master equations of the systems used to describe the CPB and the UPB.*
- *Calculate quantum correlation functions with and without time delay to analyze the ability to have antibunching effects and Sub-poissonian distributions in the systems.*
- *Study the ability to exhibit conventional and unconventional behaviors simultaneously.*

To ensure the accomplishment of these objectives, the project is organized as follows:

Chapter 2 provides the Theoretical Framework, which serves as the foundation for understanding the Photon Blockade effect. This chapter explicitly explores the essential tools necessary to grasp the concept. It encompasses a wide range of topics, starting from the fundamental principles of Quantum Mechanics. Here, we delve into significant aspects, such as the definition of transforming into the rotating frame of a laser, as well as the comprehension of Gaussian states and two-level systems.

Moreover, given the inherent connection between the Photon Blockade effect and the interaction between light and matter, an extensive section dedicated to this topic is included. This section offers a comprehensive review of critical concepts, including the quantization of the electromagnetic field. Furthermore, it examines both the semiclassical and fully quantum perspectives of this interaction, providing a well-rounded understanding of the phenomenon.

Furthermore, a dedicated section is introduced to explore the concept of Quantum correlation functions, which is based on the theory of Glauber. These correlation functions play a pivotal role in understanding the statistical properties of light, making them a fundamental notion in the classification of single photon sources. To expand upon the basic definition of quantum correlation functions, we also delve into the notion of frequency filtered quantum correlation functions. This approach involves calculating the correlation functions by considering specific segments of the emission spectrum, instead of the conventional assumption of the complete spectrum. By incorporating this perspective, we gain a deeper understanding of the intricate relationship between the correlation functions and the emission characteristics.

Additionally, we explore how the phenomenon of interference of quantum states can be linked to the statistical properties of light. This analysis allows us to highlight the significance of higher order contributions of quantum correlation functions when developing an accurate criterion for characterizing single photon sources. By considering these higher order effects, we can provide a more comprehensive and precise description of the behavior and characteristics of single photons.

Later, in Chapter 3, we present the significant outcomes derived from the simulations conducted to explore the Photon Blockade effect. Initially, we introduce the solutions associated with the models for Unconventional Photon Blockade. These solutions are obtained through numerical methods by solving the master equations, as well as through analytical approaches where we apply concepts such as Gaussian states and higher order correlation functions to analyze the phenomenon of PB.

Furthermore, we thoroughly investigate the concept of Simultaneous Photon Blockade, where a system exhibits both conventional and unconventional features by appropriately adjusting the relevant parameters. In this analysis, we not only replicate the treatment discussed in the section dedicated to UPB, but also emphasize the primary distinctions between these two types of blockades. To accomplish this, we draw upon the theory of frequency filtered correlations and the notion of phonon-mediated coupling, enabling a comprehensive understanding of the contrasting characteristics.

Additionally, we introduce an innovative model for a photon source, which not only enables on-demand single photon generation but also offers the capability to control the polarization state of the photons by simply tuning the magnetic field. This advancement holds significant potential for various applications in quantum technologies, as it grants researchers precise control over the polarization properties of photons, opening doors to new possibilities in the field.

Finally, in Chapter 4, we summarize the main contributions and findings of our work regarding the Photon Blockade effect, as well as discuss the limitations and possible future directions of this research.

Theoretical framework

In this chapter, the theoretical tools that will be used in order to analyze the quantum optics systems related to Photon Blockade will be presented, with the hope to help those who want to learn about the beautiful (but complicated) field that is quantum optics.

In the opening section of this chapter, *Formalism of quantum mechanics*, we establish the fundamental concepts essential for comprehending quantum optics systems. We begin by introducing the transformation into a rotating frame of a laser, which proves crucial in effectively handling time-dependent contributions in the Hamiltonian. This transformation allows us to disentangle the effects of coherent pumping and facilitates a clearer analysis of the Photon Blockade phenomenon. Furthermore, we delve into Gaussian states, which play a vital role in understanding the Unconventional Photon Blockade effect. By combining coherent and squeezed states, these optimally squeezed Gaussian states exhibit minimized second-order correlation functions when specific parameters are chosen appropriately. We provide a thorough definition and examination of coherent and squeezed states to foster a solid understanding of their characteristics and their impact on the Photon Blockade effect. Additionally, we introduce the Wigner function, a quasiprobability distribution that visualizes quantum mechanics in the phase space. Its use allows us to explore potential connections between the optimal parameters minimizing the second-order correlation function in the Unconventional Photon Blockade and the representation of these states in the phase space.

The second section, *Light-matter interaction*, focuses on the fundamental dynamics between light and matter. We first explore the semiclassical theory, where the matter contribution is quantized, but the light is understood as a classical component. For this case, we focus on the solutions of the population dynamics of a two-level system under different driving conditions. Afterward, we briefly return to the notion of the quantization of the electromagnetic field. Finally, by quantizing the electromagnetic field, we enter the realm of quantum theory for light-matter interaction. In particular, we examine the Jaynes Cummings Hamiltonian, a key framework that provides insights into the behavior and properties of light-matter systems. These foundational concepts form the basis for our analysis of the Photon Blockade effect.

The third section, *Quantum correlation functions*, introduces the concept of quantum correlation functions proposed by Roy Glauber. We derive the mathematical formalism for second and higher-order correlation functions, enabling the characterization of photon bunching and antibunching. Furthermore, in the following

section, entitled *Frequency filtered quantum correlation functions*, we explore correlations between photons of different frequencies, providing insights into the complex behavior of light and its statistical properties. These sections contribute to a deeper understanding of the Photon Blockade effect and its manifestation across the electromagnetic spectrum.

Finally, on the fifth section, called *Interference of quantum states*, we show the theory that explores the mixing of quantum states using a beam splitter and its impact on the second-order correlation function. By analyzing this interference, we gain insights into how coherent and incoherent contributions can be combined to generate single photons, refining the understanding of classifying photon sources. This section enhances the criteria for characterizing single-photon sources, and serves to analyze whether there is a difference between the incoherent components associated to the distinct mechanisms of Photon Blockade.

Disclaimer: *This thesis builds upon the theoretical framework presented in Santiago Bermúdez Feijóo bachelor thesis, entitled “Statistical and entanglement properties of light emitted by two interacting cavities”, which was carried out with the same advisor of the present thesis. Nevertheless, the theoretical framework here presented has been significantly expanded, reorganized, and revised to include new relevant information. The modifications include a chapter regarding the formalism of quantum mechanics employed throughout the research project, a revision, and the addition of information on the subsections for coherent and squeezed states, as well as for the theory of open quantum systems. Furthermore, a complete section for light-matter interaction and its particularities has been added, as well as the theory of frequency-filtered correlations. The interested reader is referred to [42] for further information on the original framework.*

2.1 Formalisms of Quantum Mechanics

2.1.1 Laser rotating frame transformation

One theoretical method that will be repeatedly used throughout this thesis is known as the *laser rotating frame transformation*. It consists of a formalism in which the explicit time dependence of Hamiltonian terms associated with coherent driving can be removed by making an appropriate change of coordinates by means of a unitary transformation. The steps of this method will be highlighted next.

Let's suppose that we have a time dependent Hamiltonian $H(t)$ that can be split as

$$H(t) = H_0 + V(t), \quad (2.1)$$

where H_0 corresponds to the time independent Hamiltonian and $V(t)$ is the time dependent contribution. The explicit time dependence of the Hamiltonian makes the time evolution of the state of the system more complex than the case of a time independent one. However, in some cases, one can surpass this problem if a transformation that removes such dependence is performed. If such a transformation is possible, then the time dependency of the Hamiltonian disappears and the effort to find the dynamics associated with the Hamiltonian becomes straightforward.

To find the solution to this problem, first is shown that the evolution of a wave function due to a time in-

dependent Hamiltonian is calculated as

$$|\Psi(t)\rangle = \hat{\mathcal{U}}_0(t, 0) |\Psi(0)\rangle = E^{-iH_0 t/\hbar} |\Psi(0)\rangle, \quad (2.2)$$

where $\hat{\mathcal{U}}_0$ is the usual propagator. Since In this case $|\Psi(t)\rangle$ does not contain the time dependent contribution of the Hamiltonian $V(t)$, this state does not depict the correct evolution of the system. To completely describe the evolution, one must apply a formalism that rotates the current state vector,

$$|\Psi'(t)\rangle = \hat{R}(t) |\Psi(t)\rangle \iff |\Psi(t)\rangle = \hat{R}^\dagger(t) |\Psi'(t)\rangle. \quad (2.3)$$

Taking the time derivative of $|\Psi'(t)\rangle$, and multiplying by $i\hbar$ gives

$$\begin{aligned} i\hbar \partial_t |\Psi'(t)\rangle &= i\hbar (\partial_t \hat{R}(t)) |\Psi(t)\rangle + i\hbar \hat{R}(t) \partial_t |\Psi(t)\rangle \\ &= i\hbar (\partial_t \hat{R}(t)) |\Psi(t)\rangle + \hat{R}H |\Psi(t)\rangle \\ &= i\hbar (\partial_t \hat{R}(t)) \hat{R}^\dagger(t) |\Psi'(t)\rangle + \hat{R}H \hat{R}^\dagger(t) |\Psi'(t)\rangle \\ i\hbar \partial_t |\Psi'(t)\rangle &= \tilde{H} |\Psi'(t)\rangle. \end{aligned} \quad (2.4)$$

Therefore, it is obtained that the rotated state follows Schrödinger equation with a modified Hamiltonian

$$\tilde{H} = i\hbar [\partial_t \hat{R}(t)] \hat{R}^\dagger(t) + \hat{R}(t) H \hat{R}^\dagger(t). \quad (2.5)$$

The choice of $\hat{R}(t)$ depends on the structure of each Hamiltonian, and an appropriate selection will make the Hamiltonian \tilde{H} to be time independent. In most cases, $\hat{R}(t)$ will consist of an exponential of the number operator of the system.

E.g., :

$$\hat{R}_\sigma(t) = e^{i\omega_L \hat{\sigma}^\dagger \hat{\sigma} t} = e^{\alpha \hat{\sigma}^\dagger \hat{\sigma}} \quad (2.6a)$$

$$\hat{R}_a(t) = e^{i\omega_L \hat{a}^\dagger \hat{a} t} = e^{\alpha \hat{a}^\dagger \hat{a}}. \quad (2.6b)$$

As it will be shown in the next chapters, these operators are useful for moving into the laser rotating frame, where in most cases, a time independent version of the system can be obtained. When dealing with these transformations, and given that normally \hat{R} is proportional to a hermitian operator (i.e., the number operator), one encounters that the transformation $\hat{R}(t) H \hat{R}^\dagger$ translates into terms of the form $e^{\alpha \hat{A}} \hat{B} e^{-\alpha \hat{A}}$, which can be expanded as

$$e^{\alpha \hat{A}} \hat{B} e^{-\alpha \hat{A}} = \hat{B} - \alpha [\hat{A}, \hat{B}] + \frac{\alpha^2}{2!} [[\hat{A}, \hat{B}], \hat{A}] - \dots \quad (2.7)$$

The usual combinations that one finds are $\hat{A} = \hat{c}^\dagger \hat{c}$, $\hat{B} = \hat{c}(\hat{c}^\dagger)$, so one must calculate the following commutators

$$[\hat{c}^\dagger \hat{c}, \hat{c}] = \hat{c}^\dagger [\hat{c}, \hat{c}] + [\hat{c}^\dagger, \hat{c}] \hat{c} = [\hat{c}^\dagger, \hat{c}] \hat{c} = -\hat{c} \quad (2.8a)$$

$$[\hat{c}^\dagger \hat{c}, \hat{c}^\dagger] = \hat{c}^\dagger [\hat{c}, \hat{c}^\dagger] + [\hat{c}^\dagger, \hat{c}^\dagger] \hat{c} = \hat{c}^\dagger [\hat{c}, \hat{c}^\dagger] = \hat{c}^\dagger. \quad (2.8b)$$

This property holds true when \hat{c} is either a fermionic ($\hat{\sigma}$) or bosonic (\hat{a}) operator,

$$\begin{aligned} [\hat{\sigma}^\dagger \hat{\sigma}, \hat{\sigma}] &= [\hat{\sigma}^\dagger, \hat{\sigma}] \hat{\sigma} = \hat{\sigma}^\dagger \hat{\sigma}^2 - \hat{\sigma} (\hat{\sigma}^\dagger \hat{\sigma}) = -\hat{\sigma} \\ [\hat{a}^\dagger \hat{a}, \hat{a}] &= [\hat{a}^\dagger, \hat{a}] \hat{a} = (-1) \hat{a} = -\hat{a}. \end{aligned}$$

The equality for the conjugate operators is equally proven. Since in the commutators one recursively obtains either $-\hat{c}$ or \hat{c}^\dagger , then the result of the property $e^{\alpha \hat{A}} \hat{B} e^{-\alpha \hat{A}}$ for each case is

$$e^{\alpha \hat{c}^\dagger \hat{c}} \hat{c} e^{-\alpha \hat{c}^\dagger \hat{c}} = \hat{c} \left\{ 1 + \alpha + \frac{\alpha^2}{2!} + \frac{\alpha^3}{3!} + \dots \right\} = \hat{c} e^{-\alpha} \quad (2.9a)$$

$$e^{\alpha \hat{c}^\dagger \hat{c}} \hat{c}^\dagger e^{-\alpha \hat{c}^\dagger \hat{c}} = \hat{c}^\dagger \left\{ 1 - \alpha + \frac{\alpha^2}{2!} - \frac{\alpha^3}{3!} + \dots \right\} = \hat{c}^\dagger e^{\alpha}, \quad (2.9b)$$

and given that time dependent terms of coherent driving are usually of the form $\propto (\hat{c} e^{\alpha} + \hat{c}^\dagger e^{-\alpha})$, then when moving to the rotating frame of the laser the exponentials cancels out leaving only the driving term proportional to $\propto (\hat{c} + \hat{c}^\dagger)$. Equations (2.9) hold either for bosonic or fermionic operators, and the results of their transformation will be crucial for some models used in this thesis.

2.1.2 Gaussian states in Quantum Mechanics

The concept of phase space, when treated from a quantum mechanical perspective, is a little different from its classical analog. In the latter one, the state of a system is entirely represented by exactly knowing the position and momentum coordinates, which can be described in the phase space as a point. On the other side, due to the restrictions that naturally arise from the uncertainty principle, one can not represent the state of a system as a point in the phase space, because of the incompatibility to measure with infinite precision conjugated variables such as position and momentum. Nevertheless, this concept can be extrapolated into a new definition of phase space, by using generalized coordinates that are in agreement with the uncertainty principle. This means that states envisioned through the phase space will not be represented as points, but rather as areas that are in agreement with the uncertainty principle.

The concept of phase space in quantum mechanics will be a vital tool for visualizing the evolution of states to determine their quantum properties. Some significant types of states are the so-called *Gaussian states*, which means that their phase space representation has a Gaussian shape. The most famous states of this kind are the *coherent states* and *squeezed states*. In the next subsection, their definition and properties will be profoundly analyzed.

Wigner function

Regarding phase space in quantum mechanics, there are many ways in which states can be represented. Among them, the most common tool that facilitates the exploration of dynamics in phase space is the *Wigner function*, introduced by Eugene Wigner in 1932. It is a quasiprobability distribution, which means that it can take negative

values, commonly related to nonclassical states [43]. It is defined in terms of the density operator as

$$W(x, p) = \frac{1}{2\pi\hbar} \int_{-\infty}^{\infty} dx' e^{-ipx'/\hbar} \langle x + x'/2 | \rho | x - x'/2 \rangle \quad (2.10a)$$

$$\int_{-\infty}^{\infty} dx \int_{-\infty}^{\infty} dp W(x, p) = 1. \quad (2.10b)$$

Now, we will calculate the Wigner representation for some states, highlighting their most relevant properties. We will start by giving the representation of Fock states $|n\rangle$.

An equivalent form of writing the Wigner function employs the *characteristic function*, $\hat{C}_\rho(\lambda) = \text{Tr}\{\rho \hat{D}(\lambda)\}$, where $\hat{D} = \exp\{-|\lambda|^2/2\} \exp\{\lambda \hat{a}^\dagger\} \exp\{-\lambda^* \hat{a}\}$ is referred to as the *displacement operator*, whose nature will be clarified when we introduce the formal definitions of coherent states. The Wigner representation using the characteristic function is,

$$W(\alpha) = \frac{1}{\pi^2} \int e^{\lambda^* \alpha - \lambda \alpha^*} \hat{C}_\rho(\lambda) d^2 \lambda \quad (2.11)$$

Since the characteristic function depends on the density matrix, it will have a particular representation for each state. For the case of the Fock basis, $\rho = |n\rangle \langle n|$, and $C_\rho(\lambda)$ turns to be

$$\hat{C}_{\text{Fock}}(\lambda) = \sum_{m=0}^{\infty} \langle m|n\rangle \langle n|\hat{D}(\lambda)|m\rangle = \langle n|\hat{D}(\lambda)|n\rangle = e^{-|\lambda|^2/2} \langle n|e^{\lambda \hat{a}^\dagger} e^{-\lambda^* \hat{a}}|n\rangle$$

using the series expansion for the exponential operator yields,

$$\begin{aligned} \hat{C}_{\text{Fock}}(\lambda) &= e^{-|\lambda|^2/2} \sum_{m=0}^{\infty} \langle n| \frac{(\lambda \hat{a}^\dagger)^m}{m!} \frac{(-\lambda^* \hat{a})^m}{m!} |n\rangle = e^{-|\lambda|^2/2} \sum_{m=0}^{\infty} \frac{(-|\lambda|^2)^m}{m!^2} \langle n|\hat{a}^{\dagger m} \hat{a}^m|n\rangle \\ &= e^{-|\lambda|^2/2} \sum_{m=0}^n \frac{(-|\lambda|^2)^m}{m!^2} \binom{n}{m} = (-1)^n e^{-|\lambda|^2/2} L_n(|\lambda|^2) \end{aligned}$$

Where $L_n(|x|^2)$ are the Laguerre polynomials. This means that the Wigner function for the Fock states can be written as

$$W(\alpha) = \frac{1}{\pi^2} \int e^{\lambda^* \alpha - \lambda \alpha^*} (-1)^n e^{-|\lambda|^2/2} L_n(|\lambda|^2) d^2 \lambda$$

And by using the identity $\int f(\alpha) e^{\alpha^* y - z|\alpha|^2} \pi^{-1} d^2 \alpha = z^{-1} f(z^{-1}y)$, one obtains the final representation

$$W_n(\alpha) = \frac{2}{\pi} (-1)^n e^{-2|\alpha|^2} L_n(4|\alpha|^2) \quad (2.12)$$

Where α is a complex number whose nature will be revealed afterward. An example of the first four Wigner functions of the Fock states can be seen in Figure (2.1). The negative values on the Wigner function highlight the nonclassical properties inherent to Fock states, which is a characteristic of non-Gaussian states. The Wigner function for Gaussian states will be calculated after the formal definition of coherent and squeezed states.

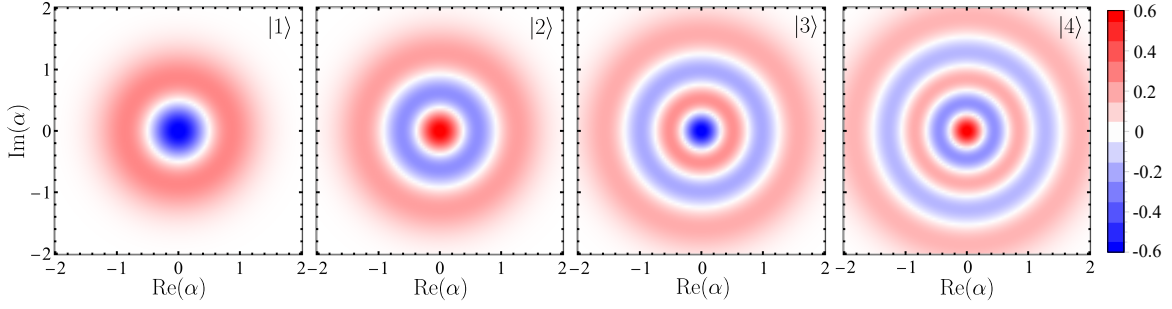


Figure 2.1 Wigner functions for the Fock state $|n\rangle$, for $n \in [1, 4]$.

Coherent states

Since their original proposal by Schrödinger, these states have been rigorously studied, especially by Roy Glauber, who developed the theory of optical coherence [11] by the use of coherence states to describe the quantum properties of light.

Coherent states have been described in several ways. First, they are defined as the “most classical” states allowed by quantum mechanics, which means that they correspond to the states that have the lowest possible uncertainties. They are also defined as the eigenstates of the annihilation operator of the electromagnetic field. These two properties can be summed up as

$$(\langle \hat{x}^2 \rangle - \langle \hat{x} \rangle^2) (\langle \hat{p}^2 \rangle - \langle \hat{p} \rangle^2) \geq \left(\frac{[\hat{x}, \hat{p}]}{2} \right)^2 = \frac{1}{4} \quad (2.13a)$$

$$\hat{a}|\alpha\rangle = \alpha|\alpha\rangle. \quad (2.13b)$$

To understand better the phase state representation of a coherent state is useful to construct the dimensionless momentum and position operators, denominated the quadrature operators, which are defined as

$$\hat{X}_1 = \frac{\hat{a} + \hat{a}^\dagger}{2} \quad (2.14a)$$

$$\hat{X}_2 = \frac{\hat{a} - \hat{a}^\dagger}{2i}. \quad (2.14b)$$

Their expected value over coherent states is,

$$\langle \alpha | \hat{X}_1 | \alpha \rangle = \langle \alpha | \left\{ \frac{\hat{a} + \hat{a}^\dagger}{2} \right\} | \alpha \rangle = \frac{\alpha + \alpha^*}{2} = \text{Re}(\alpha) \quad (2.15a)$$

$$\langle \alpha | \hat{X}_2 | \alpha \rangle = \langle \alpha | \left\{ \frac{\hat{a} - \hat{a}^\dagger}{2i} \right\} | \alpha \rangle = \frac{\alpha - \alpha^*}{2i} = \text{Im}(\alpha), \quad (2.15b)$$

this means that the complex α – plane acts as a phase space, with $\text{Re}(\alpha)$ and $\text{Im}(\alpha)$ being regarded as momentum and position, respectively. This corresponds to the axis used in Figure (2.1). The Wigner representation of the coherent states can now be calculated. Starting once again by calculating the characteristic function,

$$\hat{C}_{\text{coherent}}(\lambda) = \langle \alpha_0 | \hat{D}(\lambda) | \alpha_0 \rangle = e^{-|\lambda|^2/2} \langle \alpha_0 | e^{\lambda \hat{a}^\dagger} e^{-\lambda^* \hat{a}} | \alpha_0 \rangle = e^{-|\lambda|^2/2} e^{\lambda \alpha_0^* - \lambda^* \alpha_0},$$

where the second property of Equation (2.13) was applied. Inserting this characteristic function into the Wigner function (2.11) gives

$$W_{\alpha_0}(\alpha) = \int d^2\lambda e^{(\alpha-\alpha_0)\lambda^* - (\alpha_0^* - \alpha^*)\lambda} e^{-|\lambda|^2/2} = \frac{2}{\pi} e^{-2|\alpha-\alpha_0|^2}. \quad (2.16)$$

This means that the phase space representation of a coherent state $|\alpha_0\rangle$ corresponds to a displaced circle with origin in the complex value α_0 , and its area, as mentioned earlier, is related to the uncertainty of the state. The results of this can be seen in Figure (2.2), where a value of $\alpha_0 = 1 + i$ has been used.

Another important result from coherent states is obtained by expanding them in a base of Fock states

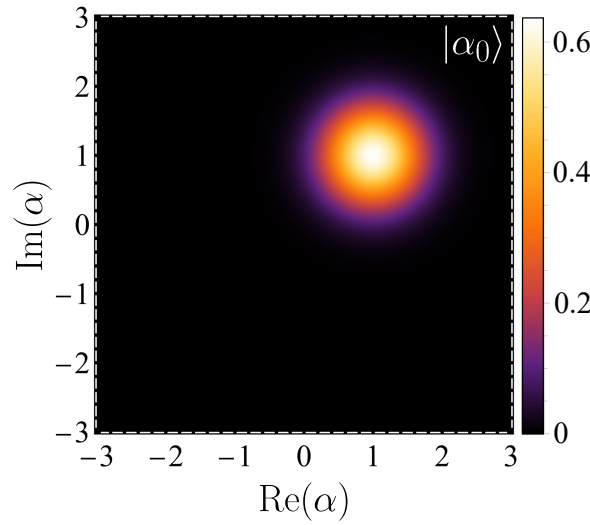


Figure 2.2 Wigner's function of the coherent state $|\alpha_0\rangle$, where $\alpha_0 = 1 + i$.

since they form a complete set

$$|\alpha\rangle = \sum_{n=0}^{\infty} C_n |n\rangle. \quad (2.17)$$

By applying the annihilation operator and remembering that coherent states are their eigenstates, then

$$\hat{a}|\alpha\rangle = \alpha|\alpha\rangle = \sum_{n=0}^{\infty} C_n \hat{a}|n\rangle = \sum_{n=0}^{\infty} C_n \sqrt{n} |n-1\rangle.$$

The recurrence relationship for the C_n coefficients is

$$C_n = \frac{\alpha}{\sqrt{n}} C_{n-1} = \frac{\alpha^2 C_{n-2}}{\sqrt{n(n-1)}} C_{n-2} = \dots = \frac{\alpha^n}{\sqrt{n!}} C_0.$$

By founding the normalization requirement for coherent states, C_0 can be obtained, and thus, coherent states can be represented in the Fock basis as

$$|\alpha\rangle = e^{-|\alpha|^2/2} \sum_{n=0}^{\infty} \frac{\alpha^n}{\sqrt{n!}} |n\rangle, \quad (2.18)$$

which is the textbook expression for coherent states. The previous formula helps to find some relevant quantities of coherent states, such as the probability of finding n photons, $P(n)$:

$$\begin{aligned} i). \langle n|\alpha\rangle &= e^{-|\alpha|^2/2} \sum_{m=0}^{\infty} \frac{\alpha^m}{\sqrt{m!}} \langle n|m\rangle = e^{-|\alpha|^2/2} \sum_{m=0}^{\infty} \frac{\alpha^m}{\sqrt{m!}} \delta_{m,n} = e^{-|\alpha|^2/2} \frac{\alpha^n}{\sqrt{n!}} \\ ii). \langle \alpha|n\rangle &= e^{-|\alpha|^2/2} \frac{\alpha^{*n}}{\sqrt{n!}} \\ iii). P(n) &= |\langle n|\alpha\rangle|^2 = \langle \alpha|n\rangle \langle n|\alpha\rangle = e^{-|\alpha|^2} \frac{|\alpha|^{2n}}{n!} = e^{-\bar{n}} \frac{\bar{n}^n}{n!}. \end{aligned} \quad (2.19)$$

Therefore, it is found that the probability of finding n photons in a coherent state corresponds to a Poisson distribution, with average photon number $\langle n\rangle = \bar{n} = |\alpha|^2$. This result corresponds exactly to the photon statistics obtained by a laser far above the threshold. I will also be a fundamental limit to compare the photon statistics of different states, which will be tackled later on.

There is another useful way to envision coherent states. Recalling that any Fock state $|n\rangle$ can be thought of as an n -times application of the creation operator \hat{a}^\dagger over the vacuum, i.e.,

$$|n\rangle = \frac{(\hat{a}^\dagger)^n}{\sqrt{n!}} |0\rangle, \quad (2.20)$$

then, one can replace this in the Fock representation of coherent states

$$\begin{aligned} |\alpha\rangle &= e^{-|\alpha|^2/2} \sum_{n=0}^{\infty} \frac{\alpha^n}{\sqrt{n!}} |n\rangle \\ &= e^{-|\alpha|^2/2} \left(\sum_{n=0}^{\infty} \frac{(\alpha \hat{a}^\dagger)^n}{n!} \right) |0\rangle \\ &= e^{-|\alpha|^2/2} e^{\alpha \hat{a}^\dagger} |0\rangle. \end{aligned} \quad (2.21)$$

Taking advantage of the fact that $e^{\alpha^* \hat{a}} |0\rangle = 0$, then, one can also define a coherent state as

$$|\alpha\rangle = e^{-|\alpha|^2/2} e^{\alpha \hat{a}^\dagger} e^{\alpha^* \hat{a}} |0\rangle = \hat{D}(\alpha) |0\rangle, \quad (2.22)$$

where $\hat{D}(\alpha)$ is denoted as the displacement operator (whose first appearance was made in the characteristic function definition of the Wigner function, Equation 2.11, and now its nature will be clarified). This result shows that coherent states can also be visualized as displaced vacuum states, with the center in the complex number α , and it also indicates that the fluctuations from both states are the same. Furthermore, the zero photon state $|0\rangle$ is therefore a special case of a coherent state where $\alpha = 0$, and it does not correspond to a non Gaussian state such as the Fock states $|n\rangle$.

Resuming the discussion on the subject of the displacement operator, an equivalent way to rewrite it can be found by means of the Baker-Hausdorff formula. If \hat{A} and \hat{B} are two operators such that $[[\hat{A}, \hat{B}], \hat{A}] = [[\hat{A}, \hat{B}], \hat{B}] = 0$, then

$$e^{\hat{A}+\hat{B}} = e^{-[\hat{A}, \hat{B}]/2} e^{\hat{A}} e^{\hat{B}}. \quad (2.23)$$

Choosing $\hat{B} = -\alpha^* \hat{a}$ and $\hat{A} = \alpha \hat{a}^\dagger$,

$$e^{\alpha \hat{a}^\dagger + \alpha^* \hat{a}} = e^{-|\alpha|^2/2} e^{\alpha \hat{a}^\dagger} e^{\alpha^* \hat{a}} = \hat{D}(\alpha). \quad (2.24)$$

Now, we focus on searching what is the effect of a similarity transformation of the annihilation and creation operators as $\hat{D}^\dagger(\alpha) \hat{a} \hat{D}(\alpha)$ and $\hat{D}^\dagger(\alpha) \hat{a}^\dagger \hat{D}(\alpha)$,

$$\hat{D}^\dagger(\alpha) \hat{a} \hat{D}(\alpha) = e^{|\alpha|^2/2} e^{\alpha^* \hat{a}} e^{-\alpha \hat{a}^\dagger} \hat{a} e^{-|\alpha|^2/2} e^{\alpha \hat{a}^\dagger} e^{-\alpha^* \hat{a}} \quad (2.25)$$

$$\hat{D}^\dagger(\alpha) \hat{a} \hat{D}(\alpha) = e^{-\alpha \hat{a}^\dagger} \hat{a} e^{\alpha \hat{a}^\dagger}. \quad (2.26)$$

Once again, applying the property of Equation (2.7), and since for $\hat{A} = \hat{a}^\dagger$ and $\hat{B} = \hat{a}$ the commutators $[[\hat{a}, \hat{a}^\dagger], \hat{a}^\dagger]$ are all zero, then

$$\hat{D}^\dagger(\alpha) \hat{a} \hat{D}(\alpha) = \hat{a} + \alpha. \quad (2.27)$$

Following a similar procedure for \hat{a}^\dagger yields,

$$\hat{D}^\dagger(\alpha) \hat{a}^\dagger \hat{D}(\alpha) = \hat{a}^\dagger + \alpha^*. \quad (2.28)$$

This means that the action of $\hat{D}(\alpha)$ over the creation and annihilation operator is, as its name indicates, to displace them by a value α . This property will be used later on.

Finally, to see the possible Hamiltonian descriptions for a coherent state, we will apply the open quantum system formalism (Explained in detail in Appendix A), to find the steady state solution for a Quantum Harmonic Oscillator driven by a laser. We will consider that this system is in contact with an external environment, which leads to a loss of photons at a rate κ_a . This situation can be expressed by means of the following master equation in Lindblad form,

$$H_a = \tilde{\omega}_a \hat{a}^\dagger \hat{a} + \Omega_a (\hat{a} + \hat{a}^\dagger) \quad (2.29a)$$

$$\partial_t \rho = i[\rho, H_a] + \frac{\kappa_a}{2} (2\hat{a} \rho \hat{a}^\dagger - \hat{a}^\dagger \hat{a} \rho - \rho \hat{a}^\dagger \hat{a}) \quad (2.29b)$$

$$\partial_t \langle \hat{O} \rangle(t) = i \langle [H_a, \hat{O}] \rangle + \frac{\kappa_a}{2} (2\langle \hat{a}^\dagger \hat{O} \hat{a} \rangle - \langle \hat{a}^\dagger \hat{a} \hat{O} \rangle - \langle \hat{O} \hat{a}^\dagger \hat{a} \rangle), \quad (2.29c)$$

where $\tilde{\omega}_a = \omega_a - \omega_L$ corresponds to the laser rotating frame frequency and Ω_a refers to the strength of the coherent driving. This Hamiltonian, which is written in the laser rotating frame, is obtained after applying the transformation given in Equation (2.5). Although the exact procedure to obtain this new Hamiltonian will be omitted at this point, an example of the complete derivation of a laser rotating frame transformation will be realized in the following sections, when we deal with the problem of photon statistics in the driven Jaynes Cummings model, Sec 3.2.

We will begin by finding the steady state solutions for an operator of the form $\hat{O} = \hat{a}^{\dagger\mu} \hat{a}^\nu$. Applying the Equation (2.29 c), this yields

$$\partial_t \langle \hat{a}^{\dagger\mu} \hat{a}^\nu \rangle(t) = i \langle [\tilde{\omega}_a \hat{a}^\dagger \hat{a} + \Omega_a (\hat{a} + \hat{a}^\dagger), \hat{a}^{\dagger\mu} \hat{a}^\nu] \rangle + \frac{\kappa_a}{2} (2\langle \hat{a}^\dagger (\hat{a}^{\dagger\mu} \hat{a}^\nu) \hat{a} \rangle - \langle \hat{a}^\dagger \hat{a} (\hat{a}^{\dagger\mu} \hat{a}^\nu) \rangle - \langle (\hat{a}^{\dagger\mu} \hat{a}^\nu) \hat{a}^\dagger \hat{a} \rangle). \quad (2.30)$$

First, taking the case where $\mu, \nu = 1$, i.e., the equation of motion for the number operator, gives $\hat{a}^\dagger \hat{a}$

$$\partial_t \langle \hat{a}^\dagger \hat{a} \rangle(t) = i \langle [\tilde{\omega}_a \hat{a}^\dagger \hat{a} + \Omega_a (\hat{a} + \hat{a}^\dagger), \hat{a}^\dagger \hat{a}] \rangle + \frac{\kappa_a}{2} (2 \langle \hat{a}^\dagger (\hat{a}^\dagger \hat{a}) \hat{a} \rangle - \langle \hat{a}^\dagger \hat{a} (\hat{a}^\dagger \hat{a}) \rangle - \langle (\hat{a}^\dagger \hat{a}) \hat{a}^\dagger \hat{a} \rangle).$$

Using the operator algebra for the bosonic operators, $[\hat{a}, \hat{a}^\dagger] = 1$, one simplifies the previous equation to obtain

$$\partial_t \langle \hat{a}^\dagger \hat{a} \rangle(t) = i \Omega_a (\langle \hat{a} \rangle - \langle \hat{a}^\dagger \rangle) - \kappa_a \langle \hat{a}^\dagger \hat{a} \rangle. \quad (2.31)$$

Now, since the terms $\langle \hat{a} \rangle$ and $\langle \hat{a}^\dagger \rangle$ appear on the equation of motion for $\langle \hat{a}^\dagger \hat{a} \rangle$, we will need to apply once again the procedure for finding the corresponding equation for one of both quantities (since the missing one can be obtained by taking the complex conjugate of the equation). We take $\nu = 0$, $\mu = 1$ so we will find the equation of motion for $\langle \hat{a}^\dagger \rangle$,

$$\partial_t \langle \hat{a}^\dagger \rangle(t) = i \langle [\tilde{\omega}_a \hat{a}^\dagger \hat{a} + \Omega_a (\hat{a} + \hat{a}^\dagger), \hat{a}^\dagger] \rangle + \frac{\kappa_a}{2} (2 \langle \hat{a}^\dagger (\hat{a}^\dagger) \hat{a} \rangle - \langle \hat{a}^\dagger \hat{a} (\hat{a}^\dagger) \rangle - \langle (\hat{a}^\dagger) \hat{a}^\dagger \hat{a} \rangle).$$

Applying some useful relations, such as $\langle \hat{a}^\dagger \hat{a} \hat{a}^\dagger \rangle = \langle \hat{a}^\dagger \rangle + \langle \hat{a}^\dagger \hat{a}^\dagger \hat{a} \rangle$, the following master equation is obtained

$$\partial_t \langle \hat{a}^\dagger \rangle(t) = i (\tilde{\omega}_a \langle \hat{a}^\dagger \rangle + \Omega_a) - \frac{\kappa_a}{2} \langle \hat{a}^\dagger \rangle. \quad (2.32)$$

And by taking the hermitian conjugate one gets

$$\partial_t \langle \hat{a} \rangle(t) = -i (\tilde{\omega}_a \langle \hat{a} \rangle + \Omega_a) - \frac{\kappa_a}{2} \langle \hat{a} \rangle. \quad (2.33)$$

Using the Equations (2.31-2.33), it is possible to find the following steady state solutions.

$$|\alpha|^2 = \langle \hat{a}^\dagger \hat{a} \rangle_{ss} = \frac{4\Omega_a^2}{\kappa_a^2 + 4\tilde{\omega}_a^2} \quad (2.34a)$$

$$\langle \hat{a}^\dagger \rangle_{ss} = \frac{2i\Omega_a}{\kappa_a - 2i\tilde{\omega}_a}. \quad (2.34b)$$

So, we have been able to find an expression that relates the population of a coherent state ($|\alpha|^2$) with the parameters of the driven quantum harmonic oscillator master equation.

Squeezed states

A more general kind of state results when each quadrature must not necessarily have the same amount of uncertainty as the other, so that they have a less amount than the one related to coherent states, although their multiplication must still be equal to 1/4 in order to be considered minimum uncertainty states. These types of states are the *Squeezed states*, which in order to satisfy the uncertainty principle, must fulfill that the quadrature that is not being squeezed must have a noise increase. This property can be written as

$$\langle (\hat{X}_1)^2 \rangle < \frac{1}{4}. \quad (2.35)$$

As in the case of coherent states, squeezed states can be described by applying an operator, called the squeezing operator, to a given state.

$$|\zeta\rangle = \hat{S}(\zeta) |\psi_s\rangle, \quad (2.36)$$

where $\hat{S}(\zeta) = \exp\left(\frac{\zeta^*}{2}\hat{a}^2 - \frac{\zeta}{2}\hat{a}^{\dagger 2}\right)$ and $\zeta = re^{i\theta}$. the parameter r is called the amplitude squeezing parameter and can take values between $0 < r < \infty$. The θ angle indicates the direction in which the squeezing of the deviation takes place, satisfying $0 < \theta < 2\pi$. For the case of $|\psi_s\rangle = |0\rangle$, the states are referred to as squeezed vacuum states.

Similarly than for coherent states, the similarity transformation for \hat{a} and \hat{a}^\dagger , as given by the Baker-Hausdorff lemma are

$$\hat{S}^\dagger(\zeta)\hat{a}\hat{S}(\zeta) = \hat{a}\cosh r - e^{i\theta}\hat{a}^\dagger\sinh r = \hat{a}_\xi \quad (2.37)$$

$$\hat{S}^\dagger(\zeta)\hat{a}^\dagger\hat{S}(\zeta) = \hat{a}^\dagger\cosh r - e^{-i\theta}\hat{a}\sinh r = \hat{a}_\xi^\dagger. \quad (2.38)$$

From this, the deviation of the quadrature operators on squeezed states can be found, and from there, the squeezing of each quadrature can be quantified. Remembering that the definition of the quadrature operators is

$$\begin{aligned} \hat{X}_1 &= \frac{\hat{a} + \hat{a}^\dagger}{2} \\ \hat{X}_2 &= \frac{\hat{a} - \hat{a}^\dagger}{2i}, \end{aligned}$$

then, for the special case of squeezed vacuum states, one has to calculate the following product

$$\begin{aligned} \langle(\Delta\hat{X}_1)^2\rangle &= \langle\hat{X}_1^2\rangle - \langle\hat{X}_1\rangle^2 \\ \langle\xi|(\Delta\hat{X}_1)^2|\xi\rangle &= \langle 0|\hat{S}^\dagger(\xi)(\Delta\hat{X}_1)^2\hat{S}(\xi)|0\rangle, \end{aligned}$$

which is completely expressed as

$$\langle 0|\hat{S}^\dagger(\xi)(\Delta\hat{X}_1)^2\hat{S}(\xi)|0\rangle = \frac{1}{4} [\langle 0|\hat{S}^\dagger(\hat{a}^2 + \hat{a}\hat{a}^\dagger + \hat{a}^\dagger\hat{a} + \hat{a}^{\dagger 2})\hat{S}|0\rangle - (\langle 0|\hat{S}^\dagger(\hat{a} + \hat{a}^\dagger)\hat{S}|0\rangle)^2]. \quad (2.39)$$

Now, each one of these terms will be explicitly calculated. For the first case, it is done as follows

$$\begin{aligned} \langle 0|\hat{S}^\dagger(\hat{a}^2 + \hat{a}\hat{a}^\dagger + \hat{a}^\dagger\hat{a} + \hat{a}^{\dagger 2})\hat{S}|0\rangle &= \langle 0|(\hat{S}^\dagger\hat{a}\hat{S}\hat{S}^\dagger\hat{a}\hat{S} + \hat{S}^\dagger\hat{a}\hat{S}\hat{S}^\dagger\hat{a}^\dagger\hat{S} + \hat{S}^\dagger\hat{a}^\dagger\hat{S}\hat{S}^\dagger\hat{a}\hat{S} + \hat{S}^\dagger\hat{a}^\dagger\hat{S}\hat{S}^\dagger\hat{a}^\dagger\hat{S})|0\rangle \\ &= \langle 0|(\hat{a}_\xi^2 + \hat{a}_\xi\hat{a}_\xi^\dagger + \hat{a}_\xi^\dagger\hat{a}_\xi + \hat{a}_\xi^{\dagger 2})|0\rangle. \end{aligned} \quad (2.40)$$

The form of these transformed operators is

$$\hat{a}_\xi^2 = \hat{a}^2 \cosh^2 r - \hat{a}\hat{a}^\dagger e^{i\theta} \cosh r \sinh r - \hat{a}^\dagger\hat{a} e^{i\theta} \cosh r \sinh r + \hat{a}^{\dagger 2} e^{2i\theta} \sinh^2 r \quad (2.41a)$$

$$\hat{a}_\xi\hat{a}_\xi^\dagger = \hat{a}\hat{a}^\dagger \cosh^2 r - \hat{a}^2 e^{-i\theta} \cosh r \sinh r - \hat{a}^{\dagger 2} e^{i\theta} \cosh r \sinh r + \hat{a}^\dagger\hat{a} \sinh^2 r \quad (2.41b)$$

$$\hat{a}_\xi^\dagger\hat{a}_\xi = \hat{a}^\dagger\hat{a} \cosh^2 r - \hat{a}^{\dagger 2} e^{i\theta} \cosh r \sinh r - \hat{a}^2 e^{i\theta} \cosh r \sinh r + \hat{a}\hat{a}^\dagger \sinh^2 r \quad (2.41c)$$

$$\hat{a}_\xi^{\dagger 2} = \hat{a}^{\dagger 2} \cosh^2 r - \hat{a}^\dagger\hat{a} e^{-i\theta} \cosh r \sinh r - \hat{a}\hat{a}^\dagger e^{-i\theta} \cosh r \sinh r + \hat{a}^2 e^{-2i\theta} \sinh^2 r, \quad (2.41d)$$

and evaluating the expected value over the vacuum Fock state results in

$$\langle 0 | \hat{a}_\xi^2 | 0 \rangle = -e^{i\theta} \cosh r \sinh r \quad (2.42a)$$

$$\langle 0 | \hat{a}_\xi \hat{a}_\xi^\dagger | 0 \rangle = \cosh^2 r \quad (2.42b)$$

$$\langle 0 | \hat{a}_\xi^\dagger \hat{a}_\xi | 0 \rangle = \sinh^2 r \quad (2.42c)$$

$$\langle 0 | \hat{a}_\xi^{\dagger 2} | 0 \rangle = -e^{-i\theta} \cosh r \sinh r. \quad (2.42d)$$

The second term of $\langle 0 | \hat{S}^\dagger(\xi) (\Delta \hat{X}_1)^2 \hat{S}(\xi) | 0 \rangle$ does not contribute at all because $\langle 0 | \hat{a}_\xi | 0 \rangle$ and $\langle 0 | \hat{a}_\xi^\dagger | 0 \rangle$ is equal to zero. It is thus finally obtained

$$\begin{aligned} \langle 0 | \hat{S}^\dagger(\xi) (\Delta \hat{X}_1)^2 \hat{S}(\xi) | 0 \rangle &= \frac{1}{4} \left[\cosh^2 r + \sinh^2 r - \cosh r \sinh r (e^{i\theta} + e^{-i\theta}) \right] \\ &= \frac{1}{4} [\cosh^2 r + \sinh^2 r - 2 \cosh r \sinh r \cos \theta]. \end{aligned} \quad (2.43)$$

By an analogous procedure, the result is also obtained for the second quadrature

$$\begin{aligned} \langle 0 | \hat{S}^\dagger(\xi) (\Delta \hat{X}_2)^2 \hat{S}(\xi) | 0 \rangle &= \frac{1}{4} \left[\cosh^2 r + \sinh^2 r + \cosh r \sinh r (e^{i\theta} + e^{-i\theta}) \right] \\ &= \frac{1}{4} [\cosh^2 r + \sinh^2 r + 2 \cosh r \sinh r \cos \theta]. \end{aligned} \quad (2.44)$$

Now we will present the photon number distribution for the squeezed vacuum state, in analogy to the Poisson distribution that was found for coherent states. First, starting with the property $\hat{a} | 0 \rangle = 0$ one can multiply both sides of the equation by the squeezing operator, and introduce a unitary operator

$$\begin{aligned} \hat{a} | 0 \rangle &= \hat{S}(\xi) \hat{a} \hat{S}^\dagger(\xi) \hat{S}(\xi) | 0 \rangle = \hat{S}(\xi) \hat{a} \hat{S}^\dagger(\xi) | \xi \rangle \\ (\hat{a} \cosh r + \hat{a}^\dagger e^{i\phi} \sinh r) | \xi \rangle &= (\hat{a} \mu + \hat{a}^\dagger \nu) | \xi \rangle = 0, \end{aligned}$$

so it has been found that the squeezed vacuum operator is the zero eigenstate of the operator $(\hat{a} \mu + \hat{a}^\dagger \nu)$. Now, using this fact, we will apply this operator to the Fock basis representation of the squeezed vacuum in order to find a recursion relationship

$$\begin{aligned} | \xi \rangle &= \sum_n C_n | n \rangle \\ (\hat{a} \mu + \hat{a}^\dagger \nu) | \xi \rangle &= \sum_{n=0} C_n (\hat{a} \mu + \hat{a}^\dagger \nu) | n \rangle \\ \sum_{n=0} \left(\mu C_{n+1} \sqrt{n+1} + \nu C_{n-1} \sqrt{n} \right) | 0 \rangle &= 0. \end{aligned}$$

The recursion is solved by finding the expression for even states since they are the one that include vacuum contributions (*Gerry -Knight, 2004, pg.161*) [37]. Thus, the squeezed vacuum expression in the Fock basis is

$$| \xi \rangle = \frac{1}{\sqrt{\cosh r}} \sum_{m=0}^{\infty} (-1)^m \frac{\sqrt{(2m)!}}{2^m m!} e^{im\theta} (\tanh r) | 2m \rangle, \quad (2.45)$$

and the photon number probability for even pairs of photons is (odd states directly yield zero)

$$P_{2m} = |\langle 2m | \xi \rangle|^2 = \frac{(2m)!}{2^{2m}(m!)^2} \frac{(\tanh r)^{2m}}{\cosh r}. \quad (2.46)$$

Finally, to complete the analysis for the squeezed states, we will find the analytical expression for the Wigner function. Applying once again the characteristic function representation given by Equation (2.11)

$$\hat{C}_\xi(\lambda) = \langle \xi | \hat{D}(\lambda) | \xi \rangle = \langle 0 | \hat{S}^\dagger(\xi) \hat{D}(\lambda) \hat{S}(\xi) | 0 \rangle. \quad (2.47)$$

This quantity is a well-known property whose result is

$$\hat{S}^\dagger(\xi) \hat{D}(\lambda) \hat{S}(\xi) = \hat{D}(\lambda \mu + \lambda^* \nu), \quad (2.48)$$

where $\mu = \cosh r$ and $\nu = e^{i\theta} \sinh r$ are the similarity transformation coefficients given in Equation (2.38). With this, the resulting form for the vacuum squeezed state is

$$W_\xi(\alpha) = \frac{1}{\pi^2} \int d^2\lambda e^{\alpha\lambda^* - \alpha^*\lambda} e^{-|\lambda\mu + \lambda^*\nu|^2/2} = \frac{2}{\pi} \exp \left\{ -2 \left(\frac{\text{Re}\{\alpha\}^2}{e^{-2\xi}} + \frac{\text{Im}\{\alpha\}^2}{e^{2\xi}} \right) \right\}. \quad (2.49)$$

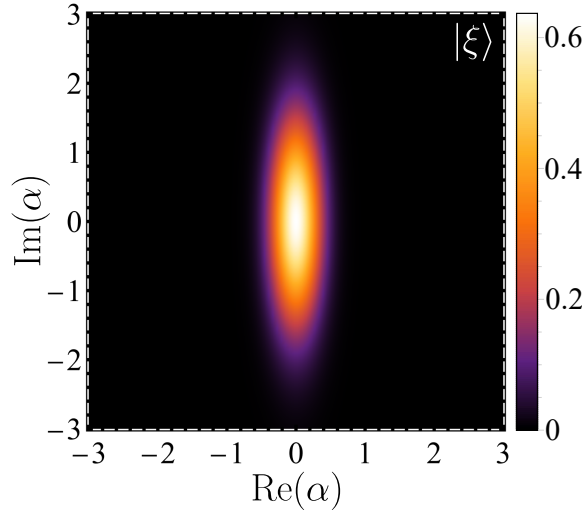


Figure 2.3 Wigner's function of the vacuum squeezed state $|\xi\rangle = \hat{S}(\xi)|0\rangle$. The squeezing parameter ξ is 0.7.

2.1.3 Two level systems

As its name indicates, Two level systems (2LS) characterize by having a Hilbert space of two independent states, normally labeled as “ground” ($|g\rangle$) and “excited” ($|e\rangle$) states, although the state $|g\rangle$ must not necessarily coincide with the lowest energy state of a quantum system. Despite their apparent simplicity, 2LS describe a wide range of physics phenomena, and their applications are essential for the development of new technologies. Some famous examples of 2LS are Spin-1/2 systems, where spins can take the values of $\pm\hbar/2$, as for the models employed in nuclear magnetic resonance [44]. Furthermore, even complicated structures such as

superconducting devices and quantum dots can be on certain occasions modeled as two level systems. Each of these systems serves to constitute the basic unit of quantum information, the qubit, whose properties can be later altered by the use of a set of operations (quantum gates) that permit the construction of complex algorithms[45]. The versatility of the construction of 2LS allows them to be the fundamental building blocks for a wide range of quantum technologies, such as for the fields of quantum computing, by the implementation of schemes using superconducting qubits [46], for quantum communication [47] and for quantum cryptography [48].

Another crucial property of two level systems refers to the process by which a system in an excited state can decay into a lower energy state by emitting a photon, i.e., *spontaneous emission*. This important feature was among the first properties that could not get a semiclassical explanation, but rather required the full quantum formalism of light matter interaction in order to understand its nature. We will derive the expression and some features in section (2.2).

In what follows, we will derive the analytical expression for the population of the 2LS ($n_\sigma = \hat{\sigma}^\dagger \hat{\sigma}$), and analyze the differences from the presence of coherent and incoherent pumping to the system.

The general operator equation that we will solve is

$$\partial_t \langle \hat{O} \rangle(t) = i \langle [H_\sigma, \hat{O}] \rangle + \frac{1}{2} \sum_k \left(2 \langle \hat{L}_k^\dagger \hat{O} \hat{L}_k \rangle - \langle \hat{L}_k^\dagger \hat{L}_k \hat{O} \rangle - \langle \hat{O} \hat{L}_k^\dagger \hat{L}_k \rangle \right). \quad (2.50)$$

Coherent driving

In analogy to the driving of a harmonic oscillator, a laser field can coherently couple to two level systems, which rises the following Hamiltonian in the laser rotating frame

$$H_\sigma = \tilde{\omega}_\sigma \hat{\sigma}^\dagger \hat{\sigma} + \Omega_\sigma (\hat{\sigma} + \hat{\sigma}^\dagger), \quad (2.51)$$

where once again $\tilde{\omega}_\sigma$ corresponds to the detuning and Ω_σ the driving strength. Using this Hamiltonian, and taking into account spontaneous emission by setting $\hat{L}_k = \sqrt{\gamma_\sigma} \hat{\sigma}$, where γ_σ indicates the excited state decay rate, the coupled differential equations are

$$\partial_t \langle \hat{\sigma}^\dagger \hat{\sigma} \rangle(t) = i\Omega_\sigma (\langle \hat{\sigma} \rangle - \langle \hat{\sigma}^\dagger \rangle) - \gamma_\sigma \langle \hat{\sigma}^\dagger \hat{\sigma} \rangle \quad (2.52a)$$

$$\partial_t \langle \hat{\sigma} \rangle(t) = i\Omega_\sigma (2\langle \hat{\sigma}^\dagger \hat{\sigma} \rangle - 1) - \left(i\tilde{\omega}_\sigma + \frac{\gamma_\sigma}{2} \right) \langle \hat{\sigma} \rangle \quad (2.52b)$$

$$\partial_t \langle \hat{\sigma}^\dagger \rangle(t) = -i\Omega_\sigma (2\langle \hat{\sigma}^\dagger \hat{\sigma} \rangle - 1) + \left(i\tilde{\omega}_\sigma - \frac{\gamma_\sigma}{2} \right) \langle \hat{\sigma}^\dagger \rangle. \quad (2.52c)$$

The steady state solution for this set of equations gives the following result for the population of the 2LS

$$n_\sigma = \frac{4\Omega_\sigma^2}{\gamma_\sigma^2 + 4\tilde{\omega}_\sigma^2 + 8\Omega_\sigma^2}. \quad (2.53)$$

This indicates that different from the population of a coherently driven harmonic oscillator (Eq. 2.34), the population of a coherently driven two level system saturates even when $\Omega_\sigma/\gamma_\sigma \rightarrow \infty$.

Incoherent pumping

For the case of also adding an incoherent pumping, the Hamiltonian will correspond to the same previously employed, while the dissipator in Equation (2.50) will have two contributions, one for spontaneous emission as previously considered, and the second one for the incoherent pumping which is given by the rate P_σ . The dissipator for the term $\hat{L}_k = \sqrt{P_\sigma}\hat{\sigma}^\dagger$ is given by,

$$\frac{P_\sigma}{2}(2\langle\hat{\sigma}\hat{\sigma}^\dagger\rangle - \langle\hat{\sigma}\hat{\sigma}^\dagger\hat{\sigma}\rangle - \langle\hat{\sigma}\hat{\sigma}^\dagger\hat{\sigma}\rangle). \quad (2.54)$$

Thus each one of the previous equations will have the following additions to the equations

$$\partial_t \langle\hat{\sigma}^\dagger\hat{\sigma}\rangle(t) = i\Omega_\sigma (\langle\hat{\sigma}\rangle - \langle\hat{\sigma}^\dagger\rangle) - \gamma_\sigma \langle\hat{\sigma}^\dagger\hat{\sigma}\rangle + P_\sigma(1 - \langle\hat{\sigma}^\dagger\hat{\sigma}\rangle) \quad (2.55a)$$

$$\partial_t \langle\hat{\sigma}\rangle(t) = i\Omega_\sigma(2\langle\hat{\sigma}^\dagger\hat{\sigma}\rangle - 1) - \left(i\tilde{\omega}_\sigma + \frac{\gamma_\sigma}{2} + \frac{P_\sigma}{2}\right) \langle\hat{\sigma}\rangle \quad (2.55b)$$

$$\partial_t \langle\hat{\sigma}^\dagger\rangle(t) = -i\Omega_\sigma(2\langle\hat{\sigma}^\dagger\hat{\sigma}\rangle - 1) + \left(i\tilde{\omega}_\sigma - \frac{\gamma_\sigma}{2} - \frac{P_\sigma}{2}\right) \langle\hat{\sigma}^\dagger\rangle. \quad (2.55c)$$

Now, the steady solution for the population turns out to be

$$n_\sigma = \frac{P_\sigma^3 + 2P_\sigma^2\gamma_\sigma + 4\gamma_\sigma\Omega_\sigma^2 + P_\sigma[\gamma_\sigma^2 + 4(\tilde{\omega}_\sigma^2 + \Omega_\sigma^2)]}{(P_\sigma + \gamma_\sigma)(P_\sigma^2 + 2P_\sigma\gamma_\sigma + \gamma_\sigma^2 + 4\tilde{\omega}_\sigma^2 + 8\Omega_\sigma^2)}. \quad (2.56)$$

Figure (2.4) displays the behavior of the population of a resonantly driven two level system when incoherent

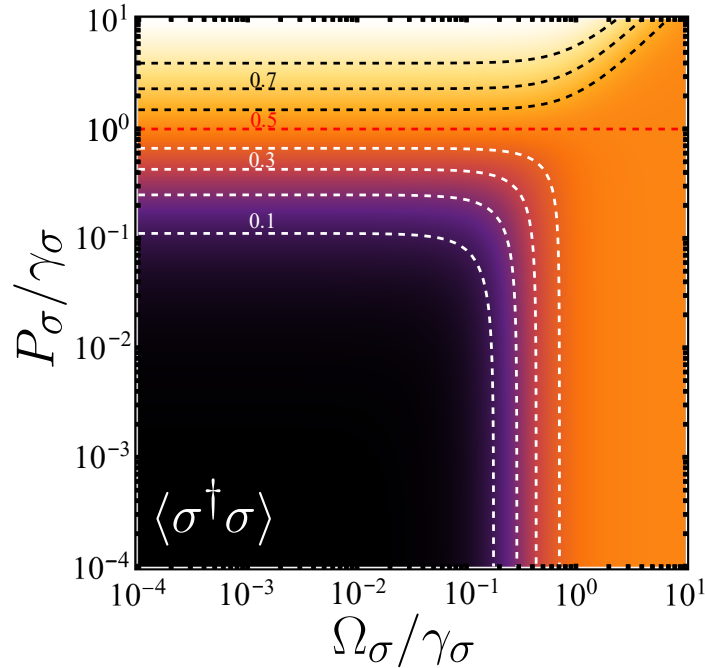


Figure 2.4 Two level system population in resonance as a function of coherent driving strength Ω_σ and rate of incoherent pumping P_σ .

pumping at a rate P_σ is also considered. This result indicates when the 2LS is only being coherently driven, as portrayed by Equation (2.53), the population has an upper limit given by $n_\sigma < 1/2$, which, as previously

mentioned, indicates that it cannot saturate. On the contrary, introducing the incoherent excitation can reach this value when the rate P_σ is bigger than the spontaneous emission decay γ_σ . The steady state value when only an incoherent driving is considered (i.e., $\Omega_\sigma = 0$) is $n_\sigma = P_\sigma / (P_\sigma + 1)$.

2.2 Light – Matter interaction

The interaction of light with matter is a fundamental problem in physics, with applications in quantum optics, chemistry, biology, and material science, as discussed in the first chapter of this thesis.

The way we understand and study these interactions depends on the physical treatment assigned to each, i.e., whether it is viewed from a classical or quantum mechanical perspective. From a classical perspective, we can understand a broad range of phenomena such as reflection, refraction, diffraction, and others. However, a more accurate description of certain phenomena requires a more refined approach. A semiclassical theory, where atoms and molecules are quantized but the light is still considered an electromagnetic wave, allows for the calculation of the probability of transitions between energy levels due to absorption or emission of radiation. This approach also correctly describes the principle of lasing in lasers, which is a key technology in many modern applications. In the purely quantum mechanical picture, phenomena such as spontaneous emission, the lamb shift, and the Casimir effect can be studied, which provides a deeper understanding of the nature of light-matter interactions. These different perspectives allow us to study light-matter interactions in various ways, each providing a unique insight into the problem, and they are all essential to the advancement of the field.

In this section, we will present the theoretical foundations of a semiclassical theory of light-matter interactions. We will also describe the process of quantizing light and explain the main features of the quantum version of light-matter interaction that will be used in subsequent chapters.

2.2.1 Semiclassical theory of light-matter interaction

The theory where an electromagnetic wave interacts with the discretized energy levels of an atom or molecule is called the semiclassical theory of light matter interaction. From this perspective, the time dependent perturbation theory of excitation with a harmonic perturbation is applicable. It is known that the Hamiltonian of a charged particle (in this case an electron) in the presence of an electromagnetic field is given as

$$H = \frac{1}{2m}(\hat{\mathbf{p}} - e\mathbf{A}(\mathbf{r}, t))^2 + e\phi(\mathbf{r}, t) + \hat{V}(r), \quad (2.57)$$

where $\mathbf{A}(\mathbf{r}, t)$ and $\phi(\mathbf{r}, t)$ are the electromagnetic field vector and scalar potentials, and $\hat{V}(r)$ is the usual binding Coulombian potential. Some considerations can be made in order to simplify the structure of this Hamiltonian. For example, the first approximation is the so-called *dipole approximation*, which consists in taking up to the first order in the multipolar expansion, i.e., $e^{i\mathbf{k} \cdot \mathbf{r}} = 1 + i\mathbf{k} \cdot \mathbf{r} - \dots \approx 1$. This consideration can only be made because of the natural scales of the problem, where the size of the atomic structure (of the order of Armstrongs, 10^{-10}) is much smaller than the characteristic wavelength of incident radiation, which for optical radiation is given by a nanometer scale. The consequence is that the vector potential can be estimated to be position independent. Furthermore, by an adequate selection of the gauge transformation, specifically to the Coulomb gauge where the radiation is transverse, i.e., $\nabla \cdot \mathbf{A} = 0$, and where $\phi(r, t) = 0$, a transformed version of the

interaction can be obtained as

$$H = \frac{\hat{\mathbf{p}}^2}{2m} + \hat{V}(r) - \hat{\mathbf{d}} \cdot \mathbf{E}(t), \quad (2.58)$$

where $\hat{\mathbf{d}}$ is the atomic dipole operator. A further simplification to this problem can be made if the atom can be considered to be a two level system (Section 2.1.3), with a ground ($|g\rangle$) and excited state ($|e\rangle$). By means of parity considerations of the dipole operator where diagonal elements are found to be zero, it can be expressed as

$$\begin{aligned} \hat{\mathbf{d}} &= d_{ge} |g\rangle \langle e| + d_{eg} |e\rangle \langle g| \\ &= d_{ge} \hat{\sigma} + d_{ge}^* \hat{\sigma}^\dagger \end{aligned} \quad (2.59a)$$

$$d_{ge} = \langle g | \hat{\mathbf{d}} | e \rangle. \quad (2.59b)$$

Assuming that the electric fields correspond to a monochromatic wave of frequency ω , $\mathbf{E}(t) = \varepsilon E_0 \cos \omega t = (\varepsilon E_0/2) (e^{i\omega t} + e^{-i\omega t})$, the semiclassical Hamiltonian transforms to

$$H = \hbar\omega_\sigma \hat{\sigma}^\dagger \hat{\sigma} - \frac{\langle g | \varepsilon \cdot \hat{\mathbf{d}} | e \rangle E_0}{2} (\hat{\sigma} e^{i\omega t} + \hat{\sigma}^\dagger e^{-i\omega t} + \hat{\sigma} e^{-i\omega t} + \hat{\sigma}^\dagger e^{i\omega t}). \quad (2.60)$$

In the Heisenberg picture, the operators $\hat{\sigma}$ have an evolution of the form $\hat{\sigma} e^{-i\omega_\sigma t}$, in accordance to the evolution with the free Hamiltonian $H_0 = \omega_\sigma \hat{\sigma}^\dagger \hat{\sigma}$. This means that in this picture the interaction terms have two exponential functions that oscillate with the detuning $\Delta = \omega - \omega_\sigma$, $e^{\pm i\Delta t}$ and other two that oscillate with the sum of the frequencies, $e^{\pm i(\omega + \omega_\sigma)t}$. Assuming that the transition frequency ω_σ and driving frequency ω is close to resonance, i.e., $|\omega - \omega_\sigma| \ll \omega + \omega_\sigma$, the *rotating wave approximation* (RWA) can be performed, which focus on the slow dynamics brought by the difference in the frequencies. With these remarks, the final Hamiltonian from the semiclassical interaction of light and matter can be written as

$$H = \hbar\omega_\sigma \hat{\sigma}^\dagger \hat{\sigma} + \frac{\hbar\Omega_R}{2} (\hat{\sigma} e^{i\omega t} + \hat{\sigma}^\dagger e^{-i\omega t}), \quad (2.61)$$

where we have introduced the term $\Omega_R = -\langle g | \varepsilon \cdot \hat{\mathbf{d}} | e \rangle E_0 / \hbar$, named the *Rabi frequency*. Assuming a wave function of the form $|\Psi\rangle = c_g |g\rangle + c_e |e\rangle$, the Schrödinger equation for the previous Hamiltonian yields the following set of coupled differential equations

$$\partial_t c_g = -\frac{i\Omega_R}{2} c_e e^{i\omega t} \quad (2.62a)$$

$$\partial_t c_e = -i\omega_\sigma c_e - \frac{i\Omega_R}{2} c_g e^{-i\omega t}. \quad (2.62b)$$

Some solutions to the set of differential equations (2.62) can be seen in Figure (2.5). Panel a. calculates the populations for the ground and excited states, given by $P_\alpha(t) = |c_\alpha(t)|^2$, for the condition where light is resonant with the two level transition. It can be seen that the Rabi frequency sets the period of oscillations from the 2LS population, where some relevant pulses can be seen in dashed lines. For $\Omega_R t = \pi/2$, the so-called $\pi/2$ – pulse it can be seen that the state corresponds to a superposition of ground and excited states, while for a π – pulse all the population resides on the excited state. On panel b. the effect of detuning on the excited state population is analyzed, where it can be seen that detuning gives the known interference pattern that arises from

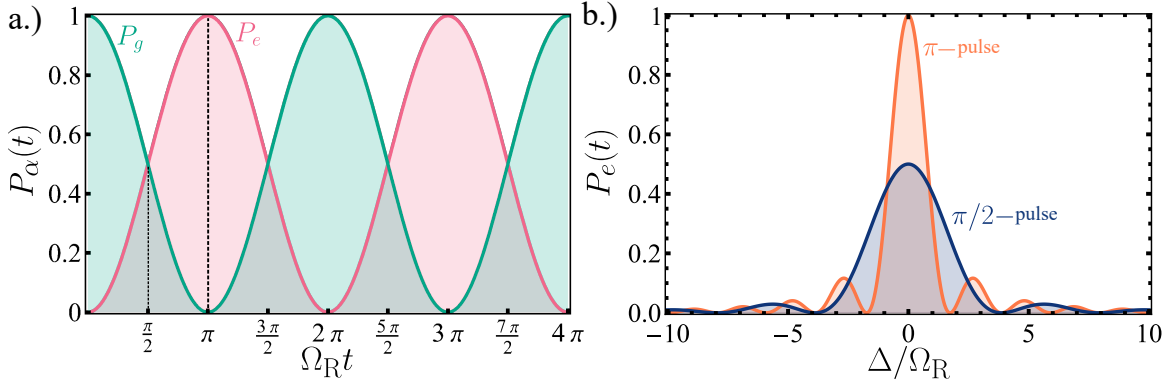


Figure 2.5 Solutions for the semiclassical model of light-matter interaction. a.) Populations $P_\alpha(t) = |c_\alpha(t)|^2$ under resonance condition. The dashed lines denote the $\pi/2$ and π pulses. b.) Excited state population as a function of detuning for $\pi/2$ and π pulses.

the time dependent modulation theory of an atom driven by a harmonic perturbation (e.g., *N.Zettili (2009), pg. 580 [49]*).

2.2.2 Quantization of the Electromagnetic Field

As previously mentioned, quantizing the electromagnetic field was necessary to explain phenomena that were at odds with classical physics, such as the photoelectric effect and the blackbody radiation problem. This process is now a standard topic in quantum mechanics courses and textbooks. Here, an analogous procedure to the one by Scully and Zubairy (*1997, chp. 1 [50]*) will be performed, in order to establish the foundations for a quantum theory of light-matter interaction.

The process starts from the framework on which classical electromagnetism was built: The *Maxwell equations*. They consist of a self-containing set of equations that explain the behavior of electric and magnetic fields. They are given by

$$\begin{aligned}
 \nabla \cdot \mathbf{E} &= \frac{\rho}{\epsilon_0} \\
 \nabla \times \mathbf{E} &= -\frac{\partial \mathbf{B}}{\partial t} \\
 \nabla \cdot \mathbf{B} &= 0 \\
 \nabla \times \mathbf{B} &= \mu_0 \mathbf{J} + \epsilon_0 \mu_0 \frac{\partial \mathbf{E}}{\partial t}.
 \end{aligned} \tag{2.63}$$

The process of quantization begins as follows. First, one must derive a wave equation for the electromagnetic field. This is achieved by taking the curl on Faraday's law,

$$\nabla^2 \mathbf{E} - \mu_0 \epsilon_0 \frac{\partial^2 \mathbf{E}}{\partial t^2} = \frac{\nabla \rho}{\epsilon_0} + \mu \frac{\partial \mathbf{J}}{\partial t}.$$

This last equation is recognized as the wave equation for the electric field \mathbf{E} . If there are no sources, it takes the simpler form $\nabla^2 \mathbf{E} - c^{-2} \partial_t^2 \mathbf{E} = 0$. The next step consists of confining the electromagnetic radiation into a resonating cavity with volume $V = LA$. The electric field \mathbf{E} is taken polarized upon the x-direction and \mathbf{B} upon

the y-direction so that the electromagnetic field is directed into the z-direction. This confinement generates that the electric and magnetic fields can be expanded into the normal mode oscillations of the cavity,

$$E_x(z, t) = \sum_j A_j q_j(t) \sin(k_j z) = \sum_j A_j q_j(t) \sin\left(\frac{j\pi z}{L}\right), \quad (2.64)$$

where $q_j(t)$ refers to the normal mode amplitudes, $A_j = \sqrt{\frac{2v_j^2 m_j}{V\epsilon_0}}$, v_j are the eigenfrequencies of the cavity, and m_j is a constant with the dimensions of mass. The expansion for the magnetic field can be obtained using this expression for $E_x(z, t)$, and making use of Ampère-Maxwell law with no sources, yielding

$$H_y = \sum_j A_j \left(\frac{\dot{q}_j(t) \epsilon_0}{k_j} \right) \cos(k_j z). \quad (2.65)$$

The classical Hamiltonian for the electromagnetic field is $\mathcal{H} = \frac{1}{2} \int_V dv' \left(\epsilon_0 |\vec{E}|^2 + \mu_0 |\vec{H}|^2 \right)$. Replacing the obtained relationships for the electric and magnetic field leads to

$$\begin{aligned} \mathcal{H} &= \frac{1}{2} \int_V dv' \sum_j A_j^2 \{ q_j^2 \epsilon_0 \sin^2(k_j z) + \frac{\dot{q}_j^2 \mu_0 \epsilon_0^2}{k_j^2} \cos^2(k_j z) \} \\ &= \int_V dv' \sum_j \frac{v_j^2 m_j}{V} \{ q_j^2 \sin^2(k_j z) + \frac{\mu_0 \epsilon_0}{k_j^2} \dot{q}_j^2 \cos^2(k_j z) \}. \end{aligned}$$

Since $v_j = k_j c$, then $k_j = v_j / c$, and $\mu_0 \epsilon_0 / k_j^2 = 1 / v_j^2$. The integration is done upon all volume V . Because the variables only depend on z , the surface volume will result in A , and dividing with respect to V simply results in $A/V = 1/L$

$$\begin{aligned} \mathcal{H} &= \frac{1}{L} \left\{ \sum_j m_j v_j^2 q_j^2 \int_0^L \sin^2\left(\frac{j\pi z}{L}\right) dz + m_j \dot{q}_j^2 \int_0^L \cos^2\left(\frac{j\pi z}{L}\right) dz \right\} \\ &= \frac{1}{L} \left\{ \sum_j m_j v_j^2 q_j^2 \frac{L}{4} \left(2 - \frac{\sin(2\pi j)}{\pi j} \right) + m_j \dot{q}_j^2 \frac{L(2\pi j) + \sin(2\pi j)}{4\pi j} \right\}. \end{aligned}$$

Remembering that the sum is made in integer values, then $\sin(2\pi j)$ is always zero, which simplifies to

$$\mathcal{H} = \frac{1}{2} \sum_j m_j v_j^2 q_j^2 + m_j \dot{q}_j^2 = \frac{1}{2} \sum_j \left(m_j v_j^2 q_j^2 + \frac{p_j^2}{m_j} \right).$$

The last equation indicates that each mode of the field is equivalent to an harmonic oscillator. Transforming the generalized coordinates q_j and p_j into operators that satisfy the known rules of commutation $[\hat{q}_j, \hat{p}_k] = i\hbar \delta_{j,k}$ and $[\hat{q}_j, \hat{q}_k] = [\hat{p}_j, \hat{p}_k] = 0$, gives the quantized result of the problem.

Alternatively, one can use another approach to understand the quantized version of the Hamiltonian, by using the creation and annihilation operators for the harmonic oscillator. These set of operators are defined as

$$\hat{a}_j e^{-iv_j t} = \frac{1}{\sqrt{2m_j \hbar v_j}} (m_j v_j \hat{q}_j + i\hat{p}_j) \quad (2.66)$$

$$\hat{a}_j^\dagger e^{iv_j t} = \frac{1}{\sqrt{2m_j \hbar v_j}} (m_j v_j \hat{q}_j - i\hat{p}_j). \quad (2.67)$$

Multiplying the creation and annihilation operators gives

$$\begin{aligned}\hat{a}_j^\dagger \hat{a}_j + \frac{1}{2} &= \frac{1}{2\hbar m_j v_j} (m_j^2 v_j^2 \hat{q}_j^2 + \hat{p}_j^2) \\ \hbar v_j \left(\hat{a}_j^\dagger \hat{a}_j + \frac{1}{2} \right) &= \frac{1}{2} (m_j v_j^2 \hat{q}_j^2 + \hat{p}_j^2).\end{aligned}$$

It has thus been proven that the quantized version of the Hamiltonian can also be written as

$$\mathcal{H} = \sum_j \hbar v_j \left(\hat{a}_j^\dagger \hat{a}_j + \frac{1}{2} \right) \quad (2.68)$$

2.2.3 Quantum theory of light-matter interaction

We will treat the quantum theory of light matter interaction by stating the most simple problem, the interaction of a single cavity mode with a two level system. The Hamiltonian from this interaction is

$$\begin{aligned}H &= \hbar \omega_\sigma \hat{\sigma}^\dagger \hat{\sigma} + \hbar \omega_a (\hat{a}^\dagger \hat{a}) - \hat{\mathbf{d}} \cdot \mathbf{E} \\ H &= H_A + H_F + H_{AF}.\end{aligned} \quad (2.69)$$

The electric field operator of a single mode can be written as

$$\mathbf{E} = -\epsilon \sqrt{\frac{\hbar \omega}{2\epsilon_0 V}} (\hat{a} + \hat{a}^\dagger) \sin kz. \quad (2.70)$$

For the interaction, the same approximation from the semiclassical theory will be applied (The dipole approximation). This means that the Hamiltonian yields

$$H_{AF} = -\epsilon \cdot \mathbf{d}_{ge} \sin kz \sqrt{\frac{\hbar \omega}{2\epsilon_0 V}} (\hat{\sigma} + \hat{\sigma}^\dagger) (\hat{a} + \hat{a}^\dagger) = \hbar g (\hat{\sigma} + \hat{\sigma}^\dagger) (\hat{a} + \hat{a}^\dagger). \quad (2.71)$$

The parameter $g = g_0 \sin kz$, known as the Cavity QED coupling constant, is one of the most important quantities in physics, since different regimes of light matter interaction could be accessed, depending on its value with respect to dissipation rates and natural frequencies of the system. The full quantum Hamiltonian is thus

$$H = \hbar \omega_\sigma \hat{\sigma}^\dagger \hat{\sigma} + \hbar \omega_a \hat{a}^\dagger \hat{a} + \hbar g (\hat{\sigma} \hat{a} + \sigma \hat{a}^\dagger + \hat{\sigma}^\dagger \hat{a} + \hat{\sigma} \hat{a}^\dagger). \quad (2.72)$$

It is referred to as the *Rabi Hamiltonian*. By moving once again into the Heisenberg picture, an analogous result to the one obtained in the semiclassical treatment gives that the interaction term has rapidly and slowly rotating exponentials, with frequencies $(\omega_a + \omega_\sigma)$ and $(\omega_a - \omega_\sigma)$. It is therefore possible to construct a second quantization version of a rotating wave approximation, in which rapidly oscillating terms are neglected, considering near resonance between atomic and light frequencies. Nevertheless, the validity of this approximation is not only related to the near resonance requirement but also must be in agreement with the restriction that the c-QED coupling constant must be much smaller than the frequencies, $g \ll \omega_a, \omega_\sigma$. This constriction can be seen if one performs a time independent perturbation theory for the interaction term, in which only terms of the form $g^2/(\omega_a - \omega_\sigma)$ contribute to the second order corrections to the energy. However, when the ratio $g^2/(\omega_a - \omega_\sigma)$ becomes nearly of the same order, the counter-rotating terms must be taken into account and the

RWA cannot be made.

In the *strong coupling regime* the condition $g \ll \omega_a, \omega_\sigma$ is fulfilled and thus the RWA can be applied. This gives the simpler Hamiltonian,

$$H = \omega_\sigma \hat{\sigma}^\dagger \hat{\sigma} + \omega_a a^\dagger a + g(\hat{a}^\dagger \hat{\sigma} + \hat{a} \hat{\sigma}^\dagger). \quad (2.73)$$

This is the famous *Jaynes-Cummings model* (JC model), first derived by Edwin Jaynes and Frederic Cummings in 1963 [51], and which corresponds to the first solvable model of a quantum picture of light matter interaction (An analytical solution to the complete Rabi Hamiltonian was found by Braak [52] in 2011, but it is considerably more difficult than the ones of the JC model).

The starting point for diagonalizing this Hamiltonian begins by defining the Hilbert space of this system, understood as the outer product of the 2LS states and Fock states, $|\Psi\rangle = |\alpha\rangle \otimes |n\rangle$, where $\alpha = g, e$. Noticing the fact that the interaction term of the JC model yields transitions of the form $|g, n\rangle \longleftrightarrow |e, n-1\rangle$, the Hamiltonian can be written in this basis as

$$H^{(n)} = \begin{pmatrix} n\omega_a & g\sqrt{n} \\ g\sqrt{n} & \omega_\sigma + (n-1)\omega_a \end{pmatrix} m, \quad (2.74)$$

and the corresponding eigenenergies are

$$E_n^{(\pm)} = \frac{\omega_\sigma + (2n-1)\omega_a}{2} \pm \frac{1}{2} \sqrt{4ng^2 + (\omega_a - \omega_\sigma)^2}. \quad (2.75)$$

These results will be substantially used when we present the main results of this thesis in Chapter 3.

2.3 Quantum Correlation Functions

The concept of coherence has an essential role in the field of optics and quantum mechanics. In optics, it is useful in the sense that it helps to indicate the capacity that two waves have to interfere. It, therefore, explains a relationship between these waves and helps to quantify to what extent (of time or space) this relationship remains invariant. From the classical theory of coherence, the standard setup for analyzing the interference properties of a system consists of Young's experiment proposal, where a plane wavefront is interrupted by a barrier containing two slits. From each slit, the new-forming spherical wave propagates until the intensity is detected on a screen. Depending on the correlation properties between the two waves, an interference pattern will be obtained. This can be mathematically expressed as

$$I(r, t) = I_1 + I_2 + 2\sqrt{I_1 I_2} |\gamma_{12}(\tau)| \cos(\alpha_{12} - \varphi), \quad (2.76)$$

where I_i corresponds to the intensity of each light source, $\gamma_{12}(\tau)$ is referred to as the degree of coherence and $\varphi = \frac{2\pi}{\lambda}(r_2 - r_1)$ corresponds to a phase difference arising from the discrepancy in the optical path taken by each front. The degree of coherence is a crucial ingredient that helps to quantify the interference procedure.

This can be seen depending on its value, where the following limits are obtained

$$|\gamma_{12}(\tau)| = \begin{cases} 0, & \text{incoherent limit} \\ 1, & \text{coherent limit.} \end{cases} \quad (2.77)$$

For the in-between case, $0 < |\gamma_{12}| < 1$ the source is referred to as partially coherent.

The case for quantum coherence functions is analogous. The method starts by considering the quantized electromagnetic field and splitting it into its positive and negative frequency components

$$\hat{E}(r, t) = E_0(r)\hat{a}e^{-i\omega t} + E_0(r)\hat{a}^\dagger e^{i\omega t} = \hat{E}^{(+)} + \hat{E}^{(-)}. \quad (2.78)$$

The probability of measuring a photon consists of a detector that absorbs it, and the incident energy is sufficient to eject a photo-electron. Consequently, the term that will contribute to this probability is the one that destroys the photon, $\hat{E}^{(+)}$. This probability is then calculated as

$$P_{fi} = \left| \langle f | \hat{E}^{(+)} | i \rangle \right|^2, \quad (2.79)$$

where $|i\rangle, |f\rangle$ indicates the initial and final states after the absorption procedure. Since one is not interested in the final field, the recorded intensity can be taken by summing up all possible fields

$$I(r, t) = \sum_f P_{fi} = \sum_f \langle i | \hat{E}^{(-)}(r, t) | f \rangle \langle f | \hat{E}^{(+)}(r, t) | i \rangle = \langle i | \hat{E}^{(-)}(r, t) \hat{E}^{(+)}(r, t) | i \rangle.$$

For the general case of a statistical mixture,

$$I(r, t) = \sum_i P_i \langle i | \hat{E}^{(-)}(r, t) \hat{E}^{(+)}(r, t) | i \rangle = \text{Tr} \left\{ \rho \hat{E}^{(-)}(r, t) \hat{E}^{(+)}(r, t) \right\}. \quad (2.80)$$

These intensity relationships will be the basis for calculating the coherence functions. The n order coherence function is

$$G^{(n)}(x_1, x_2, \dots, x_n) = \text{Tr} \left\{ \rho \hat{E}^{(-)}(x_1) \dots \hat{E}^{(-)}(x_n) \hat{E}^{(+)}(x_n) \dots \hat{E}^{(+)}(x_1) \right\}. \quad (2.81)$$

For $n = 1$, this can be expressed only as $G^{(1)}(x_1, x_2) = \text{Tr} \{ \rho \hat{E}^{(-)}(x_1) \hat{E}^{(+)}(x_2) \}$ and is referred as the first order coherence function. The normalized version of this can be written as

$$g^{(1)}(x_1, x_2) = \frac{G^{(1)}(x_1, x_2)}{[G^{(1)}(x_1, x_1) G^{(1)}(x_2, x_2)]^{1/2}}. \quad (2.82)$$

As in the case of classical coherence theory, the first quantum coherence function helps to discern the degree of coherence in a system, establishing the same boundaries as in the stated equation (2.77).

The second-order correlation function is a significant quantity that leads not with amplitudes of fields, but rather with intensities. For this reason, it constitutes a suitable quantity to measure on interferometric setups (Hanbury

Brow-Twiss, for example). It is given by

$$G^{(2)}(x_1, x_2; x_2, x_1) = \text{Tr} \left\{ \rho \hat{E}^{(-)}(x_1) \hat{E}^{(-)}(x_2) \hat{E}^{(+)}(x_2) \hat{E}^{(+)}(x_1) \right\}, \quad (2.83)$$

where once again, the normalized version of this quantity is

$$g^{(2)}(x_1, x_2; x_2, x_1) = \frac{G^{(2)}(x_1, x_2; x_2, x_1)}{[G^{(1)}(x_1, x_1) G^{(1)}(x_2, x_2)]}. \quad (2.84)$$

Expressing it as a quantity that only takes into account the time difference of the detection of a photon, this is given by

$$g^{(1)}(t, \tau) = \frac{\langle \hat{E}^{(-)}(t) \hat{E}^{(+)}(t + \tau) \rangle}{\sqrt{\langle \hat{E}^{(-)}(t) \hat{E}^{(+)}(t) \rangle \langle \hat{E}^{(-)}(t + \tau) \hat{E}^{(+)}(t + \tau) \rangle}}. \quad (2.85)$$

$$g^{(2)}(t, \tau) = \frac{\langle \hat{E}^{(-)}(t) \hat{E}^{(-)}(t + \tau) \hat{E}^{(+)}(t + \tau) \hat{E}^{(+)}(t) \rangle}{\langle \hat{E}^{(-)}(t) \hat{E}^{(+)}(t) \rangle \langle \hat{E}^{(-)}(t + \tau) \hat{E}^{(+)}(t + \tau) \rangle}. \quad (2.86)$$

Finally, considering the quantization of light for a single mode, the last equation takes the form

$$g^{(2)}(t, \tau) = \frac{\langle \hat{a}^\dagger(t) \hat{a}^\dagger(t + \tau) \hat{a}(t + \tau) \hat{a}(t) \rangle}{\langle \hat{a}^\dagger(t) \hat{a}(t) \rangle \langle \hat{a}^\dagger(t + \tau) \hat{a}(t + \tau) \rangle}. \quad (2.87)$$

This expression is one of the most employed quantities in Quantum Optics, giving rise to the study of *photon statistics*. The physical interpretation of this function is that of the detection of photons at a delayed time $t + \tau$, given that others were already detected at the previous time t . This gives the correlations between photons at different times, which is related to the intrinsic structure of the way photons are being emitted.

Some useful inequalities can be established by means of this correlation function. Defining the two-timed intensity correlations as $G^{(2)}(t, t + \tau) = \langle I(t) I(t + \tau) \rangle$, a version of the Cauchy-Schwarz inequality can be written for the classical intensities as

$$|\langle I(t) I(t + \tau) \rangle|^2 \leq \langle I^2(t) \rangle \langle I^2(t + \tau) \rangle. \quad (2.88)$$

It can be re-expressed by means of the second order correlation function as

$$[G^{(2)}(t, t + \tau)] \leq G^{(2)}(t, t) G^{(2)}(t + \tau, t + \tau). \quad (2.89)$$

Using the normalized version of the correlation function, and taking the emission for a steady state field gives

$$g^{(2)}(\tau) \leq g^{(2)}(0). \quad (2.90)$$

This equation is always fulfilled by classical fields. However, quantum fields violate this inequality yielding

$$g^{(2)}(0) < g^{(2)}(\tau). \quad (2.91)$$

This is the famous result of *photon antibunching*, which is a purely quantum mechanical effect that is directly related to the quantized nature of light [12]. The relationships between $g^{(2)}(0)$ and $g^{(2)}(\tau)$ allow the possibility to establish a threefold classification: If $g^{(2)}(0) > g^{(2)}(\tau)$, the emission is called to be *bunched*. If $g^{(2)}(0), g^{(2)}(\tau) = 1$, the emission is said to be uncorrelated. And finally as expressed before, if $g^{(2)}(0) < g^{(2)}(\tau)$ the emission is *antibunched*. An alternative scheme from this same classification is used when the delay time is taken to infinity. For this case, the detection of a photon is completely uncorrelated from another detected at a sufficiently later time, and therefore $\lim_{\tau \rightarrow \infty} g^{(2)}(\tau) = 1$, therefore the classification can also be expressed as follows. $g^{(2)}(0) > 1$ corresponds to bunched light, $g^{(2)}(0) = 1$ represents uncorrelated light, and $g^{(2)}(0) < 1$ is related to antibunched light.

The quantity $g^{(2)}(0)$ is easier to calculate than the two timed expressions given in Equation (2.87), and thus it is a useful result for some particular quantum states. For example, starting for the Fock states, the $g^{(2)}(0)$ yields

$$g_n^{(2)}(0) = \frac{\langle n | \hat{a}^{\dagger 2} \hat{a}^2 | n \rangle}{\langle n | \hat{a}^{\dagger} \hat{a} | n \rangle^2} = \frac{n(n-1)}{n^2} = 1 - \frac{1}{n}. \quad (2.92)$$

This means that when the number in the Fock basis is small, a regime where this quantity is less than one is obtained, which corresponds to quantum behavior. Specifically, when the system has only one photon, the value of this function is zero. Also, it is seen that when n increases, it tends to the uncorrelated limit.

The second useful state to calculate this quantity are the coherent state. Recalling that they are defined as the eigenstates of the annihilation operator (2.13 b), it takes the simple value

$$g_{\alpha}^{(2)}(0) = \frac{\langle \alpha | \hat{a}^{\dagger 2} \hat{a}^2 | \alpha \rangle}{\langle \alpha | \hat{a}^{\dagger} \hat{a} | \alpha \rangle^2} = \frac{|\alpha|^4}{|\alpha|^4} = 1. \quad (2.93)$$

This is a property that is not unique to the second order correlation function. In fact, correlation functions at all orders take the value of 1 for coherent states. For that reason, it is said that they pose an n th-order degree of coherence. This value will represent a limit when classifying the statistical properties of emission of various systems.

Another useful state is the previously studied Squeezed vacuum state defined as $|\xi\rangle = \hat{S}(\xi)|0\rangle$. The second order correlation function can be written as

$$\begin{aligned} g_{\xi}^{(2)}(0) &= \frac{\langle \xi | \hat{a}^{\dagger 2} \hat{a}^2 | \xi \rangle}{\langle \xi | \hat{a}^{\dagger} \hat{a} | \xi \rangle^2} = \frac{\langle 0 | \hat{S}^{\dagger} \hat{a}^{\dagger 2} \hat{a}^2 \hat{S} | 0 \rangle}{\langle 0 | \hat{S}^{\dagger} \hat{a}^{\dagger} \hat{a} \hat{S} | 0 \rangle^2} \\ &= \frac{\langle 0 | \hat{S}^{\dagger} \hat{a}^{\dagger} \hat{S} \hat{S}^{\dagger} \hat{a}^{\dagger} \hat{S} \hat{S}^{\dagger} \hat{a} \hat{S} \hat{S}^{\dagger} \hat{a} \hat{S} | 0 \rangle}{\langle 0 | \hat{S}^{\dagger} \hat{a}^{\dagger} \hat{S} \hat{S}^{\dagger} \hat{a} \hat{S} | 0 \rangle^2} \\ &= \frac{\langle \xi | \hat{a}_{\xi}^{\dagger 2} \hat{a}_{\xi}^2 | \xi \rangle}{\langle \xi | \hat{a}_{\xi}^{\dagger} \hat{a}_{\xi} | \xi \rangle^2}, \end{aligned} \quad (2.94)$$

where we have used the fact that $\hat{S}\hat{S}^{\dagger}$ is a unitary operator, and the expressions for \hat{a}_{ξ}^{\dagger} and \hat{a}_{ξ} previously defined in Equations (2.41). Employing the expectation values defined in Equation (2.42), the second order correlation

function for the squeezed vacuum state is

$$g_{\xi}^{(2)}(0) = 2 + \coth r^2. \quad (2.95)$$

For large values of the squeezing parameter r , the second order correlation function tends to 3, which is an intrinsic characteristic of squeezed vacuum states.

Now another important discussion is the one related to *photon statistics*, which represents the field that studies photon distributions that are generated from photon counting experiments, which indicates that is also bounded to the emission properties of light. Photon statistics arise when a light beam is detected using a device such as a photomultiplier tube. This device then records the detection of a photon by emitting a photoelectron and registering it as a pulse, allowing the construction of a statistical distribution of photon counts.

We have already built some steps for the classification of light by photon statistics. When coherent states were defined, it was found that the probability of finding n photons corresponded to a Poissonian distribution, where the λ parameter corresponds to the average photon number in a coherent state $\bar{n} = |\alpha|^2$. A crucial characteristic for analyzing photon distributions stems from the comparison between the mean and the variance, defined as

$$(\Delta n)^2 = \sum_n (n - \bar{n})^2 P(n) \quad (2.96)$$

The classification of photon statistics is also threefold as before, and is given as follows: *Poissonian statistics* corresponds to distributions where the variance is equal to the mean, $(\Delta n)^2 = \bar{n}$. On the other hand, *Super Poissonian statistics* refers to distributions where the variance is larger than the mean, $(\Delta n)^2 > \bar{n}$. Finally, *Sub Poissonian statistics* are those distributions where the variance is smaller than the mean, $(\Delta n)^2 < \bar{n}$. Super Poissonian light can be found eg. for single mode thermal fields, whose mean photon number is described by the Bose Einstein distribution, $\bar{n} = (\exp\{\hbar\omega/\kappa_B T\})^{-1}$. For those fields, it is found that $(\Delta n)^2 = \bar{n}(\bar{n} + 1)$ is always greater than for the Poisson distribution. On the contrary, Sub Poissonian statistics, which has a narrower distribution than for coherent states, is related to the quantum properties of light.

Photon statistics can be related to the discussion of quantum correlation functions, by writing the zero delay second order correlation function in terms of the variance and the mean as

$$g^{(2)}(0) = 1 + \frac{\langle(\Delta\hat{n})^2\rangle - \langle\hat{n}\rangle}{\langle\hat{n}\rangle^2} \quad (2.97)$$

Although most of the time a Sub Poissonian distribution corresponds to a light source that displays antibunching, it is not always the case. For example, in 1982 Surendra Singh [53] performed experiments of resonance fluorescence, on which light was always antibunched, but may present regimes on which the photon distribution could even correspond to Super Poissonian statistics. The contrary statement, that antibunching necessarily generates Sub Poissonian distributions was also disproved by Zou and Mandel [54]. Therefore, although both classification schemes serve to analyze the quantum properties of light, the correlation between both of them must be treated carefully.

The final discussion for this section corresponds to the experimental realizations that helped to constitute the field of Quantum Optics. It is worth mentioning two seminal experiments: The interferometric setup

established by Hanbury Brown and Twiss [55, 56], and later on, the discovery of antibunching from Resonance Fluorescence by Kimble, Dagenais and Mandel [12].

Robert Hanbury Brown and Richard Twiss were a couple of British astronomers who had an interest in improving the methods for measuring the diameter of stars. At that time, the current method to measure such quantities was made through a Michelson stellar interferometer, which was composed of two mirrors split by a distance d . Each mirror directed the collected light upon a telescope, and if the light exhibited spatial coherence, an interference pattern would form. This method was employed to measure the diameter of Betelgeuse, which was found to be roughly 300 times bigger than the sun, giving rise to the discovery of red giants in astronomy. The big limitation of this setup was that the distance between the mirrors could not be too large, since that would complicate the generation of the interference fringes. To come around this issue, in 1954 Hanbury Brown and Twiss proposed a simpler setup, known as an intensity interferometer. It consisted of two separated detectors separated over a distance d that registered photocurrents which were afterward correlated. They used the intensity interferometer to measure the diameter of the star Sirius. In this context of intensity correlations, the concept of the second order correlation function is introduced naturally and helped to explain the photon bunching results from the HBT experiment, which was understandable from a classical perspective.

The second relevant experiment was the discovery of photon antibunching in Resonance Fluorescence in 1977 by Kimble, Dagenais and Mandel. They used a sodium atomic beam that was excited with a laser that is resonant to the $3^2S_{1/2} F = 2$ and $3^2P_{3/2} F = 3$ transition, which enabled them to describe the sodium atoms as two level systems. Afterward, the light from resonance fluorescence was directed into an HBT interferometer, which consisted of a 50:50 beam and two photomultipliers at the end of each path. The correlations given by $g^{(2)}(\tau)$ exhibited the characteristic dip for $\tau = 0$, which conclusively demonstrated the effect of photon antibunching, thus proving the quantized nature of light.

2.4 Frequency filtered quantum correlation functions

As we have seen until now, quantum correlations are a powerful tool for exploring the inherent properties of certain systems, and specifically, for analyzing the quantum nature of the emission of light and its statistical properties.

A critical concept that arises when measuring such correlation functions is known as *frequency resolved correlation functions*, understood as the correlation between photons of different frequencies. This issue was first presented by Eberly and Wodkiewicz, when they discussed the *time dependent spectrum of light from an observational point of view* and define a *time dependent physical spectrum based on counting rates at a photodetector* [57]. This method deals with the resolution of a number of integrals and time-ordered operations that substantially increase the complexity of the problem as the order of the correlation functions grows.

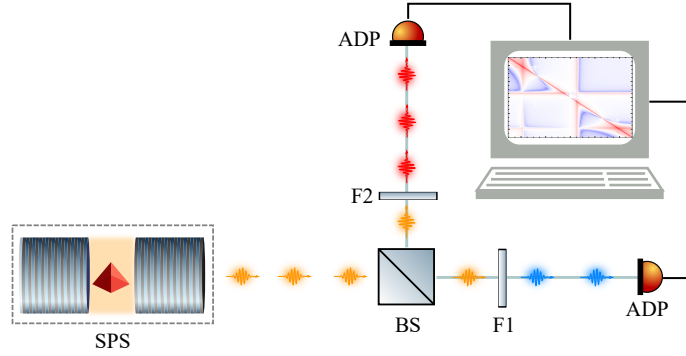


Figure 2.6 Scheme of a Hanbury Brown set up for measuring frequency correlations, by using two filters before the detectors.

However, there are two additional formalisms that allow overcoming this complexity issue, facilitating the calculation of frequency-resolved correlation functions. Each one will be introduced next.

2.4.1 Sensor method

The sensor method was introduced in 2012 by Elena del Valle *et al.* [58] as an alternative to the complex methods previously employed to calculate frequency-resolved correlation functions. It simply consists of analyzing the dynamics of an open quantum system (Q) that is being coupled to external *sensors*. Each sensor

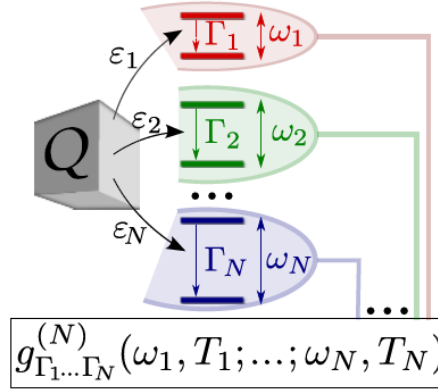


Figure 2.7 Sensor method as proposed by del Valle *et al.* [58], where an open quantum system Q is coupled to N two level systems that act as frequency sensors.

corresponds to a two level system described by an operator $\hat{\xi}_i$, with transition frequency ω_i and linewidth Γ_i . The idea is that these sensors have a vanishing coupling rate ε with the system so that the dynamics of the latter are not affected by the measurement problem. The steps to apply the sensor method will be explained by giving an example where the system consists of the Jaynes-Cummings model, given by Equation (2.73), $H_{JC} = \omega_a \hat{a}^\dagger \hat{a} + \omega_\sigma \hat{\sigma}^\dagger \hat{\sigma} + g(\hat{a}^\dagger \hat{\sigma} + \hat{a} \hat{\sigma}^\dagger)$. The open quantum system formalism takes into account the losses of photons from a cavity (κ_a), the spontaneous emission rate (γ_σ) from the 2LS and also an incoherent driving to

the 2LS (P_σ). Thus, the master equation of the system is

$$\partial_t \rho = i[\rho, H_{JC}] + \frac{\kappa_a}{2} \mathcal{L}_{\hat{a}} \rho + \frac{\gamma_\sigma}{2} \mathcal{L}_{\hat{\sigma}} \rho + \frac{P_\sigma}{2} \mathcal{L}_{\hat{\sigma}^\dagger} \rho. \quad (2.98)$$

The sensor method indicates that the terms of energy of the sensors, as well as the interaction between the sensors and the system, must be added to the Hamiltonian. For simplicity's sake, only two sensors, i.e., two scanning frequencies, will be used. The aforementioned terms are

$$H_{\text{sens}} = \omega_1 \hat{\xi}_1^\dagger \hat{\xi}_1 + \omega_2 \hat{\xi}_2^\dagger \hat{\xi}_2 \quad (2.99a)$$

$$H_{\text{int}} = \varepsilon \left(\hat{a}^\dagger \hat{\xi}_1 + \hat{a} \hat{\xi}_1^\dagger + \hat{a}^\dagger \hat{\xi}_2 + \hat{a} \hat{\xi}_2^\dagger \right) + \varepsilon \left(\hat{\sigma}^\dagger \hat{\xi}_1 + \hat{\sigma} \hat{\xi}_1^\dagger + \hat{\sigma}^\dagger \hat{\xi}_2 + \hat{\sigma} \hat{\xi}_2^\dagger \right) \quad (2.99b)$$

$$H_{\text{total}} = H_{JC} + H_{\text{sens}} + H_{\text{int}}. \quad (2.99c)$$

Adding the sensor dissipative terms $(\Gamma_i/2) \mathcal{L}_{\hat{\xi}_i} \rho$, gives the final version of the master equation of interest

$$\partial_t \rho = i[\rho, H_{\text{total}}] + \frac{\kappa_a}{2} \mathcal{L}_{\hat{a}} \rho + \frac{\gamma_\sigma}{2} \mathcal{L}_{\hat{\sigma}} \rho + \frac{P_\sigma}{2} \mathcal{L}_{\hat{\sigma}^\dagger} \rho + \frac{\Gamma}{2} \left(\mathcal{L}_{\hat{\xi}_1} \rho + \mathcal{L}_{\hat{\xi}_2} \rho \right). \quad (2.100)$$

The interest will be put in solving this ME for the steady state and finding the second order frequency filtered correlation function, which can be found as

$$g_\Gamma^{(2)}(\omega_1, \omega_2) = \lim_{\varepsilon \rightarrow 0} \frac{\langle \hat{\xi}_1^\dagger \hat{\xi}_2^\dagger \hat{\xi}_2 \hat{\xi}_1 \rangle}{\langle \hat{\xi}_1^\dagger \hat{\xi}_1 \rangle \langle \hat{\xi}_2^\dagger \hat{\xi}_2 \rangle}. \quad (2.101)$$

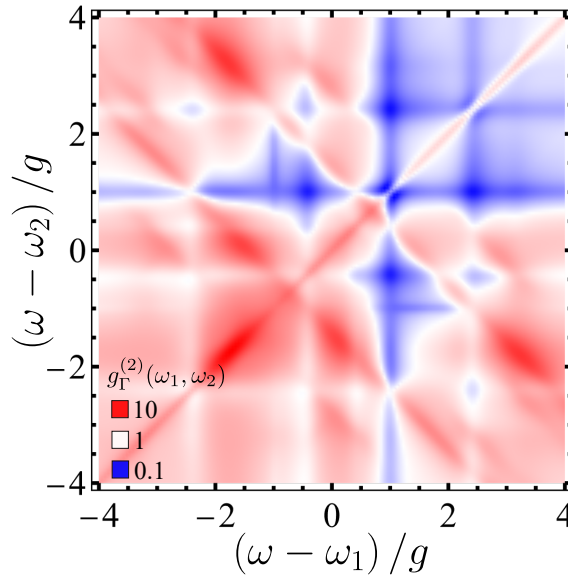


Figure 2.8 Example of the sensor method for the incoherently driven Jaynes Cummings model. *Parameters:* $\kappa_a = 0.1g$, $\gamma_\sigma = 0.001g$, $P_\sigma = 0.5g$, $\Gamma = 0.1g$.

Figure (2.8) shows the results for the frequency-filtered correlation function of the incoherently driven Jaynes Cummings model, displaying all types of photon statistics: bunching, coherent (uncorrelated), and

antibunching. Furthermore, a grid of horizontal and vertical lines can be clearly seen. This corresponds to the correlation between real states, while the diagonal lines correspond to the *leapfrog* processes, where photons are used to jump over lower manifolds. This was first identified in the work of Gonzalez Tudela *et al.* [59]. There, they explore the filtered correlations of numerous amount of systems.

Finally, the general statement of the problem for a set of system operators \hat{O}_s , and k-sensors $\hat{\xi}_k$, is given by the following master equation,

$$\partial_t \rho = i[\rho, H_s + H_\xi + H_{\xi_s}] + \frac{1}{2} \sum_s \gamma_s \mathcal{L}_{\hat{O}_s} \rho + \frac{1}{2} \sum_k \Gamma_k \mathcal{L}_{\hat{\xi}_k} \rho \quad (2.102a)$$

$$H_\xi = \sum_k \omega_k \hat{\xi}^\dagger \hat{\xi} \quad (2.102b)$$

$$H_{\xi_s} = \sum_{k,s} \varepsilon \left(\hat{O}_s^\dagger \hat{\xi}_k + \hat{O}_s \hat{\xi}_k^\dagger \right). \quad (2.102c)$$

2.4.2 Cascaded formalism

The second method for calculating frequency correlation functions is the so-called *Cascaded formalism*, which was introduced by Carmichael and Gardiner, becoming nowadays a subject of textbook material for quantum optic courses. This method consists of using the output of a quantum system, the *source*, as the means of excitation of another quantum system, the *target*, with the requirement that there is no backaction excitation from the target to the source, establishing, therefore, a unidirectional means of excitation.

The mechanism to achieve this type of excitation is derived by the application of the input-output formalism, which resides on expressing the quantum Langevin equation for the source and target operators and then connecting the output from the first quantum system as the output of the second one.

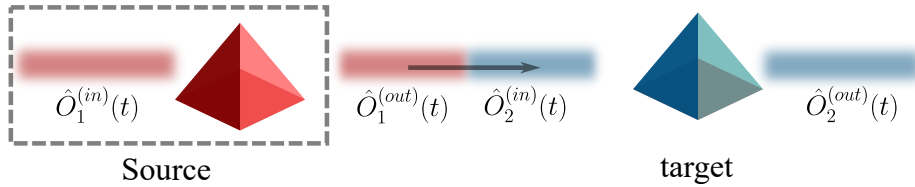


Figure 2.9 Schematics of the cascaded coupling based on the input-output formalism.

The dynamics of this treatment can be described by the following master equation,

$$\partial_t \rho = i[\rho, H_s + H_d] + \frac{1}{2} \sum_s \gamma_s \mathcal{L}_{\hat{a}_s} \rho + \frac{1}{2} \sum_k \Gamma_k \mathcal{L}_{\hat{o}_k} \rho + \sum_{ks} \sqrt{\chi_k \gamma_k \Gamma_k} \left\{ [\hat{a}_s \rho, \hat{o}_k^\dagger] + [\hat{o}_k, \rho \hat{a}_s] \right\}, \quad (2.103)$$

where H_s is the source Hamiltonian with operators \hat{a}_s and $H_d = \sum_k \omega_k \hat{o}_k^\dagger \hat{o}_k$. It is noticeable that this form of a master equation does not correspond to a Lindblad type, i.e., it can be written as $\partial_t \rho = \mathcal{L} \rho$. Nevertheless, it is possible to convert it to a Lindblad form master equation by employing a set of jump operators defined as

$$\hat{O}_k = \sqrt{\lambda_k \gamma_s} \hat{s} + \sqrt{(1 - \kappa_k) \Gamma_k} \hat{o}_k. \quad (2.104)$$

Proper selection of the rates λ_k, κ_k lead to a Lindblad equation that is equivalent to the one shown in (2.103). Using this formalism, the opportunities for studying the effect of exciting targets with quantum sources of light are possible. For this particular subject, the interested reader may refer to the excellent Ph.D. dissertation by Lopez Carreño [60], whose main topic was on exciting a plethora of quantum systems with quantum light, and exploring the consequences and differences from classical (laser) excitation.

Case of study: Mollow triplet in Resonance Fluorescence

We will provide an application of the cascaded formalism, namely, studying how the perfect antibunching from a two level system can produce a whole richness of photon correlations, once frequency measurements are involved. The model for the source simply corresponds to a coherently driven two level system,

$$H_\sigma = \tilde{\omega}_\sigma \hat{\sigma}^\dagger \hat{\sigma} + \Omega(\sigma + \sigma^\dagger) \quad (2.105a)$$

$$\partial_t \rho = i[\rho, H_\sigma] + \frac{\gamma_\sigma}{2} \mathcal{L}_{\hat{\sigma}} \rho, \quad (2.105b)$$

where $\tilde{\omega}_\sigma = \omega_\sigma - \omega_l$ is the rotating frame frequency. Using the 2LS system basis, this equation can be expressed in matrix form as $\partial_t \{\rho\} = -\mathbf{M}\{\rho\}$, with $\{\rho\} = (\rho_{gg}, \rho_{ge}, \rho_{eg}, \rho_{ee})^T$ and

$$\mathbf{M} = \begin{pmatrix} 0 & -i\Omega & i\Omega & -\gamma_\sigma \\ -i\Omega & \gamma_\sigma/2 - i\tilde{\omega}_\sigma & 0 & i\Omega \\ i\Omega & 0 & \gamma_\sigma/2 + i\tilde{\omega}_\sigma & -i\Omega \\ 0 & i\Omega & -i\Omega & \gamma_\sigma \end{pmatrix}. \quad (2.106)$$

The structure of the eigenvalues (D_p) of the Liouvillian matrix \mathbf{M} gives information about the energy regime of the system. The imaginary part of D_p indicate the energies of the transitions, while the real part is related to the broadening. A particularity of this system is that depending on the ratio Ω/γ_σ it is possible to access two different regimes: The low excitation regime, also known as *Heitler regime*, is achieved when $\Omega \ll \gamma_\sigma$. On the other hand, the *Mollow regime* is obtained when $\Omega \gg \gamma_\sigma$. For the present case of study, we will focus on the Mollow regime, whose principal characteristic is the appearance of side bands on the spectrum of emission, known as the *Mollow triplet*. The reason for referring to a triplet is that when the strong driving condition is fulfilled, the spectrum of the emission of the two level system transforms from a Lorentzian into a central peak and two *sidebands*. The most direct interpretation of this spectrum comes as a result of the study of the dressed stated formalism of semiclassical interaction of light and matter, giving rise to a manifold ladder that consists of states $\{|-\rangle, |+\rangle\}$, separated by the Rabi frequency, while subsequent manifolds are split with the incident driving frequency ω_l . With that picture in mind, the central peak arises from transitions of subsequent manifolds that do not change the state, i.e., $|\pm\rangle \rightarrow |\pm\rangle$, while sidebands correspond to transitions of the form $|\pm\rangle \rightarrow |\mp\rangle$, and are shifted in energy $\pm\Omega$ from the central peak. With this framework, it is easier to understand the following results from the cascaded formalism, which we now introduce.

Since we are interested on measuring correlations to the second order, the source will require to excite two targets. Thus, the master equation that needs to be solved is

$$\begin{aligned} \partial_t \rho = & i[\rho, H_\sigma + H_a + H_b] + \frac{\gamma_\sigma}{2} \mathcal{L}_{\hat{\sigma}} \rho + \frac{\Gamma}{2} (\mathcal{L}_{\hat{a}} \rho + \mathcal{L}_{\hat{b}} \rho) \\ & - \sqrt{\Gamma\gamma_\sigma/2} ([\hat{a}^\dagger, \hat{\sigma} \rho] + [\rho \hat{\sigma}^\dagger, \hat{a}]) - \sqrt{\Gamma\gamma_\sigma/2} ([\hat{b}^\dagger, \hat{\sigma} \rho] + [\rho \hat{\sigma}^\dagger, \hat{b}]). \end{aligned} \quad (2.107)$$

Furthermore, we will complement the study of the frequency resolved photon correlations with the *quantumness* of this system, calculated as the rate of violation of the Cauchy-Schwarz inequality (CSI) for the correlation functions. Introducing the quantity $g_{ab}^{(2)} = \langle \hat{a}^\dagger \hat{b}^\dagger \hat{b} \hat{a} \rangle / \langle \hat{a}^\dagger \hat{a} \rangle \langle \hat{b}^\dagger \hat{b} \rangle$, the CSI inequality is,

$$\left[g_{ab}^{(2)} \right]^2 \leq g_{aa}^{(2)} g_{bb}^{(2)} \quad (2.108a)$$

$$R = \left[g_{ab}^{(2)} \right]^2 / (g_{aa}^{(2)} g_{bb}^{(2)}) \leq 1. \quad (2.108b)$$

Thus, quantumness in the Mollow triplet is exhibited when $R > 1$.

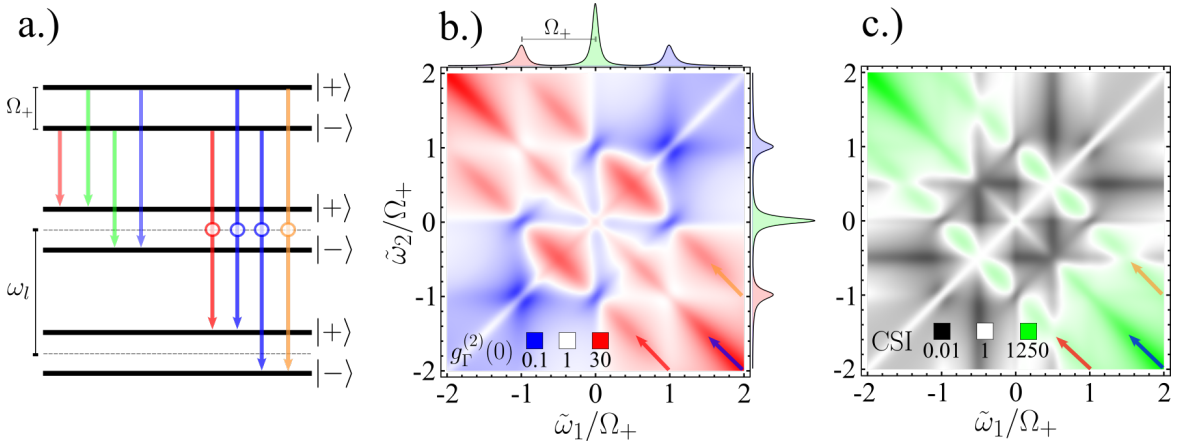


Figure 2.10 **a.)** Transitions of the Two level system in the Mollow triplet. The states $|\pm\rangle$ correspond to the dressed states. **b.)** Second order correlation function. **c.)** Violation of the Cauchy-Schwarz inequality. Parameters: $\Omega = 5\gamma_\sigma$, $\Gamma = 5\gamma_\sigma$, $\tilde{\omega}_\sigma = 0$.

The results of this system are summarized on Figure (2.10). The first panel illustrates the aforementioned dressed basis of the ladder. The transitions on the left side correspond to the ones that explain the appearance of the sidebands in the spectrum. On the other hand, other noteworthy transitions are sketched on the right of this panel, corresponding to the *Leapfrog processes* which consists of transitions from real states jumping over n manifolds, and thus involving the emission of the same number of photons. For this scheme, three possible leapfrogs can happen: $\tilde{\omega}_a + \tilde{\omega}_b = 0$, $\tilde{\omega}_a + \tilde{\omega}_b = \Omega_+$ and $\tilde{\omega}_a + \tilde{\omega}_b = -\Omega_+$. Panel b. indicates that these processes correspond to bunching behavior in the correlation functions, while correlations from the same sidebands result in an antibunched effect. Complementarily, panel c. proves that leapfrogs are accompanied by a violation of the CSI. For more in-depth theoretical discussions of these effects, the following papers are recommended [61, 59, 62].

2.4.3 Experimental measurement of frequency filtered correlations

One noteworthy example of an experimental scheme that measures the aforementioned correlation functions and Cauchy-Schwarz inequality in the Mollow triplet, was performed by Peiris *et al.* [63] in 2015.

The sample consisted of an InAs quantum dot that was grown by molecular beam epitaxy, and subject to a tunable CW laser, which leads to the Mollow spectrum of emission. The HBT setup resembles the simplified version sketched in Figure (2.6), where two tunable filters are placed before the detectors. With their

scheme, they were able to reconstruct the types of maps shown in Figure (2.10). The method they employed to reconstruct such maps was to record coincidences for each pair of filter frequencies $(\tilde{\omega}_1, \tilde{\omega}_2)$, with a fixed recording time of 165s, which corresponded to a total exposure time of 42h for each map.

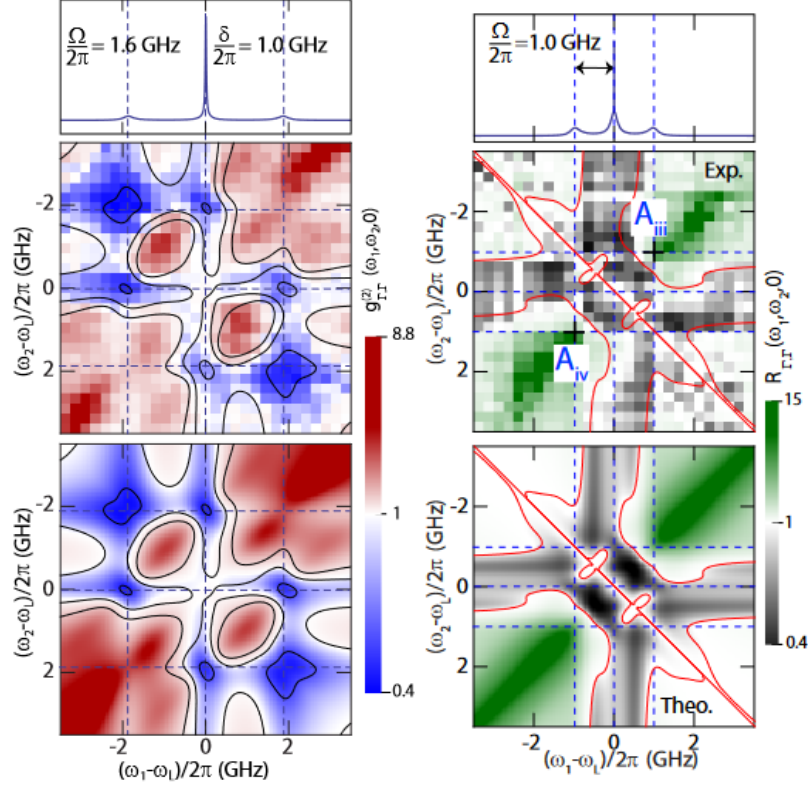


Figure 2.11 Results from experimental measurements of the frequency filtered correlations in the Mollow triplet by Peiris *et al.* [63].

The previous Figure shows the results for the second order correlation function and CSI for the Mollow triplet, comparing both the theoretical prediction with the experimental results, demonstrating the feasibility of frequency-filtered measurements.

The formalism will be applied when we return to the problem of finding differences or similarities between the conventional and unconventional photon blockade effects.

2.5 Interference of quantum states

The main idea of this section is to understand what happens when quantum states interfere with other components, whether their nature is also quantum mechanical or if they are classical contributions, and to exhibit the relationship of this interference with the tuning of photon statistics with many systems in quantum optics, as proposed by Zubizarrieta *et al.* [10]. We will thus derive the steps to formalize his calculations, which will be a crucial feature for explaining the phenomena of photon blockade in the following chapter.

In order to explore this interference, a simple setup that consists of two incident channels that are mixed

by means of a beam splitter will be used. Afterward, the correlation functions of the output beams will be analyzed.

A general formulation of this interaction can be represented as follows:

$$\begin{pmatrix} \hat{o} \\ \hat{s} \end{pmatrix} = \begin{pmatrix} iR & Td \\ T & iR \end{pmatrix} \begin{pmatrix} \hat{d} \\ \hat{a} \end{pmatrix}, \quad (2.109)$$

where \hat{a}, \hat{d} are the incident fields, R, T are the beam splitter reflection and transmission coefficients, and \hat{o}, \hat{s} correspond to the resultant fields. With this transformation, one can analyze correlations of the type $\langle \hat{s}^{\dagger n} \hat{s}^m \rangle$:

$$\langle \hat{s}^{\dagger n} \hat{s}^m \rangle = \left\langle (T\hat{d}^{\dagger} - iR\hat{a}^{\dagger})^n (T\hat{d} + iR\hat{a})^m \right\rangle. \quad (2.110)$$

By applying the Binomial theorem, the term in the parenthesis can be expanded as

$$(a + b)^n = \sum_{k=0}^n \frac{n!}{(n-k)!k!} a^{n-k} b^k \quad (2.111)$$

$$\hat{s}^{\dagger n} = (T\hat{d}^{\dagger} - iR\hat{a}^{\dagger})^n = \sum_{p=0}^n \binom{n}{p} (T\hat{d}^{\dagger})^{(n-p)} (-i)^p (R\hat{a}^{\dagger})^p \quad (2.112)$$

$$\hat{s}^m = (T\hat{d} + iR\hat{a})^m = \sum_{q=0}^m \binom{m}{q} (T\hat{d})^{(m-q)} (i)^q (R\hat{a})^q. \quad (2.113)$$

With these expressions, it is possible to find the term of the correlations according to the incident operators and the components that define the beam splitter:

$$\langle \hat{s}^{\dagger n} \hat{s}^m \rangle = \sum_{p=0}^n \sum_{q=0}^m \binom{n}{p} \binom{m}{q} \left\langle T^{(n-p)} \hat{d}^{\dagger(n-p)} (-i)^p T^p \hat{a}^{\dagger p} T^{(m-q)} \hat{d}^{(m-q)} (i)^q R^q \hat{a}^q \right\rangle \quad (2.114)$$

$$= \sum_{p=0}^n \sum_{q=0}^m \binom{n}{p} \binom{m}{q} \textcolor{red}{T}^{(n-p+m-q)} \textcolor{red}{R}^{(p+q)} (-i)^p (i)^q \left\langle \hat{d}^{\dagger(n-p)} \hat{a}^{\dagger p} \hat{d}^{(m-q)} \hat{a}^q \right\rangle. \quad (2.115)$$

The terms in red only define some normalization factors, so they can be momentarily neglected to focus on the overall result. The problem can be simplified by considering that the incident fields have no correlations between them. This means that the term that has the product of four operators can be split into two terms that measure the respective correlations of each operator

$$\langle \hat{s}^{\dagger n} \hat{s}^m \rangle = \sum_{p=0}^n \sum_{q=0}^m \binom{n}{p} \binom{m}{q} \left\langle \hat{d}^{\dagger(n-p)} \hat{d}^{(m-q)} \right\rangle \left\langle \hat{a}^{\dagger p} \hat{a}^q \right\rangle. \quad (2.116)$$

Equation (2.116) will be the starting point to analyze some specific cases of interference.

2.5.1 Interference of a classical source and a quantum source

In the specific case that \hat{d} is a quantum operator, but \hat{a} is a classical (in general complex) component, then the expression (2.116) simplifies into:

$$\langle \hat{s}^{\dagger n} \hat{s}^m \rangle = \sum_{p=0}^n \sum_{q=0}^m \binom{n}{p} \binom{m}{q} \alpha^{*p} \alpha^q \langle \hat{d}^{\dagger(n-p)} \hat{d}^{(m-q)} \rangle, \quad (2.117)$$

where $\alpha = \langle a \rangle$. Let's start by evaluating different values of n, m to observe what is the result of their correlations.

Case $n, m = 1$

The result for the simplest case, where both n, m are equal to 1 is

$$\begin{aligned} \langle \hat{s}^{\dagger} \hat{s} \rangle &= \sum_{p=0}^1 \sum_{q=0}^1 \binom{1}{p} \binom{1}{q} \alpha^{*p} \alpha^q \langle \hat{d}^{\dagger(1-p)} \hat{d}^{(1-q)} \rangle \\ &= \langle \hat{d}^{\dagger} \hat{d} \rangle + \alpha \langle \hat{d}^{\dagger} \rangle + \alpha^* \langle \hat{d} \rangle + |\alpha|^2 \\ \langle \hat{n}_s \rangle &= |\alpha|^2 + \langle \hat{n}_d \rangle + 2 \operatorname{Re} \{ \alpha^* \langle \hat{d} \rangle \}. \end{aligned} \quad (2.118)$$

This expression is reminiscent of the well-known result in both optics and mechanical physics, obtained through the phenomenon of interference. Indeed, the first two terms resemble the intensities of the incident waves, while the latter reflects the interference component between the waves.

Case $n, m = 2$

For the second order, the correlations yield,

$$\begin{aligned} \langle \hat{s}^{\dagger 2} \hat{s}^2 \rangle &= \sum_{p=0}^2 \sum_{q=0}^2 \binom{2}{p} \binom{2}{q} \alpha^{*p} \alpha^q \langle \hat{d}^{\dagger(2-p)} \hat{d}^{(2-q)} \rangle \\ &= \langle \hat{d}^{\dagger 2} \hat{d}^2 \rangle + 2\alpha \langle \hat{d}^{\dagger 2} \hat{d} \rangle + \alpha^2 \langle \hat{d}^{\dagger 2} \rangle + 2\alpha^* \langle \hat{d}^{\dagger} \hat{d}^2 \rangle + 4|\alpha|^2 \langle \hat{d}^{\dagger} \hat{d} \rangle \\ &\quad + 2\alpha |\alpha|^2 \langle \hat{d}^{\dagger} \rangle + \alpha^{*2} \langle \hat{d}^2 \rangle + 2\alpha^* |\alpha|^2 \langle \hat{d} \rangle + |\alpha|^4. \end{aligned} \quad (2.119)$$

This result itself is not very elucidating with respect to the physics it describes. However, by using the expression for the $n, m = 1$ case, a normalized version of a second-order correlation function can be obtained:

$$g_s^{(2)} = \frac{\langle \hat{s}^{\dagger 2} \hat{s}^2 \rangle}{\langle \hat{s}^{\dagger} \hat{s} \rangle^2} = \frac{\langle \hat{s}^{\dagger 2} \hat{s}^2 \rangle}{\langle \hat{n}_s \rangle^2}. \quad (2.120)$$

In this way, with the normalization to the “average number of photons” $\langle \hat{n}_s \rangle$, a result grouped in orders proportional to the classic component α can be uncovered:

$$\begin{aligned} g_s^2 &= 1 + \left(\frac{\langle \hat{d}^{\dagger 2} \hat{d}^2 \rangle - \langle \hat{d}^{\dagger} \hat{d} \rangle^2}{\langle \hat{n}_s \rangle^2} \right) + \left(\frac{4 \operatorname{Re} \{ \alpha^* (\langle \hat{d}^{\dagger} \hat{d}^2 \rangle - \langle \hat{d}^{\dagger} \hat{d} \rangle \langle \hat{d} \rangle) \}}{\langle \hat{n}_s \rangle^2} \right) \\ &\quad + 2 \left(\frac{\operatorname{Re} \{ \alpha^{*2} \langle \hat{d}^2 \rangle \} + |\alpha|^2 \langle \hat{d}^{\dagger} \hat{d} \rangle - 2 \operatorname{Re} \{ \alpha^* \langle \hat{d} \rangle \}^2}{\langle \hat{n}_s \rangle^2} \right). \end{aligned} \quad (2.121)$$

$$g_s^2 = 1 + I_0 + I_1 + I_2. \quad (2.122)$$

Equation (2.122) indicates that correlation statistics are given as a product of contributions of coherent signals, denoted by the value of 1, and incoherent parts described by the I_k factors. Depending on how much each factor weighs, the system statistics will change notably, obtaining values for purely quantum fields, coherent sources, or even thermal fields. Although it is generally difficult to describe which physics holds each I_k term, some things can be said about them.

The component I_0 indicates the statistics of the quantum part of the mixture. The reason for this is that its numerator corresponds to the variance of the operator \hat{d} , which serves to classify the nature of the distribution (Sub-Poissonian, Poissonian, Super-Poissonian). The negativity of this contribution indicates that a Sub-Poissonian statistic is being accessed, i.e., when $\langle \hat{d}^{\dagger 2} \hat{d}^2 \rangle < \langle \hat{d}^{\dagger} \hat{d} \rangle^2$. For values where I_0 has a dominant value, the resulting statistics will surely correspond to quantum states. On the contrary, the I_1 factor is not as straightforward to physically understand, since it relates the correlations between the intensity and the fluctuations of the field. This effect represents something anomalous that not all states present, however, a *squeezed coherent* state presents these types of correlations. Finally, the component of the numerator I_2 is related to *squeezing*, because its numerator can be rewritten in terms of quadratures of the operator \hat{d} , so it indicates the variance of the quadratures of the field. The fact that $I_2 < 0$ proves that there is a light squeezing component involved in the photon statistics.

A fundamental case that of the coherent decomposition (2.122) results when the same system provides both the coherent and the quantum contribution to the interference, an effect known as self-homodyning. This means that the quantum operator \hat{s} can be described as a superposition of its mean field (coherent contribution) and its fluctuations (quantum contribution)

$$\hat{s} = \langle s \rangle + \hat{d}, \text{ where } \hat{d} = \hat{s} - \langle s \rangle. \quad (2.123)$$

Obviously, by construction, the quantum operator \hat{d} has no mean-field, ($\langle \hat{d} \rangle = 0$) which greatly reduces the terms of the Equation. (2.122). This can be done by replacing $\alpha \rightarrow \langle s \rangle$ and $\hat{d} \rightarrow \hat{s} - \langle s \rangle$, which results as the followings expressions for the decomposition I_k in terms of the system operator \hat{s}

$$\begin{aligned} I_0 &= \frac{\langle s^{\dagger 2} s^2 \rangle - \langle s^{\dagger} s \rangle^2 - 4|\langle s \rangle|^4 + 6|\langle s \rangle|^2 \langle s^{\dagger} s \rangle + 2\text{Re} \{ \langle s^{\dagger} \rangle^2 \langle s^2 \rangle - 2\langle s^{\dagger} \rangle \langle s^{\dagger} s^2 \rangle \}}{\langle s^{\dagger} s \rangle^2} \\ I_1 &= 4 \frac{\text{Re} [\langle s^{\dagger} \rangle \langle s^{\dagger} s^2 \rangle - \langle s^{\dagger} \rangle^2 \langle s^2 \rangle] + 2|\langle s \rangle|^2 (|\langle s \rangle|^2 - \langle s^{\dagger} s \rangle)}{\langle s^{\dagger} s \rangle^2} \\ I_2 &= 2 \frac{\text{Re} [\langle s^{\dagger} \rangle^2 \langle s^2 \rangle] + |\langle s \rangle|^2 \langle s^{\dagger} s \rangle - 2|\langle s \rangle|^4}{\langle s^{\dagger} s \rangle^2}. \end{aligned} \quad (2.124)$$

The previous set of equations will be crucial for analyzing the second order correlation of any system operator \hat{s} . I will therefore appeal to Equation. (2.124) repeatedly in subsequent sections.

2.6 Theoretical criteria for single photon sources

In order to be able to study how well a system behaves as a single photon source, some criteria have to be evaluated as a function of relevant parameters. Typically, the single photon nature of a system is based on the measurement of the second order correlation function, where coincidences of the emission are measured as a function of the delay τ , normally by means of a Hanbury Brown - Twiss setup [56]. A dip in the count histogram when the delay time equals zero means that coincidences at the two detectors have not been registered and thus, single photon emission can be confirmed. Furthermore, another important characteristic that the SPS must sustain is that the emitted photons must be indistinguishable, which is evaluated through a Hong Ou Mandel setup [36].

The fundamental classification criteria changed later on, from not on identifying photon antibunching, given by $g^{(2)}(0) < g^{(2)}(\tau)$, but also on finding subpoissonian fluctuations in the field, which are characterized by $g^{(2)}(0) < 1$. The theoretical goal was therefore to obtain $g^{(2)}(0) = 0$, which is the result for the Fock $|1\rangle$ state photon ($g_n^{(2)}(0) = 1 - 1/n$). For this reason, the main focus for the classification of a system as a plausible single photon source was made through the minimization of the $g^{(0)}(0)$, although never reaching zero.

A true photon source is defined by the cancellation of multiphoton events, holding only one excitation at a time. However, since the current classification schemes only rely on the measurements up to the second order, this does not constitute a suitable element for examining the single photon emission of a system. This is the main justification that Lopez Carreño *et al.* exploit in their work [64] for finding an adequate substitute that classifies systems as single photon sources. As an example of the previous statement about the suppression of the correlation functions, they came up with a state that has an arbitrarily low $g^{(2)}(0)$ (but nonzero), and high $g^{(n)}(0)$ for $n > 2$.

$$\begin{aligned} \rho &= \alpha |0\rangle\langle 0| + \beta |1\rangle\langle 1| + \gamma |3\rangle\langle 3|, \alpha = \frac{297001}{300000}, \beta = \frac{1999}{200000}, \gamma = \frac{1}{600000} \\ \langle \hat{a}^\dagger \hat{a} \rangle &= \text{Tr}[\rho \hat{a}^\dagger \hat{a}] = \sum_n n \langle n | \rho | n \rangle = \beta + 3\gamma \\ g^{(2)}(0) &= \frac{\langle \hat{a}^{\dagger 2} \hat{a}^2 \rangle}{\langle \hat{a}^\dagger \hat{a} \rangle^2} = \frac{6\gamma}{(\beta + 3\gamma)^2} = \frac{1}{10} \\ g^{(3)}(0) &= \frac{\langle \hat{a}^{\dagger 3} \hat{a}^3 \rangle}{\langle \hat{a}^\dagger \hat{a} \rangle^3} = \frac{6\gamma}{(\beta + 3\gamma)^3} = 10. \end{aligned}$$

This example helps to illustrate that $g^{(2)}(0) \rightarrow 0$ is a necessary but not sufficient requirement to classify a system as a source of single photons. To avoid this issue, we propose employing an alternative method. The idea behind this is to simply compute higher-order correlation functions, in a way that the behavior of a source is not restricted to two photon coincidences, but rather, to map the whole statistical dependence of the system. Afterward, it only takes a simultaneous minimization process, such as the least square method, or more refined tools such as multi-objective optimization algorithms, to find the set of parameters that provide the best joint antibunched behavior.

Regarding the experimental proposal for this criterion which relies on the measurement of higher-order correlation functions, Figure (2.12) presents a mock-up scheme and an actually employed setup for such a task. In the Top row of this figure, it is shown a draft of a possible extension of a Hanbury Brown Twiss setup,

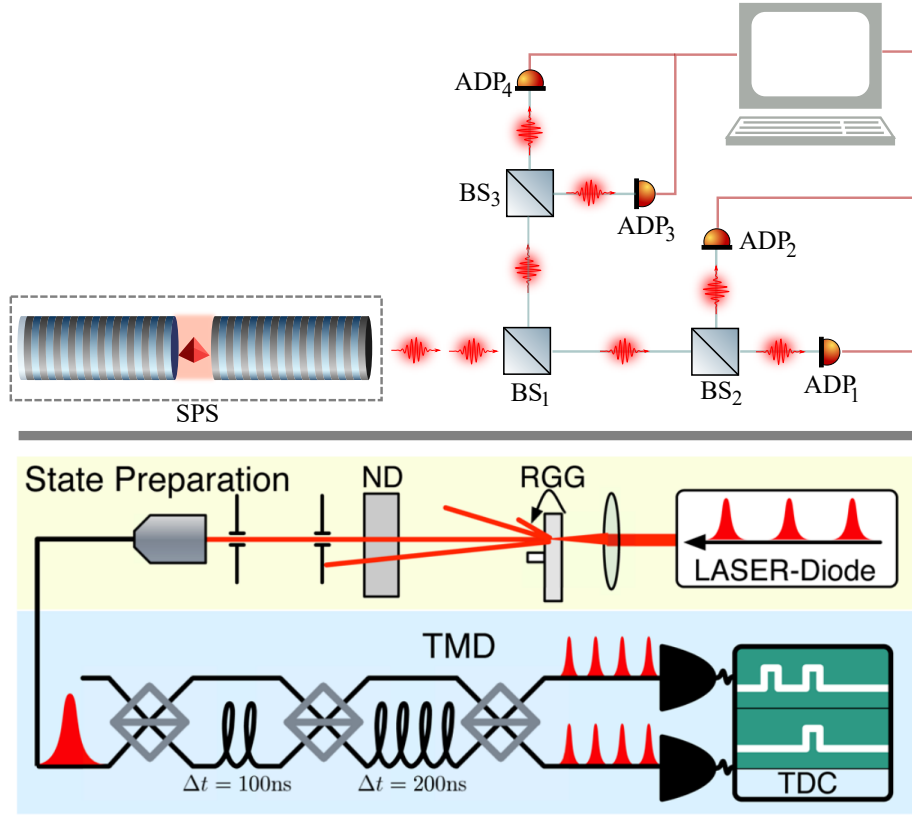


Figure 2.12 Experimental setups for measuring higher-order correlation functions. **(Top row)** Sketch of a possible extension of a Hanbury Brown Twiss setup for measuring higher order correlation functions up to $g^{(4)}(0)$. **(Bottom row)** Experimental scheme from Avenhaus *et al.* for measuring $g^{(n)}$ for coherent and chaotic states by employing Time Multiplexing Detectors (TMD)[65].

on which it is possible to find coincidences in up to four detectors, meaning that it is possible to calculate $g^{(2)}$, $g^{(3)}$ and $g^{(4)}$. The consequence of adding more detectors would be of extending the experimental process in order to obtain a relevant amount of coincidences. On the other hand, the bottom row shows the scheme used by Avenhaus *et al.* [65] for measuring higher order correlation functions of coherent and chaotic states, by employing *Time Multiplexing Detectors* (TMD) [66]. With their techniques, they were able to measure correlation functions up to the eighth order, founding an excellent agreement for the theory and experiment of the measurement of coherent states (error of 0.01% for $g^{(4)}$) and chaotic thermal states (error of 2.3% for $g^{(4)}$).

Results

In this chapter, we provide the main results regarding the analysis of the quantumness of photon blockade.

First, we derive the analytical and numerical solutions for the models associated with the Unconventional Blockade effect (3.1), specifically, finding optimal conditions for the *two interacting cavities model* in order to correctly obtain single photon emission by means of the higher order minimization criteria mentioned in section (2.6). We also compare some modifications made to the original model by Liew and Savona, to clarify if they improve the single photon criteria.

Afterward, we deal with the problem of simultaneous photon blockade. For that reason, we analyze the *driven dissipative Jaynes Cummings model*. We provide the analytical conditions for obtaining CPB and UPB in such a system, analyzing the result of different contributions, such as an admixing of the coherent drives to the cavity and QD. We discuss feasible experimental schemes and intrinsic differences between the two blockade mechanisms that arise when frequency filtering and phonon-mediated coupling are taken into consideration.

Finally, we apply all the tools to analyze a new system, namely, an elliptical micropillar with an embedded QD subject to an external magnetic field and coherent driving. We provide the framework for generating photon blockade in such setup, demonstrating the realization of a *single photon polarization with* by means of the conventional photon blockade mechanism.

3.1 Unconventional photon blockade

3.1.1 Original proposal

As mentioned in Section 1.1, the idea of obtaining single photons by means of weak nonlinearities was initially proposed by Liew and Savona in 2010 [4]. In their work, they considered a scheme of *two coupled quantum modes* with small nonlinear interactions. As an example of the quantum modes, they mentioned that solid-state implementations that use the tunneling of polaritons between quantum boxes, as well as coupled photonic crystal cavities are suitable systems for that type of interaction.

The model for such an interaction can be written as

$$H = \tilde{\omega}_a \hat{a}^\dagger \hat{a} + \tilde{\omega}_b \hat{b}^\dagger \hat{b} + U (\hat{a}^{\dagger 2} \hat{a}^2 + \hat{b}^{\dagger 2} \hat{b}^2) + J (\hat{a}^\dagger \hat{b} + \hat{a} \hat{b}^\dagger) + \Omega_a (\hat{a} + \hat{a}^\dagger), \quad (3.1)$$

where $\tilde{\omega}_i$ corresponds to the frequency in the laser rotating frame of mode i , U is understood as a polariton-polariton interaction, normally considered as a Kerr-type self-interaction mechanism, J is a tunneling rate between the quantum boxes, and Ω_a represents the CW excitation of the mode a . This was the birth of the framework of the so-called *Unconventional photon blockade*, where the blockade is based on the use of weak nonlinearities, rather than on strong couplings, which in principle is easier to generate experimentally, due to the fact that many systems exhibit such weak nonlinearities naturally [67]. In their simulations, Liew and Savona found that the coupling of the pair of quantum boxes can notably improve the statistics of the emission, compared to those systems that rely on strong interactions (CPB), and for that reason, single photon emitters based on the principle of the UPB were considered to provide optimal applications for further technological developments. There are two different methods employed to understand the results from Liew and Savona. Each one will be discussed next

Wave function approximation method

Inspired by this work, the group of Bamba *et al.*[5], used the same theoretical proposal, but explained the nature of the UPB, identifying that specific quantum interference are responsible for that type of blockade. The process to understand these results will be shown up next.

First, one must use the denoted *wavefunction approximation*, which considers an expansion of the wavefunction into the bare state basis, truncating up to a certain manifold, and solving the Schrödinger equation by using an effective Hamiltonian which includes the dissipative processes (That in this case correspond to the losses from both quantum boxes at a rate γ_i) and therefore leads to a non-Hermitian Hamiltonian.

Considering the original problem by Liew and Savona, given by Equation (3.1), the effective Hamiltonian and the wavefunction of interest are

$$H_{\text{eff}} = \tilde{\omega}'_a \hat{a}^\dagger \hat{a} + \tilde{\omega}'_b \hat{b}^\dagger \hat{b} + U (\hat{a}^{\dagger 2} \hat{a}^2 + \hat{b}^{\dagger 2} \hat{b}^2) + J (\hat{a}^\dagger \hat{b} + \hat{a} \hat{b}^\dagger) + \Omega_a (\hat{a} + \hat{a}^\dagger) \quad (3.2a)$$

$$|\Psi\rangle = C_{00} |00\rangle + C_{10} |10\rangle + C_{01} |01\rangle + C_{20} |20\rangle + C_{11} |11\rangle + C_{02} |02\rangle \quad (3.2b)$$

$$i\hbar \partial_t |\Psi\rangle = H_{\text{eff}} |\Psi\rangle, \quad (3.2c)$$

where $\tilde{\omega}'_c = \tilde{\omega}_c - i\gamma_c/2$. With the set of Equations (3.2), it is possible to find the steady state by solving the coupled algebraic equations of the C_{nm} terms. To allow a closed set of equations, the conditions $C_{00} \gg C_{10}, C_{01} \gg C_{20}, C_{11}, C_{20}$, and $C_{00} = 1$, are imposed.

$$\begin{pmatrix} \tilde{\omega}'_a & J & 0 & 0 & 0 \\ J & \tilde{\omega}'_b & 0 & 0 & 0 \\ \sqrt{2}\Omega_a & 0 & 2(\tilde{\omega}'_a + U) & \sqrt{2}J & 0 \\ 0 & \Omega_a & \sqrt{2}J & \tilde{\omega}'_a + \tilde{\omega}'_b & \sqrt{2}J \\ 0 & 0 & 0 & \sqrt{2}J & 2(\tilde{\omega}'_b + U) \end{pmatrix} \begin{pmatrix} C_{10} \\ C_{01} \\ C_{20} \\ C_{11} \\ C_{02} \end{pmatrix} = \begin{pmatrix} -\Omega_a \\ 0 \\ 0 \\ 0 \\ 0 \end{pmatrix}. \quad (3.3)$$

From Equation (3.3) it can be seen that the coefficients that are related to C_{20} are C_{10} and C_{11} , meaning that those are responsible for the quantum interference. Indeed, the paths to access to the $|20\rangle$ states are

$$\text{Path 1: } |0, 0\rangle \xrightarrow{\Omega_a} |1, 0\rangle \xrightarrow{\Omega_a} |2, 0\rangle \quad (3.4)$$

$$\text{Path 2: } |0, 0\rangle \xrightarrow{\Omega_a} |1, 0\rangle \xrightarrow{J} |0, 1\rangle \xrightarrow{\Omega_a} |1, 1\rangle \xrightarrow{J} |2, 0\rangle. \quad (3.5)$$

The steady state solutions for the coefficients are

$$C_{10} = \frac{2\Omega_a(2\tilde{\omega}_b - i\gamma)}{4J^2 + \gamma^2 + 2i\gamma\tilde{\omega}_b - 4\tilde{\omega}_a\tilde{\omega}_b} \quad (3.6a)$$

$$C_{01} = \frac{4J\Omega_a}{4J^2 + \gamma^2 + 2i\gamma\tilde{\omega}_b - 4\tilde{\omega}_a\tilde{\omega}_b} \quad (3.6b)$$

$$C_{20} = [2\sqrt{2}\omega_a^2(2U\gamma\tilde{\omega}_a + 6U\gamma\tilde{\omega}_b + 4\gamma\tilde{\omega}_a\tilde{\omega}_b + 8\gamma\tilde{\omega}_b^2 - \gamma^3) + i(4J^2U - 2U\gamma^2 - \gamma^2\tilde{\omega}_a - 5\gamma^2\tilde{\omega}_b + 4U\tilde{\omega}_a\tilde{\omega}_b + 4U\tilde{\omega}_b^2 + 4\tilde{\omega}_a\tilde{\omega}_b^2 + 4\tilde{\omega}_b^3)] / [(4J^2 + \gamma^2 - 4\tilde{\omega}_a\tilde{\omega}_b + 2i\gamma\tilde{\omega}_a + 2i\gamma\tilde{\omega}_b)(4J^2\gamma - 4U^2\gamma + \gamma^3 - 8U\gamma\tilde{\omega}_a - 2\gamma\tilde{\omega}_a^2 - 8U\gamma\tilde{\omega}_b - 8\gamma\tilde{\omega}_a\tilde{\omega}_b - 2\gamma\tilde{\omega}_b^2 + 8iJ^2U + 4iU^2\gamma + 4iJ^2\tilde{\omega}_a - 4iU^2\tilde{\omega}_a + 3i\gamma^2\tilde{\omega}_a - 4iU\tilde{\omega}_a^2 + 4iJ^2\tilde{\omega}_b - 4iU^2\tilde{\omega}_b + 3i\gamma^2\tilde{\omega}_b - 8iU\tilde{\omega}_a\tilde{\omega}_b - 4i\tilde{\omega}_a^2\tilde{\omega}_b - 4iU\tilde{\omega}_b^2 - 4i\tilde{\omega}_a\tilde{\omega}_b^2)] \quad (3.6c)$$

$$C_{11} = -[8J\Omega_a^2(U - i\gamma + \tilde{\omega}_a + \tilde{\omega}_b)(2U - i\gamma + 2\tilde{\omega}_b)] / [(4J^2 + \gamma^2 - 4\tilde{\omega}_a\tilde{\omega}_b + 2i\gamma\tilde{\omega}_a + 2i\gamma\tilde{\omega}_b)(4iJ^2\gamma - 4iU^2\gamma + i\gamma^3 - 8iU\gamma\tilde{\omega}_a - 2i\gamma\tilde{\omega}_a^2 - 8iU\gamma\tilde{\omega}_b - 8i\gamma\tilde{\omega}_a\tilde{\omega}_b - 2i\gamma\tilde{\omega}_b^2 + 8J^2U + 4U^2\gamma + 4J^2\tilde{\omega}_a - 4U^2\tilde{\omega}_a + 3\gamma^2\tilde{\omega}_a - 4U\tilde{\omega}_a^2 + 4J^2\tilde{\omega}_b - 4U^2\tilde{\omega}_b + 3\gamma^2\tilde{\omega}_b - 8U\tilde{\omega}_a\tilde{\omega}_b - 4\tilde{\omega}_a^2\tilde{\omega}_b - 4U\tilde{\omega}_b^2 - 4\tilde{\omega}_a\tilde{\omega}_b^2)] \quad (3.6d)$$

$$C_{02} = [8\sqrt{2}J2\Omega_a^2(U - i\gamma + \tilde{\omega}_a + \tilde{\omega}_b)] / [(4J^2 + \gamma^2 - 4\tilde{\omega}_a\tilde{\omega}_b + 2i\gamma\tilde{\omega}_a + 2i\gamma\tilde{\omega}_b)(4iJ^2\gamma - 4iU^2\gamma + i\gamma^3 - 8iU\gamma\tilde{\omega}_a - 2i\gamma\tilde{\omega}_a^2 - 8iU\gamma\tilde{\omega}_b - 8i\gamma\tilde{\omega}_a\tilde{\omega}_b - 2i\gamma\tilde{\omega}_b^2 + 8J^2U + 4U^2\gamma + 4J^2\tilde{\omega}_a - 4U^2\tilde{\omega}_a + 3\gamma^2\tilde{\omega}_a - 4U\tilde{\omega}_a^2 + 4J^2\tilde{\omega}_b - 4U^2\tilde{\omega}_b + 3\gamma^2\tilde{\omega}_b - 8U\tilde{\omega}_a\tilde{\omega}_b - 4\tilde{\omega}_a^2\tilde{\omega}_b - 4U\tilde{\omega}_b^2 - 4\tilde{\omega}_a\tilde{\omega}_b^2)] \quad (3.6e)$$

Although the set of Equations (3.6) are quite bulky and not elucidating at first sight, they are useful for calculating relevant observables, especially, to understand the conditions for perfect antibunching due to quantum interference associated with the UPB. Contrary to the solutions given by [5], this set of expressions are far more general and pose no constraints among the detunings $\tilde{\omega}_i$, which Bamba *et al.* imposes to be equal. With (3.6), the observables n_a and $g_a^{(2)}(0)$ can be found as

$$n_a = \langle \Psi | \hat{a}^\dagger \hat{a} | \Psi \rangle \approx |C_{10}|^2 \quad (3.7)$$

$$g_a^{(2)}(0) = \frac{\langle \Psi | \hat{a}^{\dagger 2} \hat{a}^2 | \Psi \rangle}{\langle \Psi | \hat{a}^\dagger \hat{a} | \Psi \rangle^2} \approx 2 \frac{|C_{20}|^2}{|C_{10}|^4}, \quad (3.8)$$

so only by using the coefficients C_{10} and C_{20} , the mean photon number and second order correlation function can be analytically studied. Furthermore, It can be seen that the condition $g_a^{(2)}(0) = 0$ can be achieved by making the numerator of C_{20} equal to zero. This results in two conditions

$$2U\tilde{\omega}_a + 6U\tilde{\omega}_b + 4\tilde{\omega}_a\tilde{\omega}_b + 8\tilde{\omega}_b^2 - \gamma^2 = 0 \quad (3.9a)$$

$$4J^2U - 2U\gamma^2 - \gamma^2\tilde{\omega}_a - 5\gamma^2\tilde{\omega}_b + 4U\tilde{\omega}_a\tilde{\omega}_b + 4U\tilde{\omega}_b^2 + 4\tilde{\omega}_a\tilde{\omega}_b^2 + 4\tilde{\omega}_b^3 = 0. \quad (3.9b)$$

Following the lead of Bamba *et al.*, for the simpler case where $\tilde{\omega}_a = \tilde{\omega}_b = \tilde{\omega}$, the previous equations can be solved to obtain optimal expressions for $\tilde{\omega}$ and U can be found, as functions of J, γ . This is achieved first by solving for U in the simplified version of Equation (3.9 b), which gives $U(\omega)$, and then replacing that value on (3.9 a) and solving for ω . This results in the following optimal relationships

$$\tilde{\omega}_{\text{opt}} = \frac{1}{2} \sqrt{-3J^2 - \gamma^2 + J\sqrt{9J^2 + 8\gamma^2}} \quad (3.10a)$$

$$U_{\text{opt}} = \frac{3\gamma^2 \tilde{\omega}_{\text{opt}} - 4\tilde{\omega}_{\text{opt}}^3}{2J^2 - \gamma^2 + 4\tilde{\omega}_{\text{opt}}^2} = \frac{\tilde{\omega}_{\text{opt}}(5\gamma^2 \tilde{\omega}_{\text{opt}} + 4\tilde{\omega}_{\text{opt}}^2)}{2(2J^2 - \gamma^2)}. \quad (3.10b)$$

These optimal equations synthesize the efforts of Bamba *et al.* to enlighten the mechanism responsible for UPB constitutes a major contribution to the field, and which inspired numerous works that employed their analytical treatment.

Optimally Squeezed Gaussian states

A second major contribution to the understanding of UPB came in 2014 in the work of Lemonde *et al.* [6], where they related the nature of UPB to a much more intrinsic characteristic of the states that the *two coupled quantum modes* were able to generate. The steady state of these systems turns out to be a special case of a Gaussian state (As the ones explained in section 2.1.2), which are known as *Optimally Squeezed Gaussian states*.

The most general Gaussian state corresponds to a displaced squeezed thermal state, which has a density matrix of the form

$$\hat{\rho}_{\alpha, \xi, \bar{n}} = \hat{D}(\alpha) \hat{S}(\xi) \hat{\rho}_{\bar{n}} \hat{S}^\dagger(\xi) \hat{D}^\dagger(\alpha), \quad (3.11)$$

with $\alpha = \bar{\alpha}e^{i\phi}$, $\xi = re^{i\theta}$ and where $\hat{D}(\alpha), \hat{S}(\xi)$ are the displacement and squeezing operators, and $\hat{\rho}_{\bar{n}}$ is the density matrix of a thermal state with thermal population \bar{n} . The proposal from Lemonde *et al.* is that by optimally displacing and squeezing this type of state, one can achieve non-classical states. Using similarities transformations with the displacement and squeezing operators over the number operators, one can find (after some algebra) compact expressions for the mean photon number and the general density matrix $\hat{\rho}_{\alpha, \xi, \bar{n}}$ and recalling that $\langle \hat{O} \rangle = \text{Tr}[\hat{\rho}_{\alpha, \xi, \bar{n}} \hat{O}]$:

$$\langle \hat{a}^\dagger \hat{a} \rangle = \bar{\alpha}^2 + (\bar{n} + 1/2) \cosh 2r - 1/2 = \bar{\alpha}^2 + n \quad (3.12)$$

$$g^{(0)}(0) = 1 + \frac{2\bar{\alpha}^2(n-s) + s^2 + n^2}{(\bar{\alpha}^2 + n)^2}, \quad (3.13)$$

where s is defined as $s = (\bar{n} + 1/2) \sinh 2r$, and where the displacement and squeezing angles were chosen in order to squeeze the amplitude quadrature ($\theta = 2\phi$). It is therefore possible to study the dependence of the expression (3.13) as a function of the squeezing parameter r , and the displacement parameter $\bar{\alpha}$ (which for notation's sake will be written now on as α).

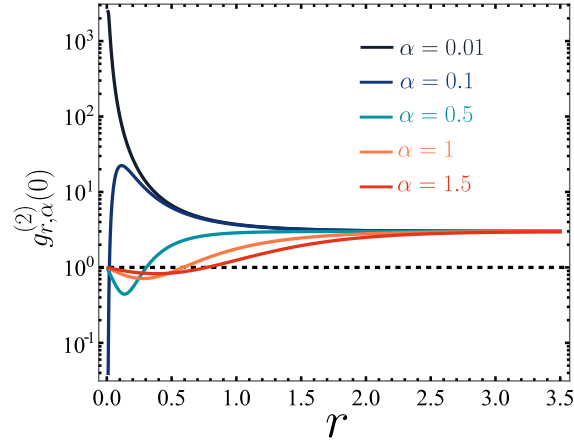


Figure 3.1 Second order correlation function calculated for the *optimally squeezed Gaussian states* as a function of the squeezing parameter r for various values of the displacement α .

For the case that there is no thermal contribution to the optimally squeezed Gaussian states, i.e. $\bar{n} = 0$, Figure (3.1) shows the behavior of the $g^{(2)}(0)$ as a function of r for several values of α . It can be seen that for an optimal choice of the squeezing parameter for each value of the displacement, there are regions where $g_{r,\alpha}^{(2)}(0) < 1$, proving that this condition is not unique to non-Gaussian states (e.g. Fock states) and therefore it is not a suitable proof of non-Gaussianity of a state. There are also two relevant aspects of this graph: First, it can be seen that the value of the antibunching can be brought closer to zero, by making small enough displacements and squeezing to the state. Secondly, it is understood that arbitrarily increasing the squeezing factor r does not decrease the second order correlation function but rather all plots tend to the value of 3, which means that increasing r , and thus, reducing the fluctuations does not translate into a smaller $g^{(2)}(0)$. These two assertions will be further inspected next.

To examine the first statement, it is relevant to study how $g^{(2)}(0)$ acts when α, r are both small. This is explored in the figure below.

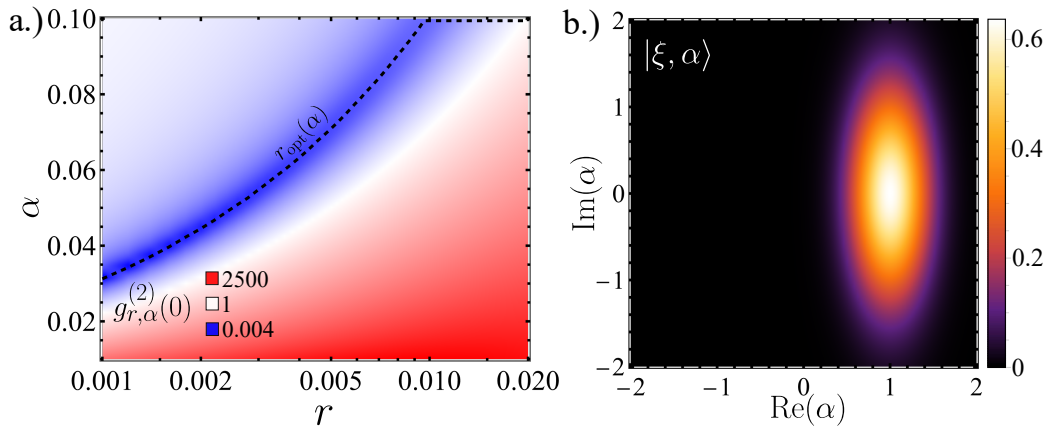


Figure 3.2 a.) Second order correlation function of the *optimally squeezed Gaussian state* for small deviations of r, α . The dashed lines indicate the optimal relationship between r and α that minimize $g^{(2)}$. b.) Wigner function of a Squeezed Coherent state $|\xi, \alpha\rangle$, where $r = 0.5$ and $\alpha = 1$.

Figure (3.2 a) shows the statistics of $g_{r,\alpha}^{(2)}(0)$ for small deviations of r, α over the vacuum state. It can be seen that by properly selecting a squeezing quantity for each displacement on the phase space, one can obtain antibunching with the use of Gaussian states. The optimal relationship for antibunching is displayed in this figure as a dashed black line, whose functional form has a quadratic nature in α , so it can be seen that in order to get antibunching with Gaussian states, one must use a squeezing $r = r_{\text{opt}}(\alpha) \approx \alpha^2$, for small values of α . It is also possible to find an optimal relationship between r and α that always minimizes $g^{(2)}(0)$, but since for big values of these pairs the second order correlation function does not display a Subpoissonian nature, it is not of my interest to explore this connection.

Now, since Gaussian state have an analytical calculation for their representation on phase space, as indicated in Section (2.1.2), it results interesting to analyze whether their Wigner function has some differences since there is a large difference for the states $g_{r,\alpha}^{(2)}$ depending on the selection of the parameters. Using the techniques of the aforementioned section, it can be proven that the expression for the Wigner function of a Squeezed Coherent state is

$$W_{\xi, \alpha_0}(\alpha) = \frac{2}{\pi} \exp \left\{ -2 \left(\frac{\text{Re}\{\alpha - \alpha_0\}^2}{e^{-2\xi}} + \frac{\text{Im}\{\alpha - \alpha_0\}^2}{e^{2\xi}} \right) \right\}. \quad (3.14)$$

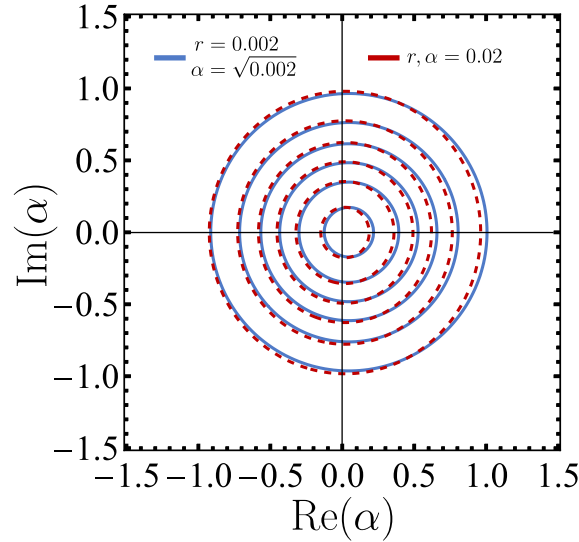


Figure 3.3 Comparison of the Wigner function of the displaced squeezed vacuum for the conditions that generate antibunching $r, \alpha = 0.02$ (Red) and bunching $r = 0.002, \alpha = \sqrt{r}$ (Blue)

Thus, $|\xi, \alpha\rangle$ is a squeezed state with a displacement given by α_0 . Figure (3.3) shows a calculation of the Wigner function of these states, for two sets of parameters: I. $r, \alpha = 0.02$ (Red), which corresponds to a bunching condition in Figure (3.2), and $r = 0.002, \alpha = \sqrt{r}$, corresponding to antibunching. As it can be seen, although the deviation from both conditions is small, it is sufficient to generate a difference in the second order correlation function of the order of 10^6 , however, the intrinsic cause remains missing. Further explorations for these types of states must be made in order to clarify the nature of such behavior.

To conclude this statement, it can be seen that for the specific model of the *two coupled quantum modes*

the Kerr interaction is the one responsible for carrying the squeezed nature in the Hamiltonian, while the coherent contribution is given by the CW driving. For this reason, it is seen that the suppression in the $g^{(2)}(0)$ in this model is a particular case for the realization of optimally squeezed Gaussian states, which corresponds to the steady state of the driven mode.

To analyze the next statement, on the reason these states tend to a value of 3, it is useful to directly inspect the squeezed vacuum states, since the behavior of the plots acts independently of α . For this purpose, one must calculate the expectation values of the number operator and the $g^{(2)}(0)$ in the squeezed state $|\xi\rangle = \hat{S}(\xi)|0\rangle$. Recalling the similarities transformation given in Equation (2.38), and that the operator $\hat{S}(\xi)$ is unitary, the expressions can be obtained as follows

$$\langle \hat{a}^\dagger \hat{a} \rangle_\xi = \langle 0 | \hat{S}^\dagger(\xi) \hat{a}^\dagger \hat{a} \hat{S}(\xi) | 0 \rangle = \langle 0 | \hat{S}^\dagger(\xi) \hat{a}^\dagger \hat{S}(\xi) \hat{S}^\dagger(\xi) \hat{a} \hat{S}(\xi) | 0 \rangle = \langle 0 | \hat{a}_\xi^\dagger \hat{a}_\xi | 0 \rangle = \sinh^2 r = n \quad (3.15a)$$

$$\langle \hat{a}^{\dagger 2} \hat{a}^2 \rangle_\xi = \langle 0 | \hat{a}_\xi^{\dagger 2} \hat{a}_\xi^2 | 0 \rangle = 2 \sinh^4 r + \sinh^2 r \cosh^2 r \quad (3.15b)$$

$$g_\xi^{(2)}(0) = \frac{2 \sinh^4 r + \sinh^2 r \cosh^2 r}{\sinh^4 r} = 3 + \frac{1}{\sinh^2 r} = 3 + \frac{1}{n}. \quad (3.15c)$$

Therefore it has been proven that for large enough n , the squeezed vacuum state second order correlation function (Equation 3.15c) tends to 3.

Numerical solution for the master equation

Now, having understood all the frameworks on which the UPB can be explained, it is time to proceed with the numerical confirmation of the analysis, which will be performed by solving the following master equation,

$$\partial_t \rho = i[\rho, H] + \frac{\gamma_a}{2} \mathcal{L}_{\hat{a}} \rho + \frac{\gamma_b}{2} \mathcal{L}_{\hat{b}} \rho, \quad (3.16)$$

where H is the original Hamiltonian from Liew and Savona (Equation 3.1). Solving for the steady state and calculating $g^{(2)}(0)$ as a function of the mode detunings $\tilde{\omega}_i$ yields

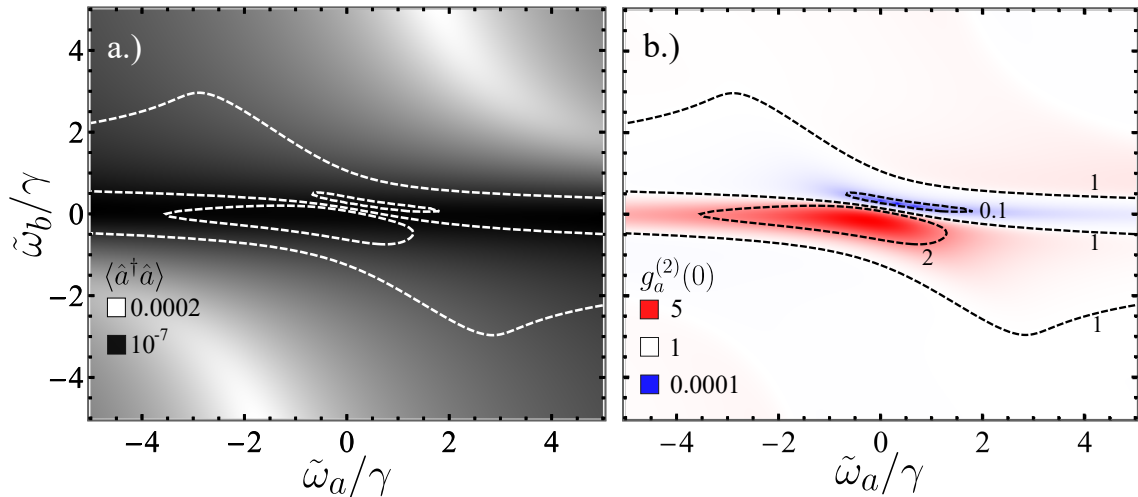


Figure 3.4 a.) Mean photon number and b.) $g^{(2)}$ of the two coupled quantum modes model, as reproduced from the references [4, 5]. U/γ is chosen to optimize antibunching as given by Equation (3.10 b). Parameters: $U = 0.0428\gamma$, $J = 3\gamma$, $\Omega_a = 0.001\gamma$.

As shown in Figure (3.4 b), the values of the $g^{(2)}$ with the UPB scheme reach values as low as 10^{-4} , for a Kerr nonlinearity of the order of 0.01γ . This outstanding result was the one that catapulted the UPB as a feasible single photon source, since, as mentioned earlier, it does not require achieving strong coupling, but also, it doesn't employ the coupling of a cavity with an emitter, which always poses a technological challenge (Although recent developments have made this process much easier). Nevertheless, as complemented with Figure (3.4 a), it can be seen that mean photon values range between 10^{-7} and 2×10^{-4} , which drawbacks the single photon emission of this sort of systems because of the decrease in brightness (which is an essential feature for an SPS to have technological applications), meaning that a source of this type corresponds to a probabilistic source of single photons, making this sort of states inconvenient for applications.

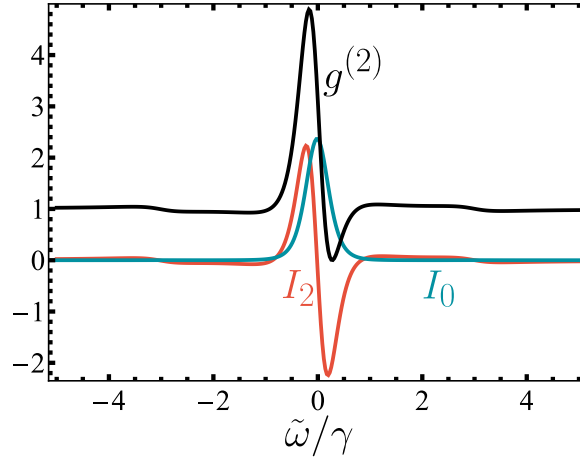


Figure 3.5 Decomposition of $g^{(2)}$ in coherent and incoherent factors, for the values where $\tilde{\omega}_a, \tilde{\omega}_b = \tilde{\omega}$ in Figure (3.4) b. The nature of the antibunching of the UPB stems from a squeezing contribution of the incoherent factor I_2 . Parameters: $U = 0.0428\gamma$, $J = 3\gamma$, $\Omega_a = 0.001\gamma$.

In Figure (3.5) the incoherent decomposition of the $g^{(2)}(0)$ is made, for the case where $\tilde{\omega}_a = \tilde{\omega}_b$. As expected, the incoherent factor associated to squeezing, i.e., I_2 is the distinctive feature for the cause of the antibunching in the UPB, which confirms the nature of the steady state as an optimally squeezed Gaussian state. I_0 and I_2 are only non-zero near the optimal minimization point, which explains the coherent nature of this source for most of the set of parameters. This optimally squeezed Gaussian state is only an infinitesimal deviation of the vacuum, therefore is not large enough to show the anomalous correlations related to squeezed coherent states, so the I_1 contribution is zero.

Furthermore, following the idea that single photon sources must provide photon blockade at all orders, Figure (3.6) shows the calculation of $g^{(n)}(0)$ up to $n = 4$, as a function of the detuning $\tilde{\omega}$ (a) and the Kerr nonlinearity strength U (b). First, it can be seen that by properly selecting the cavity and laser detuning, the second order correlation function can be adequately minimized. However, this situation contrasts with the case of higher-order correlation functions, where for both $n = 3, 4$ the behavior mostly resembles a chaotic light source. To check that this phenomenon occurs for all values of U/γ , panel b. of the same figure displays the same calculation of the higher order correlations as a function of the Kerr nonlinearity strength U , where we take the value of $\tilde{\omega}/\gamma$ that optimizes the $g^{(2)}$, i.e., $\tilde{\omega} = 0.0257\gamma$. It can be seen that by increasing the order of n , the value of U/γ that minimizes each correlation function keeps decreasing, which means that there is no value that could simultaneously provide optimal antibunching at all orders. Moreover, although the $g^{(4)}$ can be minimized,

the value it takes is greater than one, meaning that for the selection of the frequency that optimizes the second order correlation function, it is not possible to obtain the same response for higher-order correlations. This gives first insights with respect to the nature of the emission of this system, indicating that multiphotonic events are still possible.

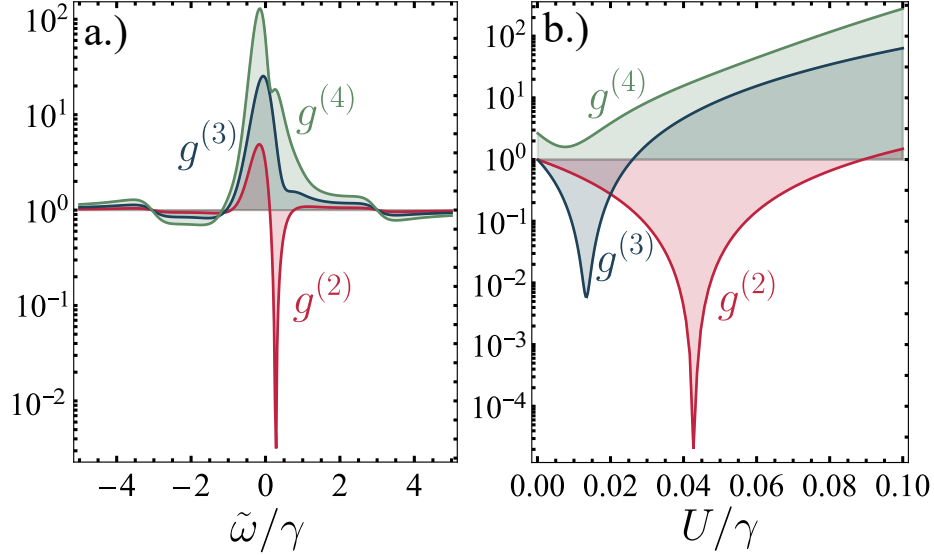


Figure 3.6 $g_a^{(n)}$ for $n = 2, 3, 4$ as a function of the detuning $\tilde{\omega}$ (a) and Kerr nonlinearity U/γ (b). In the first panel, only $g^{(2)}$ obtains values lower than one, while higher-order correlation functions exhibit a bunched nature for all frequencies. Selecting such the minimizing frequency, panel b indicates that there is no simultaneous minimization of the correlation functions. Parameters: (a) $U = 0.0428\gamma$, (b) $\tilde{\omega} = 0.0275\gamma$. The rest of the parameters are $J = 3\gamma$ and $\Omega_a = 0.001\gamma$.

To give a complete understanding of the behavior of higher-order correlation functions, in Figure (3.7) we map the previously calculated correlations, as a function of the detuning $\tilde{\omega}$ and the Kerr nonlinearity strength U . Here it can be seen that the selection of U/γ that minimizes $g^{(2)}$ yields bunching at higher order correlation functions. Proceeding with this idea, we indicate in the plot the values of U that minimize the value of $g^{(n)}$, noting that optimal antibunching in the three correlation functions is not possible, as previously indicated in Figure (3.6 b). Nevertheless, showing the minimal values for $g^{(n)}$ opens the possibility to define zones where, although not optimal, it is possible to find the same statistical behavior for all orders in the correlation function. by means of a minimization process in between the (II) and (III) zones, we found the optimal value for U that simultaneously gives the lower possible values of $g^{(n)}$. Using this value, we calculate the correlation functions with respect to the detuning. We found that this notoriously contrasts with the one observed in Figure (3.6 b), where it is now possible to simultaneously realize antibunching for all orders, at the expense of decreasing the value of the $g^{(2)}$. These results conclusively demonstrate that although the values of the model of Liew and Savona do not correspond to a true single photon emitter, it is possible to find the optimal value of the Kerr nonlinearity that gives the best simultaneous minimization of the correlation functions. Such criterion is much more robust for classifying single photon sources, because describes the statistical behavior of the source at higher orders, rather than merely relying on the values for the second order correlation function.

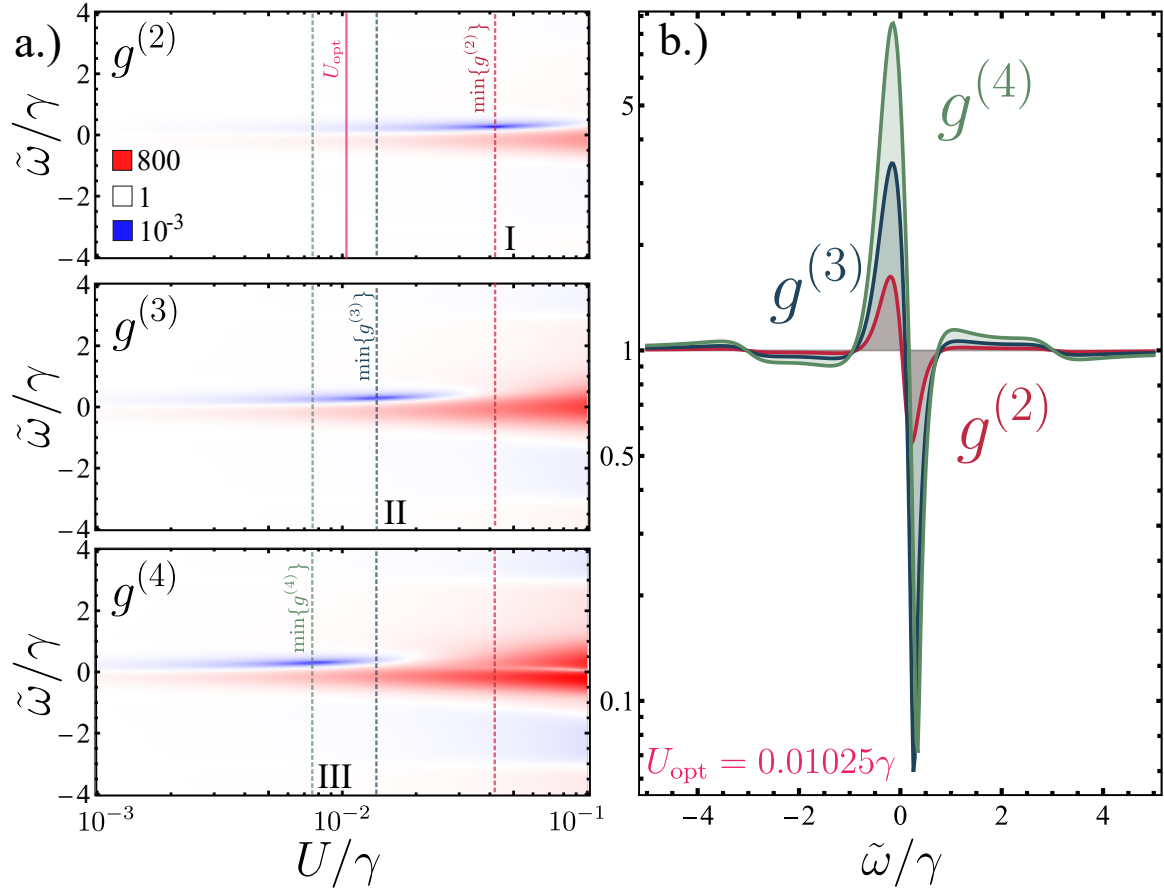


Figure 3.7 a.) Higher order correlation function analysis of the two interacting cavity model, for a mapping of the detuning $\tilde{\omega}$ and Kerr nonlinearity U . The optimal Kerr nonlinearity value, U_{opt} , that gives the best simultaneous minimization is found. **b.)** $g^{(n)}$ as a function of the detuning for the optimal Kerr nonlinearity, $U = 0.01025\gamma$. Simultaneous antibunching is observed, indicating single photon emission for a detuning value of $\tilde{\omega}/\gamma = 0.3$ Parameters: $J = 3\gamma$, $\Omega_a = 0.001\gamma$.

3.1.2 Modifications to the original model

Inspired by the original work, many derivations of the Unconventional Photon Blockade have been made, examining further systems that could minimize the second order correlation function. Most of them are synthesized into hybrid systems, which include optomechanical interactions [68, 69], others study modifications to the nature of the employed nonlinearity [70], and also have a more general approach to the original model, such as driving both polariton boxes and posing different nonlinearities values for each one[71, 72].

Here, we will only consider the easiest deviation of the original model, as proposed by Xu and Li [71], where they considered different CW strength and phase for each mode, and where the restriction for equal nonlinearity of both modes U was lifted. Their Hamiltonian is

$$H = \tilde{\omega}_a \hat{a}^\dagger \hat{a} + \tilde{\omega}_b \hat{b}^\dagger \hat{b} + J(\hat{a}^\dagger \hat{b} + \hat{a} \hat{b}^\dagger) + U_a \hat{a}^{\dagger 2} \hat{a}^2 + U_b \hat{b}^{\dagger 2} \hat{b}^2 + \Omega_a (\hat{a}^\dagger e^{i\phi_a} + \hat{a} e^{-i\phi_a}) + \Omega_b (\hat{b}^\dagger e^{i\phi_b} + \hat{b} e^{-i\phi_b}).$$

The optimal conditions that they derived are

$$\tilde{\omega}_{\text{opt}} \approx J/\eta \quad (3.17a)$$

$$U_{\text{opt}} \approx \frac{\kappa^2}{2J} \frac{\eta}{\eta^2 - 1}, \quad (3.17b)$$

with $\eta = \Omega_a/\Omega_b$, and where no relative phase between the drives was considered ($\phi_a = \phi_b$). The results of the reproduction of their main result and the comparison with the new SPS criteria are shown up next

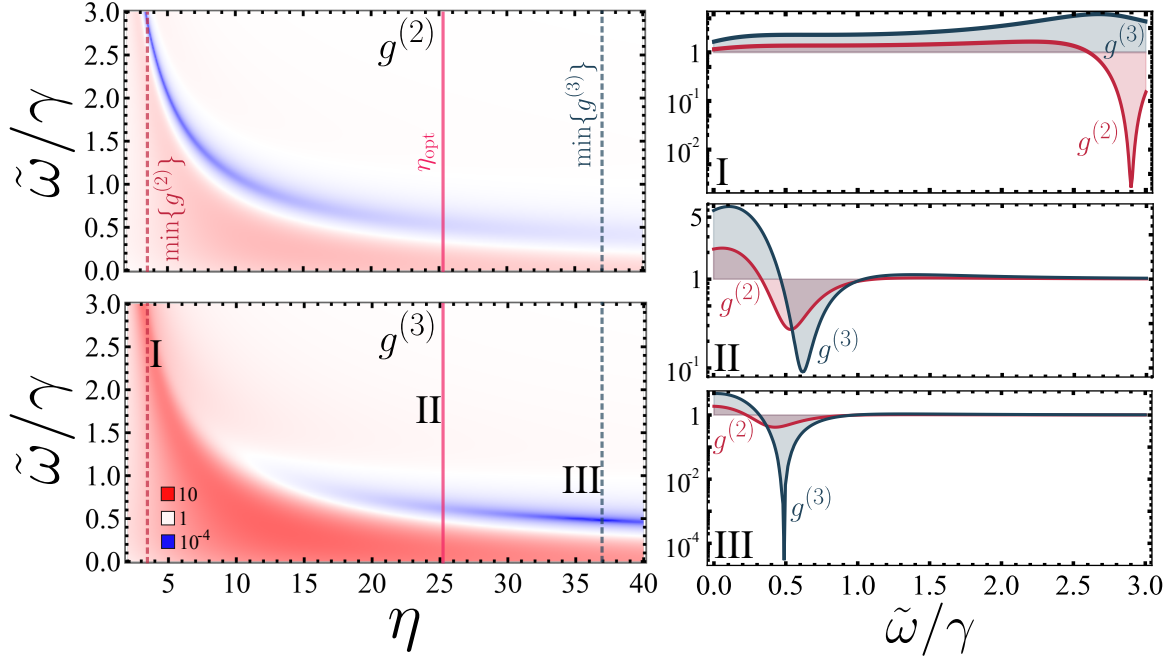


Figure 3.8 Higher order correlation function analysis for the model by Xu and Li [71], as a function of frequency and driving ratio $\eta = \Omega_a/\Omega_b$. The optimal value for the ratio of the drivings, $\eta_{\text{opt}} = 25.2$ is found by minimizing simultaneously both correlation functions.

In Figure (3.8 a) we reproduce one of the main results from [71], where the numerical calculation of the $g^{(2)}(0)$ is made as a function of the detuning $\tilde{\omega}$ and the relative driving strength $\eta = \Omega_a/\Omega_b$. Their result indicated that by properly selecting the relationship of the CW drivings for each mode, antibunching via the UPB was achievable with much more ease than from the original model, by properly tuning the detuning among the laser and the natural frequencies of the quantum modes. The optimal condition for the $g^{(2)}$ was $\eta = 3.5$. Nevertheless, as shown in the higher order correlation analysis, just by calculating the following correlation function ($g^{(3)}$) the optimal parameter yields bunching, preventing single photon emission. Once again, by applying a simultaneous minimization process, it is found that there is a value $\eta_{\text{opt}} \approx 25.2$ where both correlation functions can yield low values, namely, $g^{(2)} = 0.3$ and $g^{(3)} = 0.13$. For this system, however, the mean photon number is still of the order of 10^{-7} , so it poses the original brightness issue of the Liew and Savona model.

3.2 Simultaneous Photon Blockade

The fact that only two groups have been able to provide experiments to generate Unconventional Photon Blockade as proposed in its original form, despite the numerous setups proposed in theoretical papers, shows the limits on the implementations of these schemes, and the need to find alternative routes for generating single photon sources through the Photon Blockade Effect. In that regard, the work of Zubizarrieta *et al.* [10, 73] elucidates the path, by proving that some systems may exhibit conventional and unconventional features simultaneously, just by properly tuning the relevant parameters, and which are explained through the unified framework of admixing of coherent and squeezed states, as mentioned in section 2.5. Therefore, in this section, we will explore a particular system and evaluate its usefulness as an SPS through the higher-order correlation function minimization, as well as the discussion of their experimental realizations.

3.2.1 Driven-dissipative Jaynes Cummings model

One of the alternative systems that could serve as a real on-demand single photon source, as discussed by Zubizarrieta *et al.*, is described by the simplest, yet one of the most relevant models of Quantum Optics: The Jaynes Cummings model, which was introduced when the quantum mechanical picture of light matter interaction was discussed (section 2.2.3). The proposed system is specifically understood as a driven (and dissipative) Jaynes Cummings model, which can be described by the following Hamiltonian:

$$H(t) = \hbar\omega_a \hat{a}^\dagger \hat{a} + \hbar\omega_\sigma \hat{\sigma}^\dagger \hat{\sigma} + \hbar g (\hat{a}^\dagger \hat{\sigma} + \hat{\sigma}^\dagger \hat{a}) + \Omega_a (\hat{a} e^{i\omega_l t} + \hat{a}^\dagger e^{-i\omega_l t}) + \Omega_\sigma (\hat{\sigma} e^{i\omega_l t} + \hat{\sigma}^\dagger e^{-i\omega_l t}), \quad (3.18)$$

where $\hat{a}, \hat{\sigma}$ are the annihilation and lowering operators for radiation and matter, $\omega_{a(\sigma)}$ represents the frequency of the cavity (2LS), g is the magnitude of the dipole interaction, and $\Omega_{a(\sigma)}, \omega_l$ corresponds to the amplitude and frequency of the coherent pump to the cavity (2LS).

As it was mentioned in the previous section, moving into the laser rotating frame removes the explicit time dependence of the Hamiltonian, facilitating the solution of the system. Here we will explicitly show how this transformation can be made, in order to give full completeness to the problem. The unitary operator \hat{R} that allows this transformation is

$$\hat{R}(t) = e^{i\hbar\omega_l(\hat{a}^\dagger \hat{a} + \hat{\sigma}^\dagger \hat{\sigma})t} = e^{i\hbar\omega_l \hat{N}_T t}, \quad (3.19)$$

where $\hat{N}_T = \hat{a}^\dagger \hat{a} + \hat{\sigma}^\dagger \hat{\sigma}$ is understood as the number excitation operator for the joint system. Given that light and matter operators commute, i.e., $[\hat{a}^\dagger \hat{a}, \hat{\sigma}^\dagger \hat{\sigma}] = 0$, the exponentials of the unitary operator can be divided, resulting in

$$\hat{R}(t) = e^{i\hbar\omega_l \hat{a}^\dagger \hat{a} t} e^{i\hbar\omega_l \hat{\sigma}^\dagger \hat{\sigma} t}. \quad (3.20)$$

Once again, the transformation that allows transforming the Hamiltonian H to a new one established in the rotating laser frame H' is given by Equation (2.5)

$$H' = i\hbar \hat{R} H(t) \hat{R}^\dagger + i\hbar \partial_t \hat{R} \hat{R}^\dagger. \quad (3.21)$$

To explicitly calculate H , the Baker-Campbell-Hausdorff formula explained beforehand, is employed. The first term of the transformation is,

$$\begin{aligned} i\hbar \hat{R}H(t)\hat{R}^\dagger &= \hbar\omega_a \left(e^{i\hbar\omega_l\hat{n}_c t} \hat{a}^\dagger \hat{a} e^{-i\hbar\omega_l\hat{n}_c t} \right) + \hbar\omega_\sigma \left(e^{i\hbar\omega_l\hat{\sigma}^\dagger\hat{\sigma}t} \hat{\sigma}^\dagger \hat{\sigma} e^{-i\hbar\omega_l\hat{\sigma}^\dagger\hat{\sigma}t} \right) \\ &+ \hbar g \left(e^{i\hbar\omega_l\hat{n}_c t} e^{i\hbar\omega_l\hat{\sigma}^\dagger\hat{\sigma}t} \hat{a}^\dagger \hat{\sigma} e^{-i\hbar\omega_l\hat{\sigma}^\dagger\hat{\sigma}t} e^{-i\hbar\omega_l\hat{n}_c t} + e^{i\hbar\omega_l\hat{n}_c t} e^{i\hbar\omega_l\hat{\sigma}^\dagger\hat{\sigma}t} \hat{a} \hat{\sigma}^\dagger e^{-i\hbar\omega_l\hat{\sigma}^\dagger\hat{\sigma}t} e^{-i\hbar\omega_l\hat{n}_c t} \right) \\ &+ \hbar\Omega_a \left(e^{-i\omega_l t} e^{i\hbar\omega_l\hat{n}_c t} \hat{a}^\dagger e^{-i\hbar\omega_l\hat{n}_c t} + e^{i\omega_l t} e^{i\hbar\omega_l\hat{n}_c t} \hat{a} e^{-i\hbar\omega_l\hat{n}_c t} \right) \\ &+ \hbar\Omega_\sigma \left(e^{-i\omega_l t} e^{i\hbar\omega_l\hat{n}_c t} \hat{\sigma}^\dagger e^{-i\hbar\omega_l\hat{n}_c t} + e^{i\omega_l t} e^{i\hbar\omega_l\hat{n}_c t} \hat{\sigma} e^{-i\hbar\omega_l\hat{n}_c t} \right), \end{aligned} \quad (3.22)$$

while the second one is

$$i\hbar\partial_t\hat{R}\hat{R}^\dagger = -\hbar\omega_l (\hat{a}^\dagger\hat{a} + \hat{\sigma}^\dagger\hat{\sigma}). \quad (3.23)$$

To further simplify the calculations, some important commutators are used: $[\hat{a}^\dagger\hat{a}, \hat{a}^\dagger] = \hat{a}^\dagger$, $[\hat{a}^\dagger\hat{a}, \hat{a}] = -\hat{a}$, $[\hat{\sigma}^\dagger\hat{\sigma}, \hat{\sigma}^\dagger] = \hat{\sigma}^\dagger$, $[\hat{\sigma}^\dagger\hat{\sigma}, \hat{\sigma}] = -\hat{\sigma}$. With these results, and once again using the Baker-Campbell-Hausdorff formula, the elements that appear in (3.22) that must be calculated result in:

$$e^{i\omega_l\hat{a}^\dagger\hat{a}t} \hat{a}^\dagger \hat{a} e^{-i\omega_l\hat{a}^\dagger\hat{a}t} = \hat{a}^\dagger \hat{a} \quad (3.24a)$$

$$e^{i\omega_l\hat{\sigma}^\dagger\hat{\sigma}t} \hat{\sigma}^\dagger \hat{\sigma} e^{-i\omega_l\hat{\sigma}^\dagger\hat{\sigma}t} = \hat{\sigma}^\dagger \hat{\sigma} \quad (3.24b)$$

$$e^{i\omega_l\hat{a}^\dagger\hat{a}t} \hat{a}^\dagger e^{-i\omega_l\hat{a}^\dagger\hat{a}t} = \hat{a}^\dagger e^{-i\omega_l t} \quad (3.24c)$$

$$e^{i\omega_l\hat{a}^\dagger\hat{a}t} \hat{a} e^{-i\omega_l\hat{a}^\dagger\hat{a}t} = \hat{a} e^{i\omega_l t} \quad (3.24d)$$

$$e^{i\omega_l\hat{\sigma}^\dagger\hat{\sigma}t} \hat{\sigma}^\dagger e^{-i\omega_l\hat{\sigma}^\dagger\hat{\sigma}t} = \hat{\sigma}^\dagger e^{-i\omega_l t} \quad (3.24e)$$

$$e^{i\omega_l\hat{\sigma}^\dagger\hat{\sigma}t} \hat{\sigma} e^{-i\omega_l\hat{\sigma}^\dagger\hat{\sigma}t} = \hat{\sigma} e^{i\omega_l t}. \quad (3.24f)$$

Thus, the Hamiltonian of the coherently driven Jaynes Cumming model, expressed in the rotating frame of the laser has proven to be of the following form:

$$H = \hbar\tilde{\omega}_a \hat{a}^\dagger\hat{a} + \hbar\tilde{\omega}_\sigma \hat{\sigma}^\dagger\hat{\sigma} + \hbar g (\hat{a}^\dagger\hat{\sigma} + \hat{a}\hat{\sigma}^\dagger) + \hbar\Omega_a (\hat{a} + \hat{a}^\dagger) + \hbar\Omega_\sigma (\hat{\sigma} + \hat{\sigma}^\dagger), \quad (3.25)$$

where $\tilde{\omega}_i = \omega_i - \omega_l$, $i = \{a, \sigma\}$. As expected, the effect of moving into the laser rotating frame is to remove the explicit time dependency of the coherent pumping and to transfer its properties to the relationships between the bare frequencies of the system and the driving frequency, without modifying the light-matter interaction.

One of the principal properties of adding the coherent drive to the system is that it loses the property of commuting with the total number operator, and therefore from the Heisenberg equation it stops being a conserved quantity:

$$\begin{aligned} [\hat{N}_T, H] &= [\hat{a}^\dagger\hat{a} + \hat{\sigma}^\dagger\hat{\sigma}, \hbar\Omega_a(\hat{a}^\dagger + \hat{a}) + \hbar\Omega_\sigma(\hat{\sigma}^\dagger + \hat{\sigma})] \\ &= \hbar\Omega_a(\hat{a}^\dagger - \hat{a}) + \hbar\Omega_\sigma(\hat{\sigma}^\dagger - \hat{\sigma}) \\ \frac{d\hat{N}_T}{dt} &= \frac{1}{i\hbar} [\hat{N}_T, H] \neq 0. \end{aligned} \quad (3.26)$$

Nevertheless, for the case that the pumping magnitude is much less than the interaction term (And when the picture is upgraded to a dissipative formalism, it must also be less than the decaying parameters γ_i), the total

number operator will keep its conservation properties, which allows once again to write the Hamiltonian in a block diagonal form, finding its eigenvalues and eigenvectors for a specific manifold n .

Recalling the bare basis projection of the Jaynes Cummings Hamiltonian given in Equation (2.74), and the eigenenergies expression for each manifold (2.75), the steps for obtaining photon blockade via anharmonicities (i.e., through the mechanism of CPB) are achieved by tuning the laser frequency with energy given by $\omega_l = E_{n,\pm}/\hbar$. Specifically, if one is interested in generating one photon at a time, the proper laser frequency (taking $\hbar = 1$) is

$$E_1^{(-)} = \omega_l = \frac{\omega_\sigma + \omega_a}{2} \pm \frac{1}{2} \sqrt{4g^2 + (\omega_a - \omega_\sigma)^2}. \quad (3.27)$$

With a bit of algebra, this expression can be simplified to obtain the following condition

$$\begin{aligned} 2\omega_l &= \omega_\sigma + \omega_a - \sqrt{4g^2 + (\omega_a - \omega_\sigma)^2} \\ (\tilde{\omega}_a + \tilde{\omega}_\sigma)^2 &= 4g^2 + (\tilde{\omega}_a - \tilde{\omega}_\sigma)^2 \\ \tilde{\omega}_a \tilde{\omega}_\sigma &= g^2. \end{aligned} \quad (3.28)$$

So, by properly choosing the laser frequency one can obtain one photon in the cavity. Expression (3.28) is the *conventional photon blockade* condition for generating single photons. It will be the basis for analyzing CPB in the following calculations.

On the other hand, to understand the unconventional photon blockade within the framework of the Jaynes Cummings model, it is necessary to recall that the main mechanism relies on quantum interference, specifically, on the interference between two different pathways to access the same state. If the probabilities of both paths interfere, then this state will be unable to be reached. For the system under consideration, the paths to access the two photon state, and which result in interference are

$$\text{Path 1: } |0, g\rangle \xrightarrow{\Omega_a} |1, g\rangle \xrightarrow{\Omega_a} |2, g\rangle \quad (3.29)$$

$$\text{Path 2: } |0, g\rangle \xrightarrow{\Omega_a} |1, g\rangle \xrightarrow{g} |0, e\rangle \xrightarrow{\Omega_a} |1, e\rangle \xrightarrow{g} |2, g\rangle. \quad (3.30)$$

This allows blocking the state of two photons, and due to the low rates of pumping, higher-order states won't be commonly accessed, although they are not blockaded.

In order to obtain the analytical condition that sustains the UPB, it is necessary to apply once again the wave function approximation method. For this case, the ansatz for the wave function is,

$$|\Psi\rangle = C_{0,g} |0, g\rangle + C_{1,g} |1, g\rangle + C_{0,e} |0, e\rangle + C_{1,e} |1, e\rangle + C_{2,g} |2, g\rangle, \quad (3.31)$$

where the coefficients $|C_{n,\alpha}|^2$ denote the probability to access the state $|n, \alpha\rangle$. The effective Hamiltonian to employ is

$$H_{eff} = \hbar \tilde{\omega}_a \hat{a}^\dagger \hat{a} + \hbar \tilde{\omega}_\sigma \hat{\sigma}^\dagger \hat{\sigma} + \hbar g (\hat{a}^\dagger \hat{\sigma} + \hat{a} \hat{\sigma}^\dagger) + \hbar \Omega_a (\hat{a} + \hat{a}^\dagger) - i \frac{\kappa_a}{2} \hat{a}^\dagger \hat{a} - i \frac{\gamma_\sigma}{2} \hat{\sigma}^\dagger \hat{\sigma} \quad (3.32)$$

$$= \hbar \left(\tilde{\omega}_a - i \frac{\kappa_a}{2} \right) \hat{a}^\dagger \hat{a} + \hbar \left(\tilde{\omega}_\sigma - i \frac{\gamma_\sigma}{2} \right) \hat{\sigma}^\dagger \hat{\sigma} + \hbar g (\hat{a}^\dagger \hat{\sigma} + \hat{a} \hat{\sigma}^\dagger) + \hbar \Omega_a (\hat{a} + \hat{a}^\dagger). \quad (3.33)$$

For the moment, only driving to the cavity was considered. Once again, solving the Schrödinger equation yields a set of coupled differential equations for the coefficients $C_{n,\alpha}$

$$\partial_t C_{g,1} = \left(\tilde{\omega}_a - i \frac{\kappa_a}{2} \right) C_{g,1} + g C_{e,0} + \Omega_a \left(1 + \sqrt{2} C_{g,2} \right) \quad (3.34a)$$

$$\partial_t C_{e,0} = \left(\tilde{\omega}_\sigma - i \frac{\gamma_\sigma}{2} \right) C_{e,0} + g C_{g,1} + \Omega_a C_{e,1} \quad (3.34b)$$

$$\partial_t C_{e,1} = \left(\tilde{\omega}_a + \omega_\sigma - i \frac{\kappa_a + \gamma_\sigma}{2} \right) C_{e,1} + \sqrt{2} g C_{g,2} + \Omega_a C_{e,0} \quad (3.34c)$$

$$\partial_t C_{g,2} = 2 \left(\tilde{\omega}_a - i \frac{\kappa_a}{2} \right) C_{g,2} + \sqrt{2} g C_{e,1} + \sqrt{2} \Omega_a C_{g,1}. \quad (3.34d)$$

$$\partial_t \mathbf{C}_{1,G} = \left(\tilde{\omega}_a - i \frac{\kappa_a}{2} \right) \mathbf{C}_{1,G} + g \mathbf{C}_{0,X} + \Omega_a \left(1 + \sqrt{2} \mathbf{C}_{2,G} \right) \quad (3.35a)$$

$$\partial_t \mathbf{C}_{0,X} = \left(\tilde{\omega}_\sigma - i \frac{\gamma_\sigma}{2} \right) \mathbf{C}_{0,X} + g \mathbf{C}_{1,G} + \Omega_a \partial_t \mathbf{C}_{1,X} \quad (3.35b)$$

$$\partial_t \mathbf{C}_{1,X} = \left(\tilde{\omega}_a + \omega_\sigma - i \frac{\kappa_a + \gamma_\sigma}{2} \right) \partial_t \mathbf{C}_{1,X} + \sqrt{2} g \mathbf{C}_{2,G} + \Omega_a \mathbf{C}_{0,X} \quad (3.35c)$$

$$\partial_t \mathbf{C}_{2,G} = 2 \left(\tilde{\omega}_a - i \frac{\kappa_a}{2} \right) \mathbf{C}_{2,G} + \sqrt{2} g \partial_t \mathbf{C}_{1,X} + \sqrt{2} \Omega_a \mathbf{C}_{1,G} \quad (3.35d)$$

To solve the steady state for the previous set of equations, one assumes $\partial_t C_{n,\alpha} = 0$, and imposes the condition that lower manifolds are more probable than higher manifolds. This means that the vacuum dominates over the subsequent states, and therefore the following criterion is considered:

$$C_{g,0} \approx 1 \gg C_{e,0}, C_{g,1} \gg C_{e,1}, C_{g,2}. \quad (3.36)$$

The steady state solutions for some coefficients are

$$C_{g,1} = \Omega_a \frac{g^2 \tilde{\omega}'_\sigma - \tilde{\omega}'_a{}^2 \tilde{\omega}'_\sigma + \tilde{\omega}'_a (\Omega_a^2 - \tilde{\omega}'_\sigma{}^2)}{g^4 - g^2 (\tilde{\omega}'_a{}^2 + 2\Omega_a^2 + 2\tilde{\omega}'_a \tilde{\omega}'_\sigma) + (\tilde{\omega}'_a{}^2 - \Omega_a^2) [\tilde{\omega}'_\sigma (\tilde{\omega}'_\sigma + \tilde{\omega}'_a) - \Omega_a^2]} \quad (3.37)$$

$$C_{g,2} = \frac{\Omega_a^2}{\sqrt{2}} \frac{g^2 - \Omega_a^2 + \tilde{\omega}'_\sigma (\tilde{\omega}'_\sigma + \tilde{\omega}'_a)}{g^4 - g^2 (\tilde{\omega}'_a{}^2 + 2\Omega_a^2 + 2\tilde{\omega}'_a \tilde{\omega}'_\sigma) + (\tilde{\omega}'_a{}^2 - \Omega_a^2) [\tilde{\omega}'_\sigma (\tilde{\omega}'_\sigma + \tilde{\omega}'_a) - \Omega_a^2]}, \quad (3.38)$$

where $\tilde{\omega}'_i = \tilde{\omega}_i - i\gamma_i/2$. These expressions correspond to the complete form of the solution, differing, for example, from the ones provided by Liang *et al.* [74], which are the approximated version (Although they are proven correct since the complete solutions vary up to the third decimal). The reason for only showing the explicit solution for these two coefficients is that the observables of main interest, i.e., the mean photon number and the second order correlation function, can be completely described by these coefficients as

$$n_a = \langle \Psi | \hat{a}^\dagger \hat{a} | \Psi \rangle = |C_{g,1}|^2 + |C_{e,1}|^2 + 2|C_{g,2}|^2 \approx |C_{g,1}|^2 \quad (3.39)$$

$$g^{(2)}(0) = \frac{\langle \Psi | \hat{a}^\dagger \hat{a}^\dagger \hat{a} \hat{a} | \Psi \rangle}{\langle \Psi | \hat{a}^\dagger \hat{a} | \Psi \rangle^2} \approx 2 \frac{|C_{g,2}|^2}{|C_{g,1}|^4}. \quad (3.40)$$

From Equation (3.40) it is seen that to achieve the perfect suppression of the $g^{(2)}(0)$, it suffices that the numerator of $C_{g,2}$ equals zero. So the condition turns out to be

$$\begin{aligned} g^2 - \Omega_a^2 + \tilde{\omega}'_\sigma(\tilde{\omega}'_\sigma + \tilde{\omega}'_a) &= 0 \\ 4(\tilde{\omega}_\sigma + \tilde{\omega}_a)\tilde{\omega}_\sigma + 4g^2 - 4\Omega_a^2 - (\kappa_a + \gamma_\sigma)\gamma_\sigma - 2i[\tilde{\omega}_a\gamma_\sigma + (\kappa_a + 2\gamma_\sigma)\tilde{\omega}_\sigma] &= 0, \end{aligned} \quad (3.41)$$

Since Equation (3.41) comprises both real and imaginary parts, each one must fulfill the equality, so the criteria can be rewritten as

$$\tilde{\omega}_\sigma = \pm \sqrt{\gamma_\sigma \frac{g^2 - \Omega_a^2}{\kappa_a + \gamma_\sigma} - \frac{\gamma_\sigma^2}{4}} \quad (3.42a)$$

$$\tilde{\omega}_a = -\left(\frac{\kappa_a}{\gamma_\sigma} + 2\right)\tilde{\omega}_\sigma. \quad (3.42b)$$

With Equations (3.42) it is possible to obtain the optimal parameters to generate antibunching via the unconventional photon blockade mechanism, by properly tuning the coupling rate g and the dissipative rates κ_a, γ_σ .

A criterion similar to the relationship found in the CPB for the $(\tilde{\omega}_a, \tilde{\omega}_\sigma)$ pairs can be found for the UPB by using the real part of the criteria (3.41)

$$\begin{aligned} 4(\tilde{\omega}_\sigma + \tilde{\omega}_a)\tilde{\omega}_\sigma + 4g^2 - 4\Omega_a^2 - (\kappa_a + \gamma_\sigma)\gamma_\sigma &= 0 \\ (\tilde{\omega}_\sigma + \tilde{\omega}_a)\tilde{\omega}_\sigma + g^2 &= \Omega_a^2 + \frac{\gamma_\sigma(\gamma_\sigma + \kappa_a)}{4}. \end{aligned} \quad (3.43)$$

Therefore it has been found that for the Jaynes Cummings model, the analytical curves that allow antibunching by UPB must satisfy Equation (3.43).

Now that both the analytical conditions for the generation of photon blockade in a conventional (Equation 3.28) and unconventional (Equation 3.43) framework have been found, it is time to solve the original problem given by Equation (3.25). To do this, the master equation formalism will be once again applied, by taking into account that the cavity can present losses at a rate κ_a , while the atom presents spontaneous emission given by γ_σ . The corresponding equation is

$$\partial_t \rho = i[\rho, H] + \frac{\kappa_a}{2} \mathcal{L}_{\hat{a}} \rho + \frac{\gamma_\sigma}{2} \mathcal{L}_{\hat{\sigma}} \rho = \mathcal{L} \rho. \quad (3.44)$$

This differential equation is numerically solved, in the same basis as referred before, $|\Psi\rangle = |\alpha, n\rangle$ truncating the analysis to a manifold that guarantees the convergence of the observables, such as the mean number of photons. Since this system is analyzed in a weak driving regime ($\Omega_i < \kappa, \gamma$), and there are no further excitation channels, it is found that a manifold up to two is enough to guarantee this convergence.

Both the mean photon number and the second order correlation function for the Driven-Dissipative Jaynes Cummings model are shown in Figure (3.9) as a function of rotating frame detunings $\tilde{\omega}_i/g$. On panel b.) it can be seen that the analytical conditions for antibunching via the CPB coincides with the lower and upper polariton branches given in panel a.), meaning that this blockade occurs at the higher photon occupancy rate. The dotted red line in panel b.) corresponds to the optimal antibunching condition for UPB (Equations 3.42), which

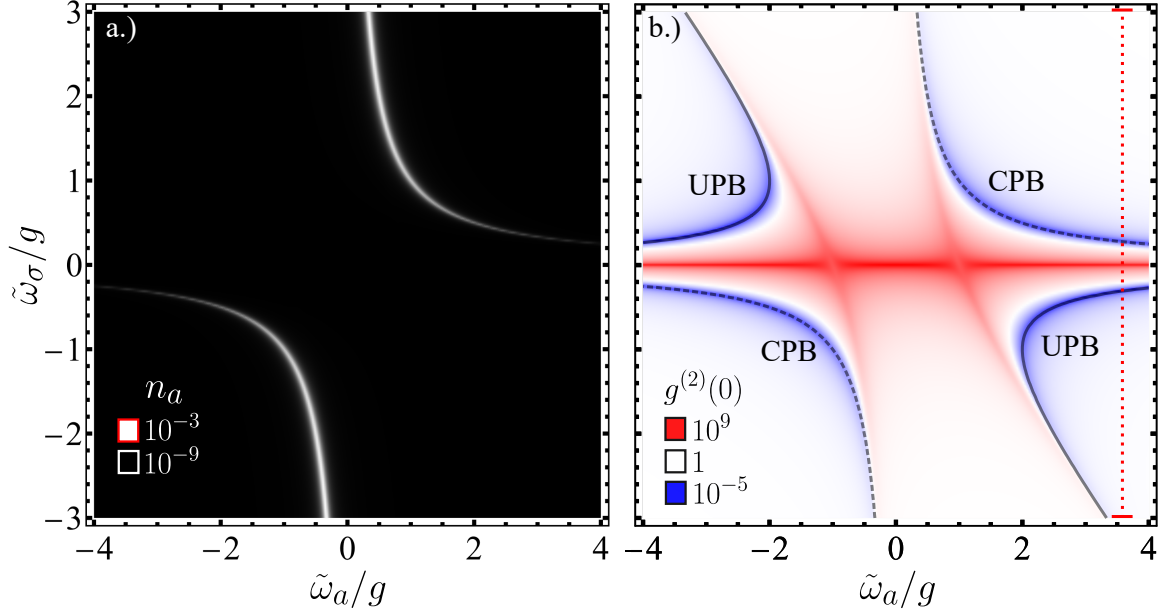


Figure 3.9 a.) Mean Photon number and b.) Second order correlation function of the Driven Dissipative Jaynes Cummings model as a function of rotating frame detunings $\tilde{\omega}_i/g$. Black lines in panel b.) Correspond to the analytical conditions given by Equations (3.28, 3.43), and the dotted red line cuts the UPB line for the minimal condition of the $g^{(2)}(0)$ given by Equations (3.42). Parameters: $\gamma_\sigma = 0.01g$, $\kappa_a = 0.1g$, $\Omega_a = 0.001g$, $\Omega_\sigma = 0$.

with the given parameters result in $\omega_a = 3.61764g$. Since a vertical line in this value exhibits all statistical dependences, i.e., antibunching due to UPB, laser statistics, superbunching, and antibunching due to CPB, it constitutes an ideal cut for analyzing the decomposition of the second order correlation function as explained in the section 2.5. The fundamental result of Figure (3.9) is proof that both CPB and UPB can coexist within the same range of parameters, and therefore it is possible with one system to explore the properties of both mechanisms. Due to this coexistence, the question of which properties each one possesses, and how they differ, arises. For this reason, it follows a characterization of the emission in order to find those relevant similarities and differences.

Starting with the correlation function decomposition, by means of the set of Equations (2.124), with $\hat{s} \rightarrow \hat{a}$, the terms I_k are calculated as a function of $\tilde{\omega}_\sigma/g$. The result of such decomposition is shown in Figure (3.10). It shows for example that the reason for obtaining coherent statistics when $\tilde{\omega}_\sigma/g = -3$ is different from the case with $\tilde{\omega}_\sigma/g = 3$, because the squeezing component I_2 tends to be less negative, together with a diminishing in the I_0 component, although both cases satisfy the relationship $I_0 \approx -I_2$. On the contrary, this figure indicates that the decomposition is not a suitable element to differentiate the nature of the blockades, because, in both conventional and unconventional features, the balance between the I_k components satisfies the same relationship, without appreciable differences for the points that minimize the blockade in both types. For that reason, in order to categorize fundamental differences between the blockades, other quantities must be considered.

Turning now not to the decomposition of the second order correlation function, but rather to the calculation of the n-th order correlation function, a fundamental difference between both types of blockades arises. Panel a.) of the Figure (3.11) shows that the conditions of conventional photon blockade, given as $\tilde{\omega}_a\tilde{\omega}_\sigma = g^2$,

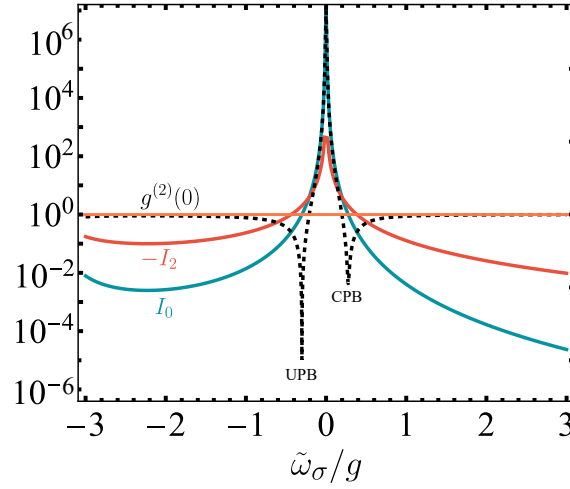


Figure 3.10 Decomposition of the $g^{(2)}(0)$ in the red line of Figure (3.9). Parameters: $\tilde{\omega}_a/g = 3.61764$, $\gamma_\sigma = 0.01g$, $\kappa_a = 0.1g$, $\Omega_a = 0.001g$, $\Omega_\sigma = 0$.

keep being completely fulfilled for all orders of the correlation functions. This contrast sharply with what is observed for the unconventional photon blockade, since it can be seen that the optimal condition for the $g^{(2)}$, given by Equations 3.42, does not coincide with the minimization curves of the UPB for increasing the order n . The consequence of this is, as shown in panel b.) is that there are no conditions for the atom and cavity detunings that could result in an *optimal antibunching* of the correlation functions for the unconventional mechanism. There is, however, a region where they can all be simultaneously minimized, in analogy to the two interacting cavities model. This value is found by the least squared methods, finding the condition that gives the best minimal value for each correlation function. This can be seen in panel c. where now, by properly selecting $\tilde{\omega}_\sigma$, it is possible to obtain $g^{(n)} < 1$ for all $n \in \{2, 3, 4\}$. However, it is important to emphasize that although the values are indeed lower than the uncorrelated limit, the $g^{(2)}$, in this case, is not sufficiently small for guaranteeing single photon emission. Therefore, the results indicate that the CPB contribution is the only mechanism that, on the driven Jaynes Cummings model, really consists of a single photon blockade, while the UPB lines are completely washed out due to the bunched nature of the higher-order correlation functions. With this set of parameters, it is proven that these systems can correctly act as a single photon source, once the criteria given by Equation (3.28) are met.

Now, having understood the nature of the blockade mechanisms in the driven Jaynes Cummings model, it is important to note that although in the original model, a coherent driving to the 2LS was included, the calculations until now have only dealt with CW pumping to the cavity. So, for completeness' sake, two conditions will be studied when this driving is taken into account: When $\Omega_\sigma = \Omega_a$, and when $\Omega_a = 0$, $\Omega_\sigma \neq 0$. Both cases will be directly evaluated next.

The general system of equations for the steady state, considering both types of drivings, can be written

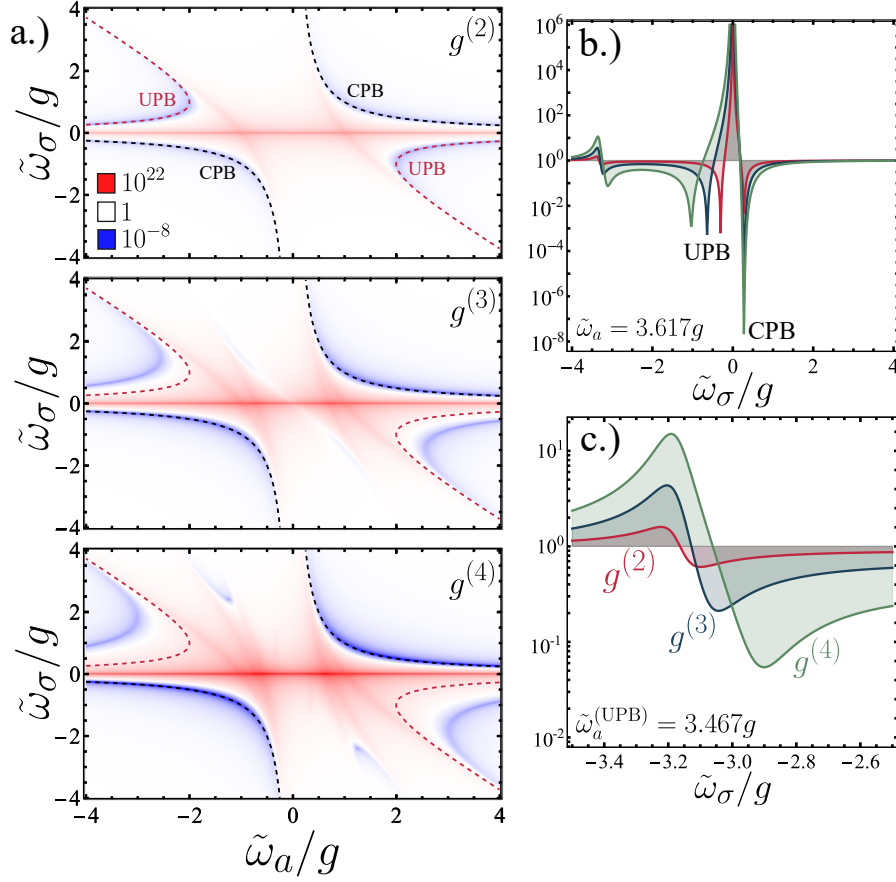


Figure 3.11 a.) Higher order correlation function analysis for the Jaynes Cummings model as a function of laser rotating frame detunings $\tilde{\omega}_i$. b.) Cut of the correlation functions through the optimal UPB value of the $g^{(2)}$, given by $\tilde{\omega}_a = 3.617g$. c.) Cut of the correlation functions through the value that provides the best simultaneous minimization for all orders, obtained by the least squares method, $\tilde{\omega}_a = 3.467g$. Parameters: $\gamma_\sigma = 0.01g$, $\kappa_a = 0.1g$, $\Omega_a = 0.001g$, $\Omega_\sigma = 0$.

in matrix form as

$$\begin{pmatrix} \tilde{\omega}'_a & g & \sqrt{2}\Omega_a & \Omega_\sigma \\ g & \tilde{\omega}'_\sigma & 0 & \Omega_a \\ \sqrt{2}\Omega_a & 0 & 2\tilde{\omega}'_a & \sqrt{2}g \\ \Omega_\sigma & \Omega_a & \sqrt{2}g & \tilde{\omega}'_a + \tilde{\omega}'_\sigma \end{pmatrix} \begin{pmatrix} C_{g1} \\ C_{e0} \\ C_{g2} \\ C_{e1} \end{pmatrix} = \begin{pmatrix} -\Omega_a \\ -\Omega_\sigma \\ 0 \\ 0 \end{pmatrix}, \quad (3.45)$$

$$\begin{pmatrix} \tilde{\omega}'_a & g & \sqrt{2}\Omega_a & \Omega_\sigma \\ g & \tilde{\omega}'_\sigma & 0 & \Omega_a \\ \sqrt{2}\Omega_a & 0 & 2\tilde{\omega}'_a & \sqrt{2}g \\ \Omega_\sigma & \Omega_a & \sqrt{2}g & \tilde{\omega}'_a + \tilde{\omega}'_\sigma \end{pmatrix} \begin{pmatrix} C_{1,G} \\ C_{0,X} \\ C_{2,G} \\ C_{1,X} \end{pmatrix} = - \begin{pmatrix} \Omega_a \\ \Omega_\sigma \\ 0 \\ 0 \end{pmatrix}, \quad (3.46)$$

where once again $\tilde{\omega}'_k = \tilde{\omega}_k - i\gamma_k/2$. From the coupled algebraic equations shown in Equation (3.45), it is once again possible to find the expression for each term C_{an} . However, as mentioned earlier, the only relevant

factor for generating the unconventional photon blockade consists of making the numerator of the coefficient C_{g2} equal to zero. For this reason, this will be the relevant expression to analyze. The condition is given in general terms as follows

$$-2g\Omega_a\Omega_\sigma(\tilde{\omega}'_a + \tilde{\omega}'_\sigma) + g^2(\Omega_a^2 + \Omega_\sigma^2) + \Omega_a^2(\Omega_\sigma^2 - \Omega_a^2 + \tilde{\omega}'_\sigma[\tilde{\omega}'_a + \tilde{\omega}'_\sigma]) = 0. \quad (3.47)$$

From this general equation, it is easy to analyze the conditions for achieving UPB. As the reader could show, making $\Omega_\sigma = 0$ in Equation (3.47) coincides with the condition presented in Equation (3.43).

To begin the analysis of the introduction of a coherent driving into the 2LS, let's start by making $\Omega_a = 0$ in Equation (3.47), while Ω_σ remains nonzero. This rapidly yields the following expression

$$g^2\Omega_\sigma = 0. \quad (3.48)$$

Since both g and Ω_σ are different from zero, the previous equation indicates that UPB in the Jaynes Cummings model cannot be achieved only through a coherent driving to the two level system. This means that all blockade mechanisms when only Ω_σ is present will be due to a conventional feature because one can still match the frequency of the driving to the energy of the $|\pm 1\rangle$ polariton, given by Equation (3.28). This can also be directly understood since the term $\Omega_\sigma(\hat{\sigma} + \hat{\sigma}^\dagger)$ only allows transitions between $|g, 0\rangle$ and $|e, 0\rangle$, therefore there are no suitable way that could access the state $|g, 2\rangle$ with Hamiltonian transitions.

For the next case, where the strength of both drivings is the same, the general condition simplifies as

$$\Omega^2[-2g(\tilde{\omega}'_a + \tilde{\omega}'_\sigma) + 2g^2 + \tilde{\omega}'_\sigma(\tilde{\omega}'_a + \tilde{\omega}'_\sigma)] = 0. \quad (3.49)$$

Expanding the terms $\tilde{\omega}'_k$ and splitting into two equations, one for the imaginary part and the other for the real one, gives (after some straightforward algebra) the following solutions for the UPB:

$$\tilde{\omega}_a = -\tilde{\omega}_\sigma \left(\frac{\kappa_a}{\gamma_\sigma} + 2 \right) + 2g \left(\frac{\kappa_a}{\gamma_\sigma} + 1 \right) \quad (3.50)$$

$$\tilde{\omega}_\sigma = 2g \pm \frac{1}{2} \sqrt{\frac{\gamma_\sigma [8g^2 - \gamma_\sigma(\gamma_\sigma + \kappa_a)]}{\gamma_\sigma + \kappa_a}}. \quad (3.51)$$

These are the conditions to enhance the minimization of the $g^{(2)}(0)$, in equivalence of the ones treated for the cavity driving (Given in Equations 3.42). To find the lines that sustain the whole UPB, rather than focusing only on the minimum point, one must calculate the real part of Equation (3.49) as a function of $\tilde{\omega}_a$ and $\tilde{\omega}_\sigma$. To understand the different forms such lines can take with varying driving strength, the next Figure takes into consideration different cases between the two types of driving.

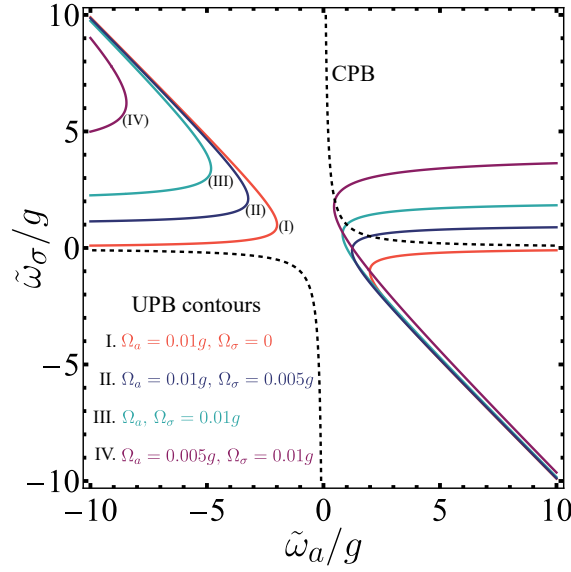


Figure 3.12 Unconventional photon blockade conditions to minimize $g^{(2)}$ for different rates of cavity and 2LS driving. For comparison, the CPB conditions are also displayed as the black dashed lines, coinciding with the case comparison, $\Omega_a = 0$ and $\Omega_\sigma \neq 0$. Parameters: $\gamma_\sigma = 0.01g$, $\kappa_a = 0.1g$.

Figure (3.12) takes into consideration several combinations between the coherent drivings to the cavity and the 2LS. The first case, where there is no driving to the 2LS, corresponds to the one analyzed in Figure (3.9). In that case, it was obtained that there must be a difference in the sign between cavity and matter detunings in order to generate UPB. Contrary to this, including the 2LS driving brings up an asymmetry that displaces the conditions, allowing to obtain UPB even when $\tilde{\omega}_a$ and $\tilde{\omega}_\sigma$ share the same sign, with the consequence that the range of $\tilde{\omega}_a$ must be extended in order to have a symmetric behavior in the conditions. Furthermore, as mentioned earlier, holding only driving to the 2LS does not allow the required transitions for interference, so the case where $\Omega_a = 0$ and $\Omega_\sigma \neq 0$ must directly correspond to a blockade in the conventional form.

Having understood the different features of the UPB when 2LS driving is also included, it is now time to proceed with the calculation of the statistics of the emission for the complete Hamiltonian given in Equation (3.25), for the cases where the driving is equal, and another where only 2LS pumping is considered.

The effects of the 2LS driving are shown in Figure (3.13). Panel a.) considers the case where Ω_a and Ω_σ are equal. For the chosen range of parameters in $\tilde{\omega}_a$ only one curve is able to generate UPB, although there is a complementary one as indicated by the line (II) in Figure (3.12). The minimum values in the statistics are of the same order in the $g^{(2)}$ as for the case where there was only driving to the cavity. Another important feature is that there is a crossing between the UPB and CPB lines, indicating that it is not only possible to generate simultaneous blockade in a system, but also, there are some conditions that hold both types of blockades, meaning that one can access the best features of each one at the same time. On the other hand, panel b.) considers uniquely a driving to the 2LS. In this case, it is obtained that the Unconventional photon blockade has no contribution to the emission, reaching a value in the $g^{(2)}$ of 10^{-6} , which is the lowest value achieved for the Jaynes Cummings model.

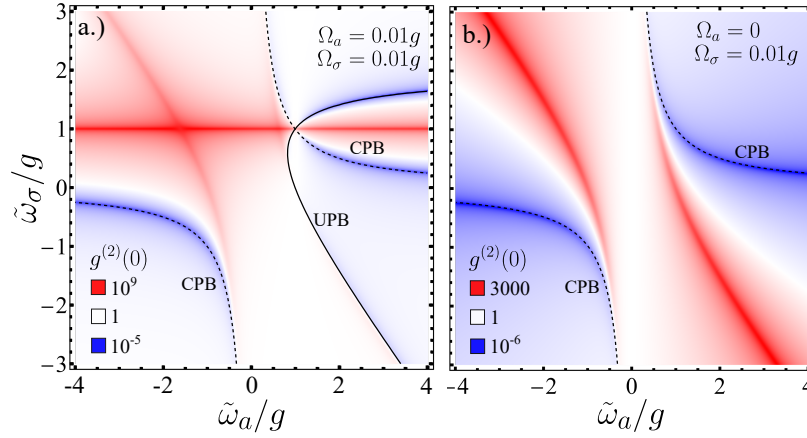


Figure 3.13 Effect of the coherent driving to the 2LS in the Jaynes Cummings statistics. The left panel (a.) considers the case where both drivings are equal, $\Omega_a, \Omega_\sigma = 0.01g$, while the right one (b.) considers only driving to the 2LS. Parameters: $\gamma_\sigma = 0.01g$, $\kappa_a = 0.1g$.

3.2.2 Experimental realizations

The theoretical results of the driven Jaynes Cummings model constitute a promising model to sustain real single photon emission through the correct tuning of the parameters. But now, to complete the landscape and prove its usefulness as a true single photon source, there must be a discussion about the experimental realizations of this model, as well as their limitations.

As previously indicated, in order to exhibit blockade in this system, it is necessary to sustain a strong coupling between light and matter. Although achieving this regime has always posed a technological challenge, current developments in semiconductor physics have allowed reaching this level of interaction with more ease. The seminal papers from Reithmaier *et al.* [75], Yoshie *et al.* [76] and Peter *et al.* [77] opened a field of research, where light and matter could experimentally hybridize to form a new quasiparticle known as polaritons. The strong coupling on those systems was confirmed by the anticrossing in the photoluminescence spectra between the cavity and exciton states, characterized by the vacuum Rabi splitting.

For our problem in consideration, we will follow the scheme proposed by Reithmaier, in which by means of molecular beam epitaxy (MBE), an InAs quantum dot is grown inside a pillar microcavity that consists of layers of distributed Bragg reflectors (DBR) of AlAs and GaAs. As shown in Figure (3.14), this setup has optical ranges of operation for the cavity and quantum dot, with $\omega \approx 1\text{eV}$, the coupling rate between light and matter is of the order of 0.1meV , while the dissipation rates are $\kappa_a = 10^{-2}\text{meV}$ and $\gamma_\sigma = 10^{-3}\text{meV}$. Taking into account that normally there is a small detuning between light and matter frequencies, that could be considered between 10meV , one could use tunable diode lasers, which nowadays range from 630nm to 2340nm (i.e. $1.968\text{eV} - 0.529\text{eV}$), in order to correctly find the optimal relationships between ω_L , g and $\omega_{a,\sigma}$ to get conventional or unconventional photon blockade. A similar setup to the one proposed has already been applied by multiple groups [30, 78, 79, 31, 41, 39, 80, 38] for building single photon sources based on semiconductor materials.

Although the previous set-up consists of a scheme of cavity QED, which has proven itself to be an adequate environment for the development of quantum technologies, there is another rising field that is suitable for achieving strong interactions between light and matter. This corresponds to the field of Circuit cavity electrody-

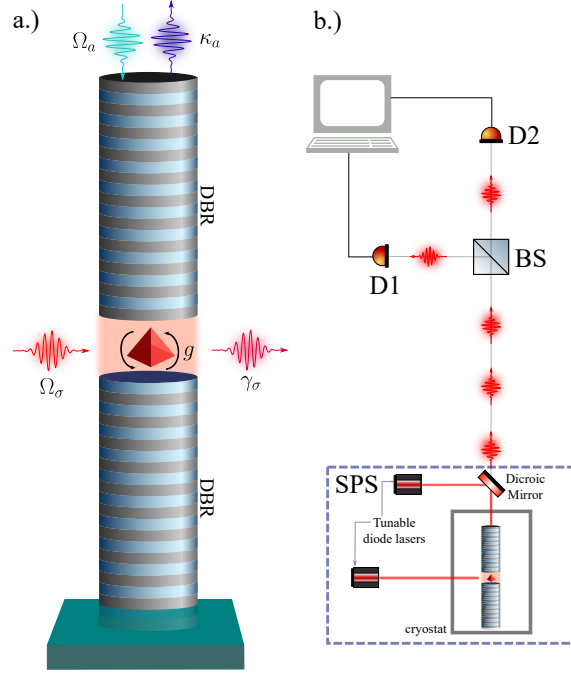


Figure 3.14 a.) Micropillar cavity of AlAs/GaAs DBR with an embedded InAs quantum dot that has been grown by molecular beam epitaxy that acts as an SPS b) Hanbury-Brown Twiss setup for measuring $g^{(2)}$.

namics (Circuit-QED), defined in which one employs superconducting circuits that act as qubits, and interact with confined light in the microwave domain. This field does not exclusively correspond to superconducting devices, but actually, it allows employing elements from circuit QED, to couple with a plethora of quantum systems, such as semiconductor quantum dots [81], generating hybrid quantum systems that get the best from the cavity and circuit QED. We refer to the excellent paper by Blais *et al.* [82] for an up-to-date review of current challenges and theoretical derivations for the superconducting elements.

For the particular experimental realization of strong coupling in circuit-QED, we refer to the seminal papers by Blais *et al.* [83] and Wallraff *et al.* [84], in which a superconducting two level system (Cooper pair box) is strongly coupled to a single photon stored in an on-chip cavity, formed by a superconducting transmission line resonator. In their system, the same condition for the Jaynes Cummings Hamiltonian is valid, but with a change in the frequency scale of the model. The coupling rate g for this model would be near 100MHz, while frequencies of the artificial atom and cavity are close to 6GHz, and dissipation rates are $\kappa_a/2\pi = 0.8\text{MHz}$, $\gamma_\sigma/2\pi = 0.7\text{MHz}$. Assuming a near resonance condition between the superconducting two level system frequency and the resonator frequency, the driving must excite the system with a frequency near of 5.9GHz and with a strength of the order of $\Omega = 0.1\text{MHz}$ in order to obtain photon blockade in the microwave regime.

3.2.3 Effects of frequency filtered correlations on photon blockade

As we previously mentioned in Section (2.4), the introduction of filters before the detection happens can alter the nature of the emission of a quantum source. The case study of such section calculated the frequency-resolved correlations from the Mollow triplet, where it was observed that the perfect antibunching associated with the

driven QD was completely changed, registering a different kind of photon statistics.

Connecting this with the framework of the photon blockade effect, the question if there are any differences between the single photon emission from the conditions of conventional and unconventional photon blockade effects naturally arises. First, we will recall that the conditions of CPB and UPB in the driven dissipative Jaynes Cummings model are given by the following relationships (3.28, 3.43):

$$\tilde{\omega}_a \tilde{\omega}_\sigma = g^2 \quad (3.52)$$

$$(\tilde{\omega}_\sigma + \tilde{\omega}_a) \tilde{\omega}_\sigma + g^2 = \Omega_a^2 + \frac{\gamma_\sigma(\gamma_\sigma + \kappa_a)}{4} \quad (3.53)$$

. We will select the same parameters that were used in Figure (3.9), i.e., $\gamma_\sigma = 0.01g$, $\kappa_a = 0.1g$, $\Omega_a = 0.001g$, $\Omega_\sigma = 0$. For the frequencies, $\tilde{\omega}_a, \tilde{\omega}_\sigma$ we will choose the same values that were employed on the decomposition of the $g^{(2)}$, which are $\tilde{\omega}_a/g = 3.61764$, $\tilde{\omega}_\sigma/g = -0.301454$ for the UPB and $\tilde{\omega}_a/g = 3.61764$, $\tilde{\omega}_\sigma/g = 1/\tilde{\omega}_a$ for CPB. Regarding the selected calculation method, we will apply the sensor method developed by Del Valle *et al.* [58], due to its facility for a computational calculation. The master equation is thus

$$H_s = \tilde{\omega}_a \hat{a}^\dagger \hat{a} + \tilde{\omega}_\sigma \hat{\sigma}^\dagger \hat{\sigma} + g(\hat{a}^\dagger \hat{\sigma} + \hat{a} \hat{\sigma}^\dagger) + \Omega_a(\hat{a} + \hat{a}^\dagger) \quad (3.54a)$$

$$H_\xi = \tilde{\omega}_{\xi_1} \hat{\xi}_1^\dagger \hat{\xi}_1 + \tilde{\omega}_{\xi_2} \hat{\xi}_2^\dagger \hat{\xi}_2 \quad (3.54b)$$

$$H_{\xi_s} = \varepsilon \left(\hat{\sigma}^\dagger \hat{\xi}_1 + \hat{\sigma} \hat{\xi}_1^\dagger + \hat{\sigma}^\dagger \hat{\xi}_2 + \hat{\sigma} \hat{\xi}_2^\dagger + \hat{a}^\dagger \hat{\xi}_1 + \hat{a} \hat{\xi}_1^\dagger + \hat{a}^\dagger \hat{\xi}_2 + \hat{a} \hat{\xi}_2^\dagger \right) \quad (3.54c)$$

$$\partial_t \rho = i[\rho, H_s + H_\xi + H_{\xi_s}] + \frac{\gamma_\sigma}{2} \mathcal{L}_\sigma \rho + \frac{\kappa_a}{2} \mathcal{L}_a \rho + \frac{\Gamma}{2} (\mathcal{L}_{\xi_1} \rho + \mathcal{L}_{\xi_2} \rho). \quad (3.54d)$$

This master equation is solved for the steady state. Afterward, the sensor cross correlated function, $g_\Gamma^{(2)} = \langle \hat{\xi}_1^\dagger \hat{\xi}_2^\dagger \hat{\xi}_2 \hat{\xi}_1 \rangle / \langle \hat{\xi}_1^\dagger \hat{\xi}_1 \rangle \langle \hat{\xi}_2^\dagger \hat{\xi}_2 \rangle$, is calculated as a function of the sensor frequencies $\tilde{\omega}_{\xi_1}, \tilde{\omega}_{\xi_2}$. By properly selecting the values of $\tilde{\omega}_a$ and $\tilde{\omega}_\sigma$ such as the conditions for the CPB and UPB are met, it is possible to study how frequency filtering alters the single photon emission rate from each one of the blockade mechanisms.

This effect is summarized in Figure (3.15), where the effects of frequency filtering for the CPB (Upper row) and UPB (Bottom row) for two values of the sensor bandwidth Γ are shown. Once again, it is proven that for both cases, adding frequency filters before the detection takes place alters the rate of emission of the photons, changing the statistical properties of emission, and thus generating a variety of correlations depending on the frequencies of the sensors. However, the most important feature is that there are some notable differences and similarities between both blockade mechanisms. For instance, With a narrow bandwidth $\Gamma = 0.001g$, a leapfrog process, such as the ones evidenced in the Mollow triplet, is observed for both types of blockades when the condition $\tilde{\omega}_{\xi_1} + \tilde{\omega}_{\xi_2} = 0$. This effect however is stronger in the UPB since by increasing the detector width, the bunched nature of the emission tends to remain present, while for the CPB this effects tend to an uncorrelated rate. Furthermore, in both graphs there is a grid of horizontal and vertical lines, which, as identified by Gonzalez-Tudela *et al.* [59] for the case of an incoherently driven Jaynes Cummings model, correspond to correlation between real states of subsequent manifolds.

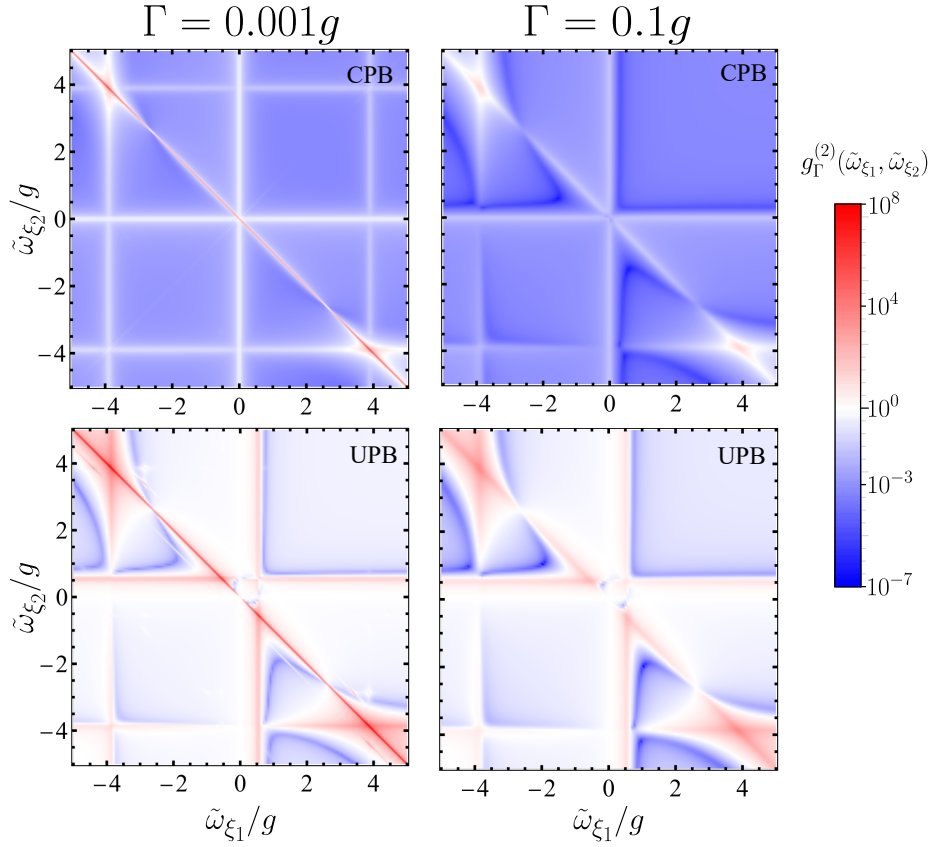


Figure 3.15 Frequency resolved correlations of the driven Jaynes Cummings model for the conditions that generate Conventional photon Blockade (Upper row) and Unconventional photon Blockade (Bottom row). Parameters: $\gamma_\sigma = 0.01g$, $\kappa_a = 0.1g$, $\Omega_a = 0.001g$, $\Omega_\sigma = 0$, $\varepsilon = 10^{-6}$.

Another striking difference between both mechanisms results when one analyzes the transition over those grids. Figure (3.16) displays a cut in the frequency-resolved correlations for a fixed value of $\tilde{\omega}_{\xi_1} = -3$, for the two previously employed detector bandwidth values. It can be observed that even for the narrow width $\Gamma = 0.001g$, CPB mostly continues to display the antibunching nature that was observed by the photons previous to the interaction with the filters, while for UPB the detection process completely alters the correlation process. This is further verified when increasing the sensor bandwidth, where UPB still exhibits bunching of the detected photons for some frequencies.

This elucidates that there is definitely a difference between the photons that are emitted from the conventional and the unconventional mechanisms, confirming that even after the introduction of frequency filters, the CPB maintains the single photon statistics of the emission.

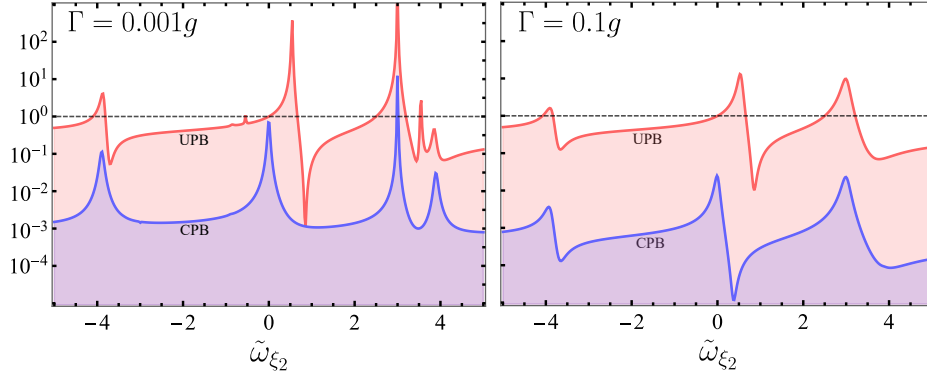


Figure 3.16 Frequency resolved correlation function of the sensors for a fixed frequency value $\tilde{\omega}_{\xi_1} = -3$, for two sensors bandwidth. The parameters are the same as in the previous figure.

3.2.4 The role of phonon mediated coupling in photon blockade

The contribution of *phonons*, i.e., the quantized vibrational modes of a solid, as mediators in light matter interaction is an effect that has been intensively studied [85, 86]. For example, in a series of papers Echeverri-Arteaga *et al.* explained that diverse effects, such as that of the appearance of an extra peak in off-resonant cavity-QED schemes [87], or a strange attraction phenomenon between cavity and exciton modes [88] can be successfully explained by the mechanism of Phonon mediated coupling (PhmC). In this section, we present how this mechanism can alter the photon blockade effect in a semiconductor QD-microcavity system.

As shown by Majumdar *et al.* [86], phonon-mediated coupling can be modeled by adding the following terms to the master equation

$$\frac{\gamma_\theta}{2} \mathcal{L}_{\hat{a}\hat{\sigma}^\dagger} \rho = \frac{\gamma_\theta}{2} (2\hat{a}\hat{\sigma}^\dagger \rho \hat{a}^\dagger \hat{\sigma} - \hat{a}^\dagger \hat{a} \hat{\sigma} \hat{\sigma}^\dagger \rho - \rho \hat{a}^\dagger \hat{a} \hat{\sigma} \hat{\sigma}^\dagger) \quad (3.55a)$$

$$\frac{P_\theta}{2} \mathcal{L}_{\hat{a}^\dagger \hat{\sigma}} \rho = \frac{P_\theta}{2} (2\hat{a}^\dagger \hat{\sigma} \rho \hat{a} \hat{\sigma}^\dagger - \hat{a} \hat{a}^\dagger \hat{\sigma}^\dagger \hat{\sigma} \rho - \rho \hat{a} \hat{a}^\dagger \hat{\sigma}^\dagger \hat{\sigma}), \quad (3.55b)$$

where γ_θ transfers an excitation of the cavity to the QD and P_θ corresponds to the inverse process. Therefore, the master equation within the framework of photon blockade is

$$\partial_t \rho = i[\rho, H] + \frac{\gamma_\sigma}{2} \mathcal{L}_{\hat{\sigma}} \rho + \frac{\kappa_a}{2} \mathcal{L}_{\hat{a}} \rho + \frac{\gamma_\theta}{2} \mathcal{L}_{\hat{a}\hat{\sigma}^\dagger} \rho + \frac{P_\theta}{2} \mathcal{L}_{\hat{a}^\dagger \hat{\sigma}} \rho. \quad (3.56)$$

With H given by Equation (3.25). We will analyze how the addition of these terms affects the previously studied conditions for photon blockade. For this reason, the same parameters that were used in Figure (3.9) will be maintained, while varying the strengths of γ_θ, P_θ . Following the procedure for the last subsection, the effects for CPB and UPB are analyzed separately, by means of the adequate tuning of the parameters $\tilde{\omega}_a, \tilde{\omega}_\sigma$, where once again, for UPB these values are $\tilde{\omega}_a/g = 3.61764$, $\tilde{\omega}_\sigma/g = -0.301454$ for the UPB and $\tilde{\omega}_a/g = 3.61764$, $\tilde{\omega}_\sigma/g = 1/\tilde{\omega}_a$ for CPB. As for the case with frequency-filtered correlations, Figure (3.17) indicates that there is also an intrinsic difference between both mechanisms against the dissipation given by photon mediate coupling. It can be observed that only for high values of the rates $\gamma_\theta/g, P_\theta/g$ the conventional photon blockade mechanism affected, however still maintaining values of $g^{(2)}(0) \approx 0.5$. On the other hand, unconventional photon blockade is much more sensitive to these effects, where even a small contribution of the phonon-mediated rates can destroy the process of quantum interference and thus generate bunching behavior on the system.

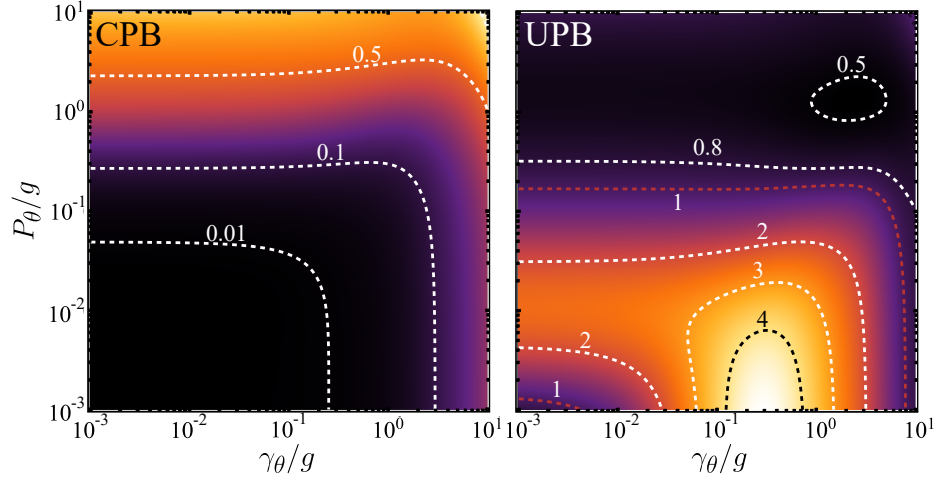


Figure 3.17 Effects of phonon mediated coupling dissipative terms γ_θ, P_θ on each mechanism of the photon blockade. Parameters: $\gamma_\sigma = 0.01g$, $\kappa_a = 0.1g$, $\Omega_a = 0.001g$, $\Omega_\sigma = 0$.

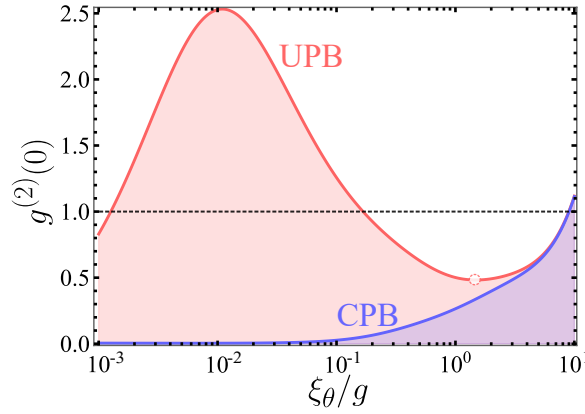


Figure 3.18 Effect of the simultaneous phonon mediated coupling rate ξ_θ on the mechanisms of photon blockade.

To further clarify this difference, we analyze the simultaneous values of the PhmC rates, i.e., $P_\theta, \gamma_\theta = \xi_\theta$ on both mechanisms of photon blockade. As it can be seen from Figure (3.18), CPB only suffers noticeable changes on the second order correlation function when $\xi_\theta/g \approx 10^{-1}$, which can be related to the value of κ_a , and then continue to increase smoothly as the factor ξ_θ grows. On the contrary, the effect that this rate has on unconventional photon blockade is to destroy all antibunched correlations, even for small values of ξ_θ . It is nonetheless interesting to notice that the second order correlation function in the UPB appears to have a polynomial tendency (The x-axis is displayed in log10 scale), showing a maximum value ($\xi_\theta/g = 10^{-2}$), which could be related to the QD dissipative rate γ_σ . After this maximum is reached, it keeps decreasing, even partially restoring antibunching, until arriving at a minimum value, which is observed for $\xi_\theta/g \approx 1.47$, from which it displays the same nature as the CPB.

These results indicate that phonon-mediated coupling directly alters the single photon emission via pho-

ton blockade in a driven dissipative Jaynes Cummings scheme, and with an adequate selection of the PhmC rates, it could be used to suppress antibunching of UPB without altering the emission due to CPB.

3.2.5 Photon blockade beyond the strong coupling regime

The most important development of light matter interaction for circuit QED was that strong coupling was easier to achieve than in cavity QED systems, where the condition of $\omega > g > |\kappa_a - \gamma_\sigma|/4$ could be accessed in the microwave region using superconducting devices. Furthermore, these setups allowed to experimentally achieve a new regime of light matter interaction: the *Ultrastrong coupling regime* (USC). This regime is theoretically defined when one has interaction strengths near the characteristic frequencies of the system, which is bounded by the limit $\omega/g < 10$ [89, 90]. Niemczyk *et al.* [91] were among the first teams to provide an experiment of USC in circuit QED. Furthermore, another regime where the interaction strength is even greater than the resonant frequencies of the system has also been proposed, the so-called *Deep strong coupling regime* (DSC), where effects such as a decoupling of light and matter interaction take place.

Using perturbation theory to calculate the corrections to the energy due to the interaction in the Jaynes-Cummings Hamiltonian, it is possible to see that when g is in the strong coupling regime, corrections due to counter-rotating terms in the Hamiltonian can be safely neglected. Contrary to this, in the USC coupling regime, since the interaction rates are comparable to the frequencies of the system, the corrections due to the terms proportional to $g^2/(\omega_a + \omega_\sigma)$ must be considered, and thus, the rotating wave approximation performed over the interaction term cannot be discarded and must be taken into account. This means that the Jaynes Cummings model must be upgraded to the full quantum interaction model, given by the quantum Rabi model

$$H = \omega_a a^\dagger a + \omega_\sigma \sigma^\dagger \sigma + g(a + a^\dagger)(\sigma + \sigma^\dagger). \quad (3.57)$$

The main difference from this model with respect to the Jaynes Cummings model is that in the strong coupling regime, the Hilbert space could be decoupled as infinite independent two level systems, each one describe by a Hamiltonian $H^{(n)}$ as given by Equation (2.74). Contrary to this, the presence of the terms $a^\dagger \sigma^\dagger + a \sigma$ connects two manifolds, where a coupling between states $|G, n\rangle$ and $|X, n+1\rangle$ is now possible. This implies that the Hamiltonian does not conserve the total number of excitations, so the solution of the spectral properties of the system becomes nontrivial. The distinctive trait of the quantum Rabi model is that it preserves the same parity of the states, given by the parity operator $\Pi = -\sigma_z(-1)^{a^\dagger a}$.

Another relevant aspect that must be inspected when treating light matter interactions in the USC regime is the fact that many of the theoretical tools employed to characterize the dynamics of the interaction, fail to provide a correct picture to describe the problem. As pointed out by Le Boité *et al.* [89], the description through a master equation approach fails to correctly account for the dynamics of the system. Furthermore, as has been substantially used throughout the calculations in this thesis, the presence of coherent driving to the cavity and atom is fundamental for the development of photon blockade. In an environment where counter-rotating terms cannot be neglected, the rotating frame transformation fails to generate a time-independent framework and more sophisticated strategies must be applied, such as using Floquet theory.

But truly the most noteworthy deviation from the strong coupling corresponds to the calculation of the correlation functions for the analysis of photon statistics, which directly relates to the topic at hand of this thesis, photon blockade. The problem is that a direct application of the correlation functions through the cavity

operators as $g^{(n)} = \langle a^{\dagger n} a^n \rangle / \langle a^{\dagger} a \rangle^n$ would predict an unphysical stream of photons, as pointed out by Ridolfo *et al.* [92]. In fact, they were also the first to address the problem of photon blockade in the ultrastrong coupling regime. They derived the correct input-output relationships, given as

$$a_{\text{out}}(t) = a_{\text{in}}(t) - i \frac{\mathcal{E}_c}{\sqrt{8\pi^2 \hbar \mathcal{E}_0 v}} \dot{X}^+.$$

The main difference is that \dot{X}^+ does not directly correspond to the cavity operator a , as in the strong coupling case. The second order correlation function is thus

$$g^{(2)}(\tau) = \lim_{t \rightarrow \infty} \frac{\langle \dot{X}^-(t) \dot{X}^-(t+\tau) \dot{X}^+(t+\tau) \dot{X}^+(t) \rangle}{\langle \dot{X}^-(t) \dot{X}^+(t) \rangle^2}.$$

The most important result from the photon statistics by Ridolfo *et al.* is that when the cavity and an atom enter an ultra strong coupling regime, the photon blockade vanishes due to the emergence of parametric processes with origin from the counter-rotating terms in the Hamiltonian. To further study this, Le Boité *et al.* [93] studied the fate of photon blockade in the deep strong coupling regime. They found that the photon statistics suffer multiple transitions as the rate g/ω_a keeps increasing, finding first a breakdown of photon blockade for values where $g \sim 0.45\omega_a$, while a subsequent revival characterized by a strong antibunching could be found in regimes where $1 \leq g/\omega_a \leq 2.5$.

We will leave the rigorous analysis of photon blockade in the USC and DSC regimes for further studies.

3.3 Single photon polarization switch via photon blockade

In this section, we will apply all the tools employed beforehand regarding the methods to analyze the phenomena of photon blockade, to characterize a particular system that could be used as a feasible single photon source: An elliptical microcavity with an embedded quantum dot that is being excited with an external magnetic field. The role of the magnetic field will be that of acting as a parameter of control to modify both the photon occupation and the emission statistics.

The Hamiltonian that describes this system consists of four contributions: Excitons, Cavity, Magnetic field, and Coherent excitation. Each term will be explained next.

On the first hand, we will assume that the embedded quantum dot presents an asymmetry that splits the exciton states into two linearly polarized states, with frequencies ω_1 and ω_2 for x and y polarizations, respectively. Both frequency modes are related through the fine structure splitting, $\delta = \omega_2 - \omega_1$, which will be taken to be $\delta = 0.1\text{meV}$.

$$H_{\text{QD}} = \omega_1 \sigma_{11} + \omega_2 \sigma_{22} + \frac{\delta}{2} (\sigma_{12} + \sigma_{21}), \quad (3.58)$$

where $\sigma_{ij} = |i\rangle \langle j|$, with $i, j = 0, 1, 2$, are the transition operators of the excitons, with $|0\rangle$ being the ground state, $|1\rangle$ the excited state for photons with x polarization and $|2\rangle$ the excited state for the ones with y polarization. On the other hand, the micropillar system is considered to have an elliptical symmetry, causing the cavity to sustain two orthogonal and linearly polarized modes, labeled as x and y cavity modes. This micropillar has an asymmetry that generates that the cavity frequencies are non-degenerate. We will fix the x-mode frequency to

be $\omega_x = 1000 \text{ meV}$, while for the y mode $\omega_y = \omega_x + 0.2$. Each mode only interacts with the exciton state that has the same polarization and does it with an interaction strength given by g

$$H_{\text{cav}} = \omega_x a_x^\dagger a_x + g(a_x^\dagger \sigma_{01} + a_x \sigma_{10}) + \omega_y a_y^\dagger a_y + g(a_y^\dagger \sigma_{02} + a_y \sigma_{20}). \quad (3.59)$$

The next relevant contribution to the Hamiltonian, as previously mentioned, will be the effect of the magnetic field, where depending on the direction of the appliance it is possible to obtain different responses from the excitonic system. The most relevant application of the magnetic field is to indirectly populate *dark excitonic* (DE) states, i.e., states that do not optically interact with light, as opposed to the *bright excitonic* (BE) states that will be considered hereafter. The reason to avoid the contributions of the DE states to the Hamiltonian is that the direction of the magnetic field will be considered to be fixed and parallel to the direction of growth of the QD, in the so-called Faraday configuration. This configuration has the characteristic that it will only open, but not mix the BE and DE states. As shown by Jiménez-Orjuela *et al.* [94] when the magnetic field is taken to be parallel to the direction of growth of the QD, the DE population is significantly reduced, and thus, the contributions can be safely neglected. The magnetic field Hamiltonian is

$$H_{\text{mag}} = i\beta(\sigma_{12} - \sigma_{21}) + \alpha B^2(\sigma_{11} + \sigma_{22}), \quad (3.60)$$

with $\beta = \mu_B B \sin \theta (g_{ez} + g_{hz})/2$, $\mu_B = 0.0579 \text{ meV/T}$ is the Bohr magneton, $g_{ez} = -0.8$ are the electron and hole $g_{hz} = -2.2$ g-factors in the z direction, and $\alpha = 0.02 \text{ meV/T}^2$ is the diamagnetic shift. These values are typical for InAs/GaAs Quantum dots. Finally, the cavity and quantum dot are exposed to coherent drivings, which are described as

$$H_{\text{pump}} = \Omega_i(a_i^\dagger e^{-i\omega_L t} + \text{c.c.}) + \Omega_\alpha(\sigma_{\alpha 0} e^{-i\omega_L t} + \text{c.c.}), \quad (3.61)$$

where $i = x, y$ is the coherent excitation to the cavity and $\alpha = 1, 2$ is the one to the QD. Therefore, having understood each particular contribution, the total Hamiltonian for the system is

$$H_{\text{total}} = H_{\text{QD}} + H_{\text{mag}} + H_{\text{cav}} + H_{\text{pump}}. \quad (3.62)$$

Once again, it is convenient to transform the total Hamiltonian (3.62) to a frame that rotates with the laser frequency, eliminating the explicit time dependence present in the coherent driving, translating the relationships to the frequencies of the cavity and the Quantum Dot. In that regard, the relevant detuning is built as the difference between the laser frequency ω_L and the central frequency of the micropillar modes, i.e., $\Delta_L = \omega_c - \omega_L$, where $\omega_c = (\omega_x + \omega_y)/2$. The excitons frequencies are detuned from the cavity central frequency by $\omega_c - \omega_0 = 0.5 \text{ meV}$, establishing $\omega_1 = \omega_0 - \delta/2$, $\omega_2 = \omega_0 + \delta/2$.

We will perform two calculations to solve the dynamics of this system. First, we will give the numerical description by solving the following master equation in the Lindblad form,

$$\begin{aligned} \partial_t \rho = & i[\rho, H_{\text{total}}] + \frac{\kappa}{2} \{ \mathcal{L}_{a_x} \rho + \mathcal{L}_{a_y} \rho \} \\ & + \frac{\gamma}{2} \{ \mathcal{L}_{\sigma_{01}} \rho + \mathcal{L}_{\sigma_{02}} \rho \}, \end{aligned} \quad (3.63)$$

where $\kappa(\gamma)$ represents the cavity(QD) dissipation rate. The relevant observables of the system are calculated by solving Equation (3.63), projecting it into a basis that corresponds to the outer product of light and matter states, $|\Psi\rangle = |n_x, n_y\rangle \otimes |\alpha\rangle$, where, as previously indicated, α applies solely to the bright exciton's basis, i.e. $\alpha \in \{0, 1, 2\}$, and n_i corresponds to the number of photons of the i th mode.

We will also apply the same analytical treatment that was extensively used in earlier sections, which consists of using the wave function approximation and solving the Schrödinger equation for a Hamiltonian that contains the dissipation rates shown in the master equation (3.63), with a wave function that is truncated up to the second manifold. To our problem under consideration, given that we have taken a weak driving limit, i.e. $\Omega \ll \gamma, \kappa$, a wavefunction up to the second manifold will suffice to describe the system. Using the same notation as for the numerical solution, $|n_x, n_y, \alpha\rangle$, the relevant wavefunction will be

$$|\Psi\rangle = C_{100}|100\rangle + C_{010}|010\rangle + C_{001}|001\rangle + C_{002}|002\rangle \\ + C_{200}|200\rangle + C_{110}|110\rangle + C_{020}|020\rangle + C_{101}|101\rangle + C_{011}|011\rangle + C_{102}|102\rangle + C_{012}|012\rangle. \quad (3.64)$$

the line break is made on purpose to separate the first and second manifolds. The non-Hermitian operator is constructed by using the Hamiltonian given in Equation (3.62) and adding the following dissipative terms, in accordance with the master equation (3.63)

$$H_{\text{eff}} = H_{\text{total}} - i\frac{\kappa}{2}(a_x^\dagger a_x + a_y^\dagger a_y) - i\frac{\gamma}{2}(\sigma_{11} + \sigma_{22}). \quad (3.65)$$

The Schrödinger equation can be written in matrix form by projecting into the basis established on the wave function, and writing a differential equation for each one of the coefficients C_{α, n_x, n_y} .

$$M = \begin{pmatrix} \tilde{\omega}'_x & 0 & g & 0 & \sqrt{2}\Omega_x & 0 & 0 & 0 & 0 & 0 & 0 \\ 0 & \tilde{\omega}'_y & 0 & g & 0 & \Omega_x & 0 & 0 & 0 & 0 & 0 \\ g & 0 & \tilde{\omega}'_1 & \delta/2 - i\beta & 0 & 0 & 0 & \Omega_x & 0 & 0 & 0 \\ 0 & g & \delta/2 + i\beta & \tilde{\omega}'_2 & 0 & 0 & 0 & 0 & 0 & \Omega_x & 0 \\ \sqrt{2}\Omega_x & 0 & 0 & 0 & 2\tilde{\omega}'_x & 0 & 0 & \sqrt{2}g & 0 & 0 & 0 \\ 0 & \Omega_x & 0 & 0 & 0 & \tilde{\omega}'_x + \tilde{\omega}'_y & 0 & 0 & g & g & 0 \\ 0 & 0 & 0 & 0 & 0 & 0 & 2\tilde{\omega}'_y & 0 & 0 & 0 & \sqrt{2}g \\ 0 & 0 & \Omega_x & 0 & \sqrt{2}g & 0 & 0 & \tilde{\omega}'_1 + \tilde{\omega}'_x & 0 & \delta/2 - i\beta & 0 \\ 0 & 0 & 0 & 0 & 0 & g & 0 & 0 & \tilde{\omega}'_1 + \tilde{\omega}'_y & 0 & \delta/2 - i\beta \\ 0 & 0 & 0 & \Omega_x & 0 & 0 & 0 & \delta/2 + i\beta & 0 & \tilde{\omega}'_2 + \tilde{\omega}'_x & 0 \\ 0 & 0 & 0 & 0 & 0 & 0 & \sqrt{2}g & 0 & \delta/2 + i\beta & 0 & \tilde{\omega}'_2 + \tilde{\omega}'_x \end{pmatrix}, \quad (3.66)$$

where the equations are written in the order given by the following coefficient vector

$$x = (C_{100}, C_{010}, C_{001}, C_{002}, C_{200}, C_{110}, C_{020}, C_{101}, C_{011}, C_{102}, C_{012})^T,$$

and the frequencies are given as $\tilde{\omega}'_{x(y)} = \tilde{\omega}_{x(y)} - i\kappa/2$ and $\tilde{\omega}'_{1(2)} = \tilde{\omega}_{1(2)} - i\gamma/2 + \alpha B^2$ (the tilde denotes that we are on the laser rotating frame). Due to the weak pumping limit, the coefficient from each manifold must be bigger than the ones from the subsequent manifold, e.g. $C_{000} = 1 \gg C_{100} \gg C_{200}$. This means that some simplifications to the M matrix can be made, such as turning to zero the higher order elements that appear on

the first manifold of equations. This allows solving each manifold iteratively:

$$M^{(1)} \rightarrow \begin{pmatrix} \tilde{\omega}'_x & 0 & g & 0 \\ 0 & \tilde{\omega}'_y & 0 & g \\ g & 0 & \tilde{\omega}'_1 & \delta/2 - i\beta \\ 0 & g & \delta/2 + i\beta & \tilde{\omega}'_2 \end{pmatrix} \begin{pmatrix} C_{100} \\ C_{010} \\ C_{001} \\ C_{002} \end{pmatrix} = \begin{pmatrix} -\Omega_x \\ 0 \\ 0 \\ 0 \end{pmatrix}. \quad (3.67)$$

$$M^{(2)} \rightarrow \begin{pmatrix} 2\tilde{\omega}'_x & 0 & 0 & \sqrt{2}g & 0 & 0 & 0 \\ 0 & \tilde{\omega}'_x + \tilde{\omega}'_y & 0 & 0 & g & g & 0 \\ 0 & 0 & 2\tilde{\omega}'_y & 0 & 0 & 0 & \sqrt{2}g \\ \sqrt{2}g & 0 & 0 & \tilde{\omega}'_x + \tilde{\omega}'_1 & 0 & \delta/2 - i\beta & 0 \\ 0 & g & 0 & 0 & \tilde{\omega}'_y + \tilde{\omega}'_1 & 0 & \delta/2 - i\beta \\ 0 & g & 0 & \delta/2 + i\beta & 0 & \tilde{\omega}'_x + \tilde{\omega}'_2 & 0 \\ 0 & 0 & \sqrt{2}g & 0 & \delta/2 + i\beta & 0 & \tilde{\omega}'_y + \tilde{\omega}'_2 \end{pmatrix} \begin{pmatrix} C_{200} \\ C_{110} \\ C_{020} \\ C_{101} \\ C_{011} \\ C_{102} \\ C_{012} \end{pmatrix} = \begin{pmatrix} -\sqrt{2}\Omega_x C_{100}^{S(1)} \\ -\Omega_x C_{010}^{S(1)} \\ 0 \\ -\Omega_x C_{001}^{S(1)} \\ 0 \\ -\Omega_x C_{002}^{S(1)} \\ 0 \end{pmatrix}. \quad (3.68)$$

We have added the notation $S(1)$ to highlight that those coefficients are not variables, but the solutions of the form $C_{\alpha,n_x,n_y}(B,\Delta_L)$ derived from the first manifold.

The analytical expression for the observables of interest can be found in terms of the coefficients $C_{n_x,n_y,\alpha}$ as (We do not provide the explicit expressions for the coefficients, since they are way too bulky to give a compact representation).

$$n_x \approx |C_{100}|^2 \quad (3.69a)$$

$$n_y \approx |C_{010}|^2 \quad (3.69b)$$

$$g_x^{(2)} \approx 2 \frac{|C_{200}|^2}{|C_{100}|^4} \quad (3.69c)$$

$$g_y^{(2)} \approx 2 \frac{|C_{020}|^2}{|C_{010}|^4}. \quad (3.69d)$$

Once the theoretical framework has been understood, it is time to show some of the most relevant results that this system displays. To start understanding the inherent properties of this system, Figure (3.19) shows the calculations of the eigenenergies of the total Hamiltonian (Eq. 3.62), which shows the anticrossings of the exciton states with the x and y cavity modes. This occurs for $B = 3T, B = 3.75T$ respectively, and repeats once again for $B = 3T, B = 3.75T$.

As previously analyzed by Jiménez-Orjuela et al. [95], the system of an elliptical micropillar with an embedded quantum dot, subject to an external magnetic field in the Faraday configuration is an ideal setup for controlling polarization states inside the cavity, just by properly selecting the strength of the magnetic field, acting thus as an optical polarization switch. This means that incident photons with a particular polarization could leave the orthogonal state after the interaction with the system has taken place.

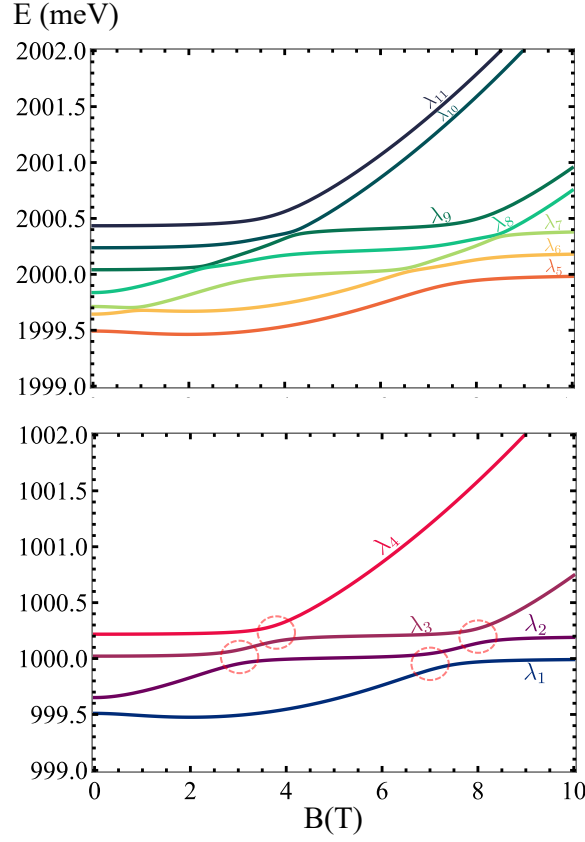


Figure 3.19 Eigenenergies of the total Hamiltonian as a function of the magnetic field. The first manifold shows clear anticrossings at $B = 3\text{T}$ and $B = 3.75\text{T}$ which corresponds to the interaction of the exciton states with the x and y mode of the cavity, respectively. This behaviour repeats itself for $B = 7\text{T}$ and $B = 8\text{T}$.

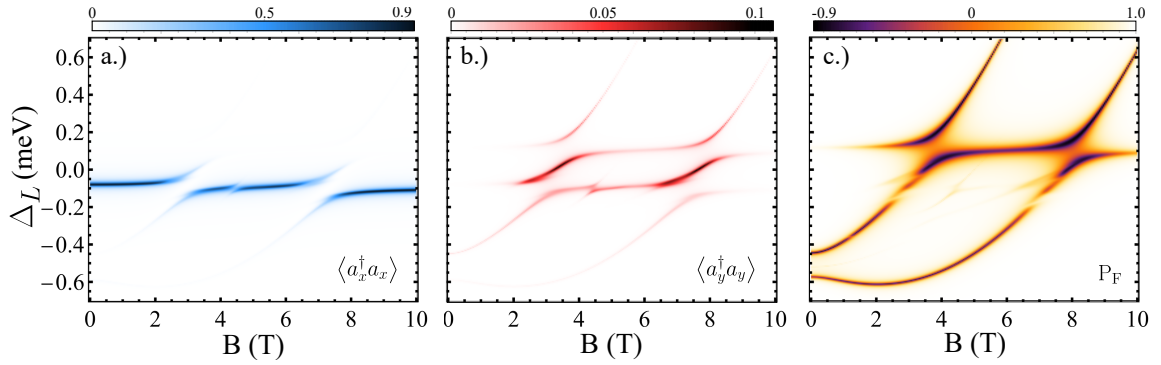


Figure 3.20 Cavity mean photon number for x (a.) and y (b.) polarization, and polarization factor (c.) as a function of the magnetic field (B) and driving frequency detuning (Δ_L). Parameters: $\Omega_x = 0.001\text{ meV}$.

The efficiency of the rate on which photons transform into the orthogonal polarization, is measured through the polarization factor (P_F) defined as

$$P_F = \frac{\langle a_x^\dagger a_x \rangle - \langle a_y^\dagger a_y \rangle}{\langle a_x^\dagger a_x \rangle + \langle a_y^\dagger a_y \rangle}. \quad (3.70)$$

Depending on the pumping to the cavity, this polarization factor will have positive or negative values. For example, when there is a coherent driving to the x mode, a value of -1 corresponds in this case to a complete switch on the polarization state, while if a coherent driving to the y mode is considered, the polarization switch would happen when P_F is 1. In accordance with [95], Figure (3.20) shows the behavior of cavity occupation and the polarization factor P_F as a function of the magnetic field strength B and laser frequency detuning Δ_L , when only driving to the x-cavity mode has been considered. The populations for cavity mode with x-polarization exhibit two anticrossings, for $B = 3$ T and $B = 7$ T, corresponding to the points where the QD interacts with the cavity with the x polarization mode which can also be seen on the diagonalization of the Hamiltonian. On the other hand, since the magnetic field mixes the x and y exciton polarization modes, the cavity occupations for the y mode presents a triple anticrossing, at $B = 3$ T where there is an interaction of the QD and the cavity with x polarization and at $B = 3.75$ T, where the interaction between the QD and the cavity with y polarization takes place. The same behaviour repeats for $B = 7$ T and $B = 8$ T, respectively. Finally, the third panel of this figure shows that the optimal polarization switch coincides with the interaction between the QD and the cavity mode with the orthogonal polarization to the driving, in this case for the y polarization mode. This means that by properly selecting the values of B and Δ_L it is possible to generate photons with a state orthogonal to the driving mode, completing the optical switch.

Now, the following relevant question is to analyze whether this system is able to sustain photon blockade, acting thus as a *single photon polarization switch*, which could have relevant potential applications in the development of quantum technologies. To this end, we follow the standard procedure performed throughout this section, by calculating the second order correlation function for both cavity modes, then analyzing the constituent factors via the incoherent decomposition (2.122) and finally, contrasting the $g^{(2)}$ results with higher order correlation functions to verify single photon behavior. We first fixed the magnetic field strength to coincide with the optimal photon conversion to the y mode cavity polarization, which happens at $B = 3.75$ T, and characterize the dependence of the statistics with the laser frequency detuning.

As shown in Fig. (3.21), for some values of Δ_L , there are regions where the mean number of photons of the orthogonal mode to the driving (y-polarization) has a higher population than the driven cavity mode. Furthermore, panel b. of this Figure analyzes the statistics of the emission by means of the $g_i^{(2)}(0)$. It can be seen that for the same values where $\langle a_y^\dagger a_y \rangle$ is enhanced over the x-cavity mode population ($\Delta_L \approx 0.05$ and $\Delta_L \approx 0.2$), there is a reduction on the second order correlation function up to an order of 10^{-2} , favoring single photon emission, and complementarily increasing the brightness of the source due to the increase in photon number. There is also a value of the frequency where $g_y^{(2)}$ is as low as 4×10^{-4} , but presenting a decrease in the cavity population, which is of the order of 10^{-3} . Contrary to this, the statistics for the x-polarization mode mostly fluctuate around the value for a coherent source ($g^{(2)} = 1$), or yields bunched behavior, as for the values of Δ_L that increases the mean population.

Since the relevant antibunching conduct is the one exhibited by the orthogonal mode of the driving, in

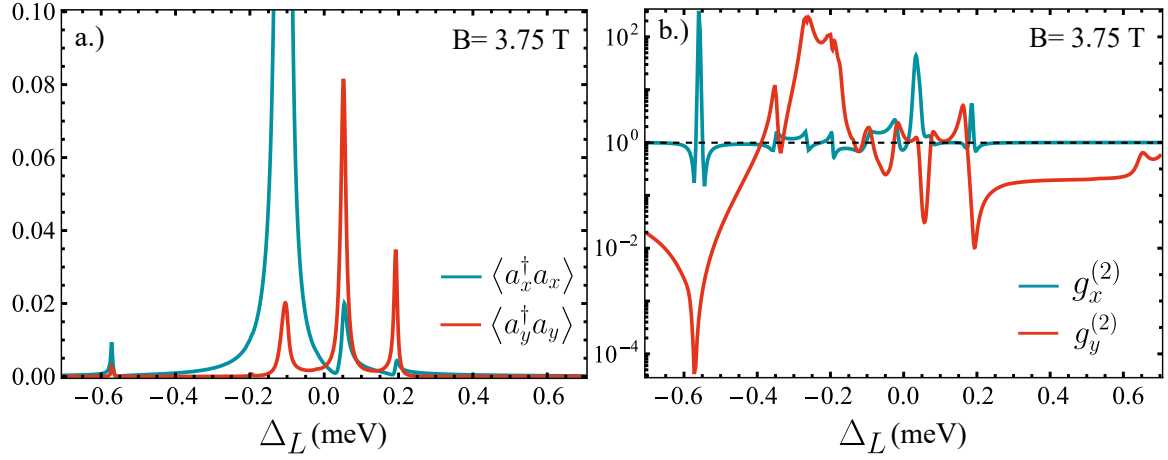


Figure 3.21 Mean photon number (a.) and second order correlation function (b.) for both cavity polarization modes as a function of the driving frequency detuning Δ_L . The magnetic field is fixed to the first anticrossing between the exciton and y-mode of the cavity. Parameters: $\Omega_x = 0.001$ meV $B = 3.75$ T.

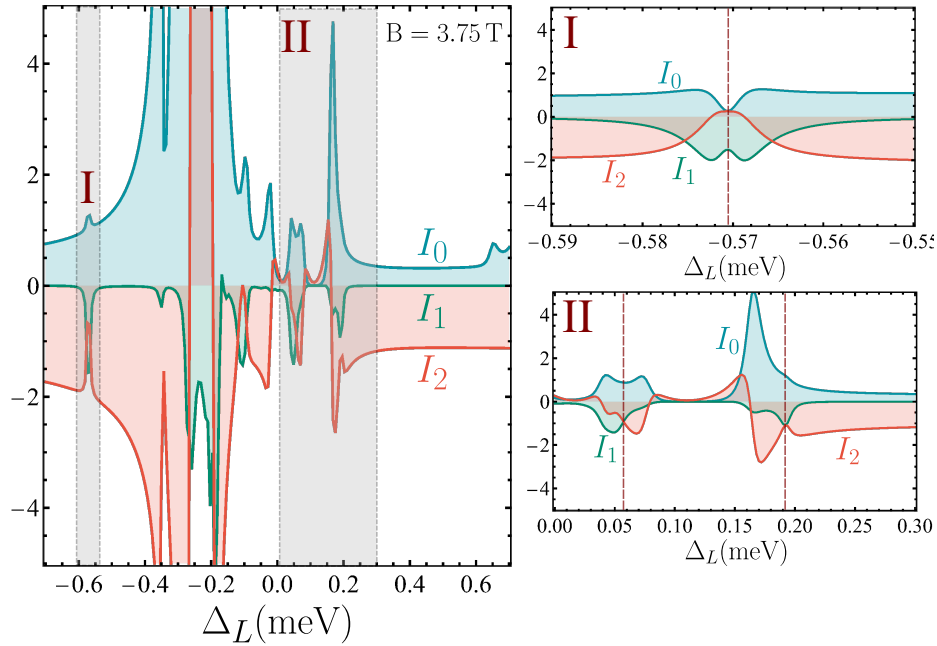


Figure 3.22 Decomposition of the second order correlation function of the y-polarization mode into coherent and incoherent fractions, as given by Equations (2.122). The dashed line on the insets indicates the position where $g_y^{(2)}$ displays antibunching. Parameters: $\Omega_x = 0.001$ meV $B = 3.75$ T.

Figure (3.22) we inspect the decomposition of the second order correlation of the y-polarization mode, as given by Equations. (2.122). The two zones where antibunching in the second correlation function is found are selected on the inset. The results from the I_0 component mostly display a positive behavior for all values of Δ_L , meaning that subpoissonian behavior is not the main mechanism for single photon statistics. Furthermore, it can be seen that the nature of the decomposition is completely different. For instance, the inset on the region (I) shows that for the point where $g_y^{(2)}$ exhibit antibunching (as denoted by the dashed lines) both I_0 and I_2

are positive, meaning there are no Sub-Poissonian or Squeezed contributions to the global nature of $g_y^{(2)}$. Rather than that, the leading factor is the enhanced anomalous correlations calculated through I_1 , indicating that with this selection of the magnetic field and laser frequency, the state could be approximated to a squeezed coherent state. On the other hand, in region (II) it is obtained that $1 + I_0 \approx 2$ is compensated by both anomalous correlations and the squeezing factor, $I_1, I_2 \rightarrow -1$.

Now, to analyze whether the antibunching of the $g_y^{(2)}$ correlation function could be truly classified as single photon emission, we perform the calculation of the higher order correlation functions up to $n = 4$, for the same cut in the magnetic field ($B=3.75$ T). The results from Figure. (3.23) specifies that there is a simultaneous minimization of all functions for the values of Δ_L previously analyzed, meaning that for that tuning not only the second order correlation function gets minimized, but higher order correlation function does it as well, stipulating that the emission corresponds to single photons. This is a particular feature related to the phenomena of conventional photon blockade, indicating that this is the leading mechanism for single photon generation in this system.

Until now, we have restricted the analysis to a fixed value of the magnetic field, while varying the laser

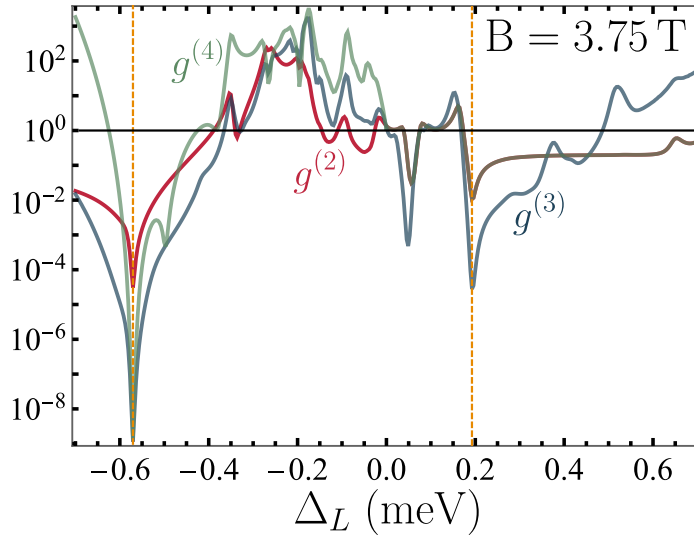


Figure 3.23 Comparison of the higher order correlation function of the y-polarization cavity mode for fixed magnetic field strength. Parameters: $\Omega_x = 0.001$ meV, $B = 3.75$ T.

frequency. However, we are interested in using both quantities as parameters of control as a way to tune the statistics of the emission of the cavity modes. To give the complete mapping of the problem, we make use of the analytical results for the correlation function explained before, and calculate the second order correlation functions with the coefficients given by Equations (3.69 c. and d.).

The results shown in Figure (3.24) indicate that, clearly, the mode that has orthogonal polarization to the incident driving is favored regarding single photon statistics. Furthermore, the black dashed lines correspond to the solution of the eigenvalue problem associated with the conventional photon blockade effect, thus demonstrating that not only it is possible to control of polarization state of the emitting light as a function of the magnetic field and the laser detuning, but also they serve as a parameter of control for tuning the desired statistics of the

system. And also, given that the regions where the polarization factor indicates a complete transformation to the orthogonal polarization state also coincide with perfect antibunching from the source, it has been demonstrated that conventional photon blockade in this system allows obtaining *single photon polarization switch*, facilitating the implementation of quantum technologies that require to create polarization qubits with single photons.

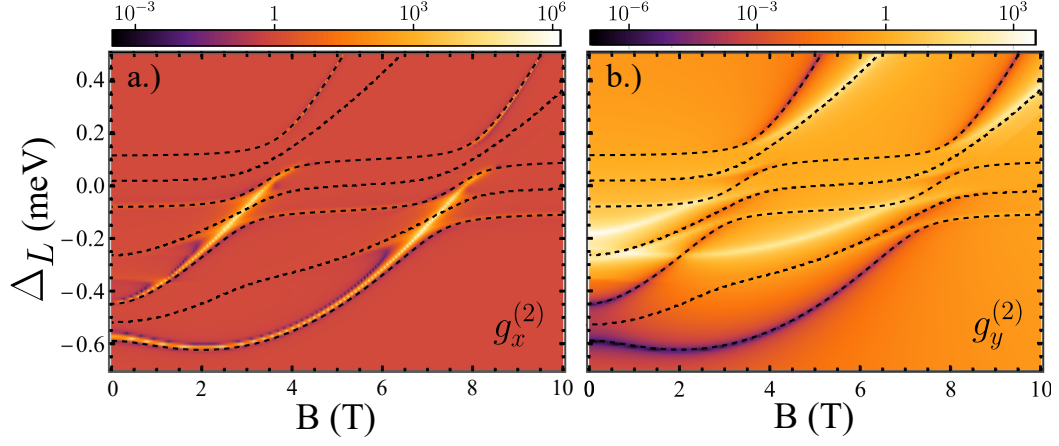


Figure 3.24 Mapping of the analytical second order correlation function for the x (a) and y-polarization (b), for pumping to the x mode, as a function of detuning Δ_L and the magnetic field B . Parameters: $\Omega_x = 0.001$ meV.

Conclusions and perspectives

In this thesis, we have studied the mechanisms that generate the so-called *photon blockade effect*, which can be divided into two categories, the *conventional photon blockade* (CPB) and the *unconventional photon blockade* (UPB). Some relevant findings are listed next.

1. We studied the original system related to the UPB, the two interacting cavity model, by numerically solving the master equations on the steady state, and calculating the second order correlation function. We have found that, while for the value of the Kerr nonlinearity proposed by Liew and Savona, this system present astonishing low values for $g^{(2)}(0)$, the calculation of higher-order correlation functions $g^{(n)}(0)$ ($n > 2$) exhibit large bunching values. Nevertheless, we applied a procedure for simultaneously minimizing higher-order correlation functions, finding the optimal value of the Kerr nonlinearity to guarantee single photon emission by this system.
2. We studied a system, namely the *driven-dissipative Jaynes Cummings model*, which is able to sustain both types of blockades simultaneously. By applying a diagonalization procedure and using the *wavefunction approximation method*, we found the optimal conditions for generating CPB and UPB, by a proper selection of the natural frequencies of the system and the incident driving frequency.
3. Exploring the differences and similarities between both mechanisms, some interesting results were found. First, the *correlation function decomposition* is not able to differentiate specific properties for each type of blockade, since the incoherent components balance exactly. However, when considering *frequency filtered correlations*, a difference between both mechanisms was found, identifying that the antibunching effect is more robust to frequency filtering, while UPB exhibits an alteration of the emission rates which generates new types of correlations that differs to sole antibunching.
4. When considering a dissipative scheme that takes into account the effect of *phonon mediated coupling* (PhmC), another important difference between CPB and UPB was found, especially when both dissipative rates increase simultaneously. For the case of CPB, only when the phonon-mediated coupling rates are close to the cavity decay rate κ_a , the second order correlation function starts to increase. On the contrary, for UPB, even low values of PhmC could destroy the quantum interference process needed to obtain antibunching through UPB. Moreover, the second order correlation function of this mechanism displays a nonlinear nature, attaining maximum bunching when $\xi_\theta/g = \gamma_\sigma$ and a lower minimum when $\xi_\theta/g \approx 1.5$.
5. We studied a system based on an elliptical pillar with an embedded quantum dot subject to an external magnetic field and coherent driving. By applying the formalisms related to photon blockade, it was found

that the magnetic field strength and the laser frequency can be used to obtain single photons from the conventional photon blockade perspective, constituting this system as a *single photon polarization switch*, which could have potential applications for the development of quantum technologies.

Regarding the perspectives that could follow from this work, the more relevant are

- Study the nature of photon blockade when the interaction strength between light and matter reaches new regimes, such as the ultrastrong and deep strong coupling regime, focusing on the different characteristics that are unique to those regimes.
- Perform quantum Montecarlo simulations of the frequency-resolved correlation in the driven dissipative Jaynes Cummings model in order to discover new differences between the blockade mechanisms.
- Study if the introduction of dark excitonic states in the model, when a tilted magnetic field is considered, has relevant differences regarding the photon blockade effect.

Open Quantum systems

The theory of open quantum systems is studied when the framework of the usual quantum mechanics, where a system under consideration is taken as isolated, is moved over for a more general and realistic perspective, where an external entity, an environment can alter the dynamics of the system. The unwanted interaction of the degrees of freedom of the environment with the system can considerably change the resulting dynamics of the system. Furthermore, in many situations, only by considering this complete framework, some experimental results can be understood. An example of this consists of the appearance of a central peak in off-resonant cavity QED systems, which can only be explained by introducing phonon-mediated couplings [87]. In the case of the present work, only by considering imperfect cavity mirrors that allow the escape of photons from the system is that the theoretical basis of light-emitting devices can be correctly described. The theoretical tools derived here are based on the calculations given in chapter 3 of the excellent book by Breuer and Petruccione, *The theory of open quantum systems* [96]. In the following, I will present all the steps in the derivation of the Lindblad master equation.

Formal derivation of Lindblad equation

The first step for constructing the open quantum system formalism results in considering the interaction of a system with an external environment. The Hilbert space will be spanned as

$$\mathcal{H}_{SB} = \mathcal{H}_S \otimes \mathbb{1}_B + \mathcal{H}_B \otimes \mathbb{1}_S + \mathcal{H}_I \quad (\text{A.1})$$

The first and middle terms refer to the system as an environment Hamiltonian, while the last term is the interaction between both of them. The density matrix approach can be used to describe the dynamics of the $S + B$ system. A first important approximation consists of the initial condition of this joint arrangement,

$$\rho_{S \otimes B}(t = 0) = \rho(t) = \rho_S(t = 0) \otimes \rho_B \quad (\text{A.2})$$

The reason for this subsists is by considering the environment as a steady-state reservoir. A vital assessment that has to be emphasized is that, even by introducing external degrees of freedom, this will be in general infinite and thus impossible to describe. The new behavior still resides in the system's density matrix; for that reason, a process of tracing out the environment or bath degrees of freedom will be continuously made throughout the

formalism. The joint density matrix (A.2) will generally evolve as

$$\rho(t) = U(t, t_0) \rho(t_0) U^\dagger(t, t_0) \quad (\text{A.3})$$

and the resulting evolved system density matrix will be obtained by a tracing process over the bath degrees of freedom

$$\rho(t) = \text{tr}_B \{ U(t, t_0) \rho(t_0) U^\dagger(t, t_0) \} \quad (\text{A.4})$$

The corresponding equation that (A.4) will follow is

$$\frac{d\rho_S(t)}{dt} = -\frac{i}{\hbar} \text{tr}_B [H(t), \rho(t)] \quad (\text{A.5})$$

The process for obtaining an equation that describes the dynamics of the system when there are correlations with the bath will begin as follows: Consider a spectral decomposition for both system and bath density matrices as

$$\rho_S = \sum_i \lambda_i |\alpha_i\rangle \langle \alpha_i| \quad (\text{A.6})$$

$$\rho_B = \sum_j \gamma_j |\beta_j\rangle \langle \beta_j| \quad (\text{A.7})$$

replacing this notation in (A.4) yields

$$\rho_S(t) = \text{tr}_B \left[\sum_{ij} U(t, 0) \lambda_i |\alpha_i\rangle \langle \alpha_i| \otimes (\gamma_j |\beta_j\rangle \langle \beta_j|) U^\dagger(t, 0) \right] \quad (\text{A.8})$$

$$\begin{aligned} &= \sum_{ijk} \lambda_i \gamma_j \langle \beta_k | U(t, 0) | \alpha_i \rangle \langle \alpha_i | \otimes |\beta_j\rangle \langle \beta_j| U^\dagger(t, 0) \\ &= \sum_{jk} \gamma_j \langle \beta_k | U(t, 0) | \beta_j \rangle \otimes \sum_i \lambda_i |\alpha_i\rangle \langle \alpha_i| \otimes \langle \beta_j | U^\dagger(t, 0) | \beta_k \rangle \\ &= \sum_{jk} \gamma_j \langle \beta_k | U(t, 0) | \beta_j \rangle \otimes \rho_S(0) \otimes \langle \beta_j | U^\dagger(t, 0) | \beta_k \rangle \end{aligned} \quad (\text{A.9})$$

defining a new set of operators, $W_{jk}(t) = \sqrt{\gamma_j} \langle \beta_k | U(t, 0) | \beta_j \rangle$ and $W_{jk}^\dagger(t) = \sqrt{\gamma_j} \langle \beta_j | U^\dagger(t, 0) | \beta_k \rangle$ allows rewriting the previous equation as

$$\rho_S(t) = \text{tr}_B \sum_{jk} W_{jk}(t) \rho_S(0) W_{jk}^\dagger(t) = V(t) \rho_S(0) \quad (\text{A.10})$$

The term $V(t)$ in (A.10) can be interpreted as a dynamical map that only evolves the subsystem S , not giving the unitary dynamics of the complete $S \otimes B$ interaction. If the correlations in the environment B decay much faster than the characteristic time scales in S , then the degrees of freedom in S only depend upon its present states, allowing to fulfill the following property

$$V(t_1 + t_2) = V(t_1) V(t_2) \quad (\text{A.11})$$

This characteristic is formally related to a dynamical semigroup, which implies the existence of a generator \mathcal{L} that creates the action of the dynamical map as

$$V(t) = e^{\mathcal{L}t} \quad (\text{A.12})$$

the generator \mathcal{L} is usually referred to as the Lindblad super operator, resulting in

$$\rho_S(t) = V(t)\rho_S(0) = e^{\mathcal{L}t}\rho_S(0) \quad (\text{A.13})$$

taking a time derivative in (A.13) yields

$$\begin{aligned} \frac{d\rho_S(t)}{dt} &= \frac{de^{\mathcal{L}t}}{dt}\rho_S(0) = \mathcal{L}e^{\mathcal{L}t}\rho_S(0) \\ \frac{d\rho_S(t)}{dt} &= \mathcal{L}\rho_S(t) \end{aligned} \quad (\text{A.14})$$

The expression (A.14) is the famous Lindblad equation, which shows that when $\mathcal{L}\rho_S(t)$ corresponds to the commutator of the Hamiltonian, then the Liouville Von Neumann equation is recovered, implying that the Lindblad equation is a more generic formalism that explains both open and closed evolution.

The following task resides in encountering a general expression of equation (A.14). The Lindblad space has dimensions of $\dim(\mathcal{L}_S) = N^2$. Defining a basis F_i that is orthonormal to the inner product $(F_i, F_j) = \text{tr}_S(F_i^\dagger F_j)$, where $i = 1, 2, \dots, N^2$ and $f_N = (N)^{-1/2}\mathbb{1}_S$. Expanding the operator $W_{jk}(t)$ and the related conjugate on the F_i basis results in

$$W_{\alpha,\beta}(t) = \sum_{i=1}^{N^2} F_i(F_i, W_{\alpha,\beta}(t)) = \sum_{i=1}^{N^2} F_i \text{tr}_S(F_i^\dagger W_{\alpha,\beta}) = \frac{1}{N} \text{tr}_S(W_{\alpha,\beta}) \mathbb{1}_S + \sum_k F_k \text{tr}_S(F_k^\dagger W_{\alpha,\beta}) \quad (\text{A.15})$$

and

$$W_{\alpha,\beta}^\dagger(t) = \frac{1}{N} \text{tr}_S(W_{\alpha,\beta}^\dagger) \mathbb{1}_S + \sum_k F_k \text{tr}_S(W_{\alpha,\beta}^\dagger F_k) \quad (\text{A.16})$$

replacing equations (A.15) and (A.16) in (A.4) gives

$$\rho_S(t) = \sum_{ij} \left[\left\{ \frac{1}{N} \text{tr}_S(W_{ij}(t)) \mathbb{1}_S + \sum_k \text{tr}_S(F_k^\dagger W_{ij}(t)) F_k \right\} \rho_S(0) \left\{ \frac{1}{N} \text{tr}_S(W_{ij}^\dagger \mathbb{1}_S) + \sum_{k'} \text{tr}_S(W_{ij}^\dagger(t) F_{k'}) F_{k'}^\dagger \right\} \right] \quad (\text{A.17})$$

$$\begin{aligned} \rho_S(t) &= \sum_{ij} \frac{1}{N^2} |\text{tr}_S W_{ij}(t)|^2 \rho_S(0) + \frac{1}{N} \sum_{ijk} (\text{tr}_S W_{ij}(t)) \text{tr}_S(W_{ij}^\dagger F_k) \rho_S(0) F_k^\dagger + \\ &\frac{1}{N} \sum_{ijk} \text{tr}_S(F_k^\dagger W_{ij}(t)) \text{tr}_S(W_{ij}^\dagger F_k) F_k \rho_S(0) + \sum_{ijkk'} \text{tr}_S(F_k^\dagger W_{ij}(t)) \text{tr}_S(W_{ij}^\dagger(t) F_{k'}) F_k \rho_S(0) F_{k'}^\dagger \end{aligned} \quad (\text{A.18})$$

defining

$$f(t) = \sum_{ij} \frac{1}{N^2} |tr_S W_{ij}(t)|^2 \quad (\text{A.19})$$

$$c_{k,k'}(t) = \sum_{ij} tr_S \left(F_k^\dagger W_{ij}(t) \right) tr_S \left(W_{ij}^\dagger(t) F_{k'} \right) \quad (\text{A.20})$$

$$F(t) = \sum_{ij} \frac{1}{N} tr_S (W_{ij}(t)) tr_S \left(W_{ij}^\dagger(t) \right) \quad (\text{A.21})$$

the equation (A.17) can be recast for an arbitrary time t' as

$$\rho_S(t) = f(t)\rho_S(t') + \rho_S(t')F^\dagger(t) + F(t)\rho_S(t) + \sum_{kk'} c_{kk'}(t) F_k \rho_S(t') F_{k'}^\dagger \quad (\text{A.22})$$

taking a derivative with respect to time and evaluating at a time $t' = t$

$$\frac{d\rho_S(t)}{dt} = \dot{f}(t)\rho_S(t) + \rho_S(t)\dot{F}^\dagger(t) + \dot{F}(t)\rho_S(t) + \sum_{kk'} \dot{c}_{kk'}(t) F_k(t)\rho_S(t) F_{k'}^\dagger(t) \quad (\text{A.23})$$

The previous equation can be more easily recognized by making the following definitions $H(t) = \frac{1}{2i} (\dot{F}^\dagger(t) - \dot{F}(t))$, $G(t) = \frac{1}{2} (\dot{f}(t) + \dot{F}^\dagger(t) + \dot{F}(t))$ and $a_{kk'}(t) = \dot{c}_{kk'}(t)$

$$\frac{d\rho_S(t)}{dt} = \frac{-i}{\hbar} [H(t), \rho_S(t)] + \{G(t), \rho_S(t)\} + \sum_{kk'} a_{kk'}(t) F_k(t)\rho_S(t) F_{k'}^\dagger \quad (\text{A.24})$$

taking a trace in the system degrees of freedom, recalling that a dynamical map preserves the trace results in

$$\frac{d}{dt} tr_S (\rho_S(t)) = 0 = \frac{-i}{\hbar} tr_S [H(t), \rho_S(t)] + tr_S \left(\sum_{kk'} a_{kk'} F_k \rho_S(t) F_{k'}^\dagger \right) \quad (\text{A.25})$$

The first and second term result in

$$tr_S (H(t)\rho_S(t) - \rho_S(t)H(t)) = tr_S (H(t)\rho_S(t) - H(t)\rho_S(t)) = 0 \quad (\text{A.26})$$

$$tr_S (G(t)\rho_S(t) + \rho_S(t)G(t)) = tr_S (G(t)\rho_S(t) - G(t)\rho_S(t)) = 2G(t)\rho_S(t) \quad (\text{A.27})$$

where the cyclic properties of the trace have been used. With these results in mind, the trace conditions transform in

$$tr_S \left\{ \left(2G(t) + \sum_{kk'} a_{kk'} F_k^\dagger F_k \right) \rho_S(t) \right\} = 0 \quad (\text{A.28})$$

This equality is satisfied when $G(t) = -\frac{1}{2} \sum_{kk'} a_{kk'} F_{k'}^\dagger F_k$. Equation (A.24) can be rewritten as

$$\frac{d\rho_S(t)}{dt} = -\frac{i}{\hbar} [H(t), \rho_S(t)] + \sum_{kk'} a_{kk'} \left(F_k \rho_S F_{k'}^\dagger - \frac{1}{2} \{F_{k'}^\dagger F_k, \rho_S\} \right) \quad (\text{A.29})$$

The coefficients $a_{kk'}$ refer to a matrix that, in general, can be diagonalized by means of a unitary matrix as $a_{kk'} = \sum_l u_{kl}(t) \gamma_l u_{k'l}^*$. This can be seen as

$$a = u \gamma u^\dagger = \begin{pmatrix} \gamma_1 & 0 & \dots & 0 \\ 0 & \gamma_2 & \dots & 0 \\ 0 & 0 & \dots & 0 \\ 0 & 0 & \dots & \gamma_{N^2-1} \end{pmatrix} \quad (\text{A.30})$$

The resulting master equation is,

$$\frac{d\rho_S(t)}{dt} = -\frac{i}{\hbar} [H(t), \rho_S(t)] + \sum_k \gamma_k \left(A_k(t) \rho_S(t) A_k^\dagger - \frac{1}{2} A_k^\dagger A_k \rho_S(t) - \frac{1}{2} \rho_S(t) A_k^\dagger A_k \right) \quad (\text{A.31})$$

This is the general form of the Lindblad equation. The coefficients A_k are named Lindblad operators, γ_k are relaxation rates that indicate different decay modes of the open system. The whole term involved in the sum over k is referred to as the dissipator.

Derivation via first principles

This was a formal approach to obtain the general form of the Lindblad equation (A.31). As a big part of physics, one of the main scopes is to derive scientific postulates on which vast quantities of statements and theorems can be obtained, aka first principles. The case of the formalism of open quantum systems is no exception. Starting once again with a Hamiltonian of the form,

$$\mathcal{H}_{SB} = \mathcal{H}_S \otimes \mathbb{1}_B + \mathcal{H}_B \otimes \mathbb{1}_S + \mathcal{H}_I \quad (\text{A.32})$$

A limit on the degree of interaction between system and bath has to be made. If the dynamics of the system does not greatly alter the corresponding dynamics of the bath, then a weak coupling approximation among them could be made. This will have some interesting consequences that will be later presented.

Moving to the interaction picture, an equation of motion of the following form is obtained

$$\frac{d\rho_S(t)}{dt} = -\frac{i}{\hbar} [\tilde{H}_I(t), \rho_I] \quad (\text{A.33})$$

And the formal solution can be written as

$$\rho(t) = \rho(0) - \frac{i}{\hbar} \int_0^t ds [\tilde{H}_I(s), \rho(s)] \quad (\text{A.34})$$

Replacing this solution on the right side of the interaction picture Liouville equation, and tracing out the bath degrees of freedom gives

$$\frac{d\rho_S(t)}{dt} = \left(\frac{-i}{\hbar} \right)^2 \int_0^t \text{tr}_B [H_I(t), [H_I(s), \rho(s)]] ds \quad (\text{A.35})$$

Born and Markov approximations: The first strong approximation that will be applied are the so-called Born and Markov approximations. The meaning of both of them will be thoroughly explained.

The first approximation corresponds to the effects that the system has over the bath dynamics. If what happens in S does not modify the behavior of B , then the evolution of the joint system can be considered separable,

$$\rho \approx \rho_S(t) \otimes \rho_B \quad (\text{A.36})$$

This also can be understood by employing the characteristic time scales of both the system and bath. If the order of magnitude of the bath relaxation time, τ_B is considerably smaller than the ones of the system, the approximation of Equation (A.36) can be made. Numerical evidence of this approximation is shown when a thermal bath with low (But nevertheless experimentally achievable) temperatures are considered,

$$\tau_B = \left(\frac{\kappa_B T}{\hbar} \right)^{-1} = \left(\frac{[1.38 \times 10^{-23} \text{JK}^{-1}][4\text{K}]}{6.63 \times 10^{-34} \text{Js}} \right)^{-1} \approx 10^{-11} \text{s} \quad (\text{A.37})$$

The characteristic times of the system are given by their own coupling constants g . An example of a two level system interacting with a cavity mode has interaction strengths of the order of 400MHz. this gives a timescale of $\tau_S = 1/400 \times 10^6 \text{Hz} \approx 10^{-9} \text{s}$, which is greater than τ_B and thus Born approximation can be made. Replacing (A.36) in (A.35)

$$\frac{d\rho_S(t)}{dt} = \left(\frac{-i}{\hbar} \right)^2 \int_0^t \text{tr}_B [H_I(t), [H_I(s), \rho_S(s) \otimes \rho_B]] ds \quad (\text{A.38})$$

The previous equation indicates that the state of the system at a given time t depends on all previous times, as the integration of $\int_0^t \rho_S(s)$ shows. If the information that S passes into B is quickly dissipated (Normally because of the size of the bath in comparison with that of the system), then the dynamics of the ρ_S only depend on its present state.

$$\frac{d\rho_S(t)}{dt} = \left(\frac{-i}{\hbar} \right)^2 \int_0^\infty \text{tr}_B [H_I(t-s), [H_I(s), \rho_S(t) \otimes \rho_B]] ds \quad (\text{A.39})$$

A replacement of $t \rightarrow t-s$ was made in the previous equation in order to obtain a quantum Markovian equation.

Secular approximation The next approximation that has to be made in order to derive the Lindblad equation is called the secular approximation. Its basis resides in disregarding fast oscillating terms that appear on the quantum master equation, which corresponds to a rotating wave approximation. To express this point, let's write the interaction Hamiltonian as a product of system and bath operators

$$H_I = \sum_{\alpha} A_{\alpha} \otimes B_{\alpha} \quad (\text{A.40})$$

Supposing that the eigenstates of the Hamiltonian of the system are known, $H_S |\eta_{\epsilon}\rangle = \epsilon |\eta_{\epsilon}\rangle$, the system operators A_{α} can be expanded in this basis as

$$A(\omega) = \sum_{\epsilon - \epsilon' = \hbar\omega} |\eta_{\epsilon}\rangle \langle \eta_{\epsilon}| A_{\alpha} |\eta_{\epsilon'}\rangle \langle \eta_{\epsilon'}| \quad (\text{A.41})$$

then, the interaction Hamiltonian results in $H_I = \sum_{\omega, \alpha} A_{\alpha}(\omega) \otimes B_{\alpha}$. Moving into the Dirac frame, the Schrödinger operators transform into

$$\tilde{H}_I = \sum_{\omega, \alpha} e^{iH_S t/\hbar} A_{\alpha}(\omega) e^{-iH_S t/\hbar} \otimes e^{iH_B t/\hbar} B_{\alpha} e^{-iH_B t/\hbar} \quad (\text{A.42})$$

The system transformed operators can be written in a more compact form introducing the system projectors

$$\begin{aligned} e^{iH_S t/\hbar} A_{\alpha}(\omega) e^{-iH_S t/\hbar} &= \sum_{\varepsilon - \varepsilon'} e^{iH_S t/\hbar} |\eta_{\varepsilon}\rangle \langle \eta_{\varepsilon}| A_{\alpha}(\omega) |\eta_{\varepsilon'}\rangle \langle \eta_{\varepsilon'}| e^{-iH_S t/\hbar} \\ &= \sum_{\varepsilon - \varepsilon'} e^{i\varepsilon t/\hbar} |\eta_{\varepsilon}\rangle \langle \eta_{\varepsilon}| A_{\alpha}(\omega) |\eta_{\varepsilon'}\rangle \langle \eta_{\varepsilon'}| e^{-i\varepsilon' t/\hbar} \\ &= \sum_{\varepsilon - \varepsilon'} e^{-i\omega t} |\eta_{\varepsilon}\rangle \langle \eta_{\varepsilon}| A_{\alpha}(\omega) |\eta_{\varepsilon'}\rangle \langle \eta_{\varepsilon'}| \\ &= e^{-i\omega t} A_{\alpha}(\omega) \end{aligned} \quad (\text{A.43})$$

The resulting Hamiltonian is

$$\tilde{H}_I(t) = \sum_{\alpha, \omega} e^{-i\omega t} A_{\alpha}(\omega) \otimes B_{\alpha}(t) \quad (\text{A.44})$$

With this expression for the Hamiltonian, an expansion on the of the term $tr_B[\tilde{H}_I(t), [\tilde{H}_I(t-s), \rho_S(t) \otimes \rho_B]]$ has to be made

$$[H_I(t), [H_I(t-s), \rho_S(t) \otimes \rho_B]] = H_I(t)H_I(t-s)\rho_S(t) \otimes \rho_B - H_I(t-s)\rho_S(t) \otimes \rho_B H_I(t) + \text{h.c} \quad (\text{A.45})$$

$$\begin{aligned} tr_B[H_I(t), [H_I(t-s), \rho_S(t) \otimes \rho_B]] &= tr_B(H_I(t)H_I(t-s)\rho_S(t) \otimes \rho_B - H_I(t-s)\rho_S(t) \otimes \rho_B H_I(t)) + \text{h.c} \\ &= tr_B(H_I(t-s)\rho_S(t) \otimes \rho_B H_I(t) - H_I(t)H_I(t-s)\rho_S(t) \otimes \rho_B) + \text{h.c} \end{aligned} \quad (\text{A.46})$$

introducing this term into Equation. (2.133) yields

$$\begin{aligned} \frac{d\rho_S(t)}{dt} &\approx -\frac{1}{\hbar^2} \int_0^\infty tr_B \sum_{\alpha\beta\omega\omega'} \left[e^{-i\omega(t-s)} A_{\alpha}(\omega) \otimes B_{\alpha}(t) (\rho_S(t) \otimes \rho_B) e^{i\omega' t} A_{\beta}^{\dagger}(\omega') \otimes B_{\beta}^{\dagger}(t) \right] \\ &\quad + \frac{1}{\hbar^2} \int_0^\infty tr_B \sum_{\alpha\beta\omega\omega'} \left[e^{i\omega' t} A_{\beta}^{\dagger}(\omega')' \otimes B_{\beta}^{\dagger}(t) e^{-i\omega(t-s)} A_{\alpha}(\omega) \otimes B_{\alpha}(t-s) \rho_S(t) \otimes \rho_B \right] + \text{h.c} \end{aligned} \quad (\text{A.47})$$

$$\begin{aligned} \frac{d\rho_S(t)}{dt} &\approx -\frac{1}{\hbar^2} \int_0^\infty \sum_{\alpha\beta\omega\omega'} tr_B \left[e^{i(\omega' - \omega)t} e^{i\omega s} \left(A_{\alpha}(\omega) \rho_S(t) A_{\beta}^{\dagger}(\omega') \omega B_{\alpha}(t-s) \rho_B B_{\beta}^{\dagger}(t) \right) \right] \\ &\quad + \frac{1}{\hbar^2} \int_0^\infty \sum_{\alpha\beta\omega\omega'} tr_B \left[e^{i(\omega' - \omega)t} e^{i\omega s} \left(A_{\beta}^{\dagger}(\omega') A_{\alpha}(\omega) \rho_S(t) \otimes B_{\beta}^{\dagger}(t) B_{\alpha}(t-s) \rho_B \right) \right] + \text{h.c} \end{aligned} \quad (\text{A.48})$$

Rearranging terms by each Hilbert subspace results in,

$$\begin{aligned} \frac{d\rho_S(t)}{dt} \approx & \sum_{\alpha\beta\omega\omega'} e^{(\omega'-\omega)t} \left(A_\alpha(\omega)\rho_S(t)A_\beta^\dagger(\omega') - A_\beta^\dagger(\omega')A_\alpha(\omega)\rho_S(t) \right) \otimes \dots \\ & \dots \otimes \frac{-1}{\hbar^2} \int_0^\infty ds e^{i\omega s} tr_B \left(B_\alpha(t-s)\rho_B B_\beta^\dagger(t) - B_\beta^\dagger(t)B_\alpha(t-s)\rho_B \right) + \text{h.c} \end{aligned} \quad (\text{A.49})$$

Which can finally be written in a more compacted way as

$$\frac{d\rho_S(t)}{dt} \approx \sum_{\alpha\beta\omega\omega'} \Gamma_{\alpha\beta}(\omega, t) e^{(\omega'-\omega)t} \left(A_\alpha(\omega)\rho_S(t)A_\beta^\dagger(\omega') - A_\beta^\dagger(\omega')A_\alpha(\omega)\rho_S(t) \right) + \text{h.c} \quad (\text{A.50})$$

where $\Gamma_{\alpha\beta}(\omega, t) = \frac{-1}{\hbar^2} \int_0^\infty ds e^{i\omega s} tr_B \left(B_\alpha(t-s)\rho_B B_\beta^\dagger(t) - B_\beta^\dagger(t)B_\alpha(t-s)\rho_B \right) = -\frac{1}{\hbar^2} \int_0^\infty ds e^{i\omega s} \left\langle B_\beta^\dagger(t)B_\alpha(t-s) \right\rangle$ are the Fourier transform of the bath correlation functions. If the bath is taken as a bosonic bath, then in the interaction picture the only important contribution is due to time differences, and therefore $\Gamma_{\alpha\beta}(\omega, t) \rightarrow \Gamma_{\alpha\beta}(\omega) = -\frac{1}{\hbar^2} \int_0^\infty ds e^{i\omega s} \left\langle B_\beta^\dagger(s)B_\alpha(0) \right\rangle$. The next approximation that has to be made is the secular approximation, which indicates that the only important dynamics that will contribute to the system occur when a time $\tau_S = \omega_S^{-1}$ has passed, meaning that the exponential terms $e^{\omega'-\omega}$ will only be relevant in the resonant case, while the other frequencies will rapidly decay and thus not contribute to the dynamics of the system.

With these two previous considerations, the final steps for obtaining the Lindblad equation will be made. Expressing $\Gamma_{\alpha\beta}(\omega)$ as

$$\Gamma_{\alpha\beta}(\omega) = \frac{1}{2}\gamma_{\alpha\beta}(\omega) + iS_{\alpha\beta} \quad (\text{A.51})$$

where $S_{\alpha\beta}(\omega) = \text{Im}(\Gamma_{\alpha\beta}(\omega))$ and $\gamma_{\alpha\beta}(\omega) = 2\text{Re}(\Gamma_{\alpha\beta}(\omega))$. Making the corresponding replacements yields

$$\frac{d\rho_S}{dt} \approx \sum_{\alpha\beta\omega} \left(\frac{1}{2}\gamma_{\alpha\beta}(\omega) + iS_{\alpha\beta}(\omega) \right) \left(A_\alpha(\omega)\rho_S(t)A_\beta^\dagger(\omega') - A_\beta^\dagger(\omega')A_\alpha(\omega)\rho_S(t) \right) \quad (\text{A.52})$$

$$+ \sum_{\alpha\beta\omega} \left(\frac{1}{2}\gamma_{\alpha\beta}^*(\omega) - iS_{\alpha\beta}^*(\omega) \right) \left(A_\beta^\dagger(\omega)\rho_S(t)A_\alpha(\omega') - \rho_S(t)A_\alpha^\dagger(\omega)A_\beta(\omega) \right) \quad (\text{A.53})$$

Taking into account that $\gamma_{\beta\alpha}^* = \gamma_{\alpha\beta}$ and $S_{\beta\alpha}^* = S_{\alpha\beta}$, a dummy index replacement of $\alpha \rightarrow \beta$ and $\beta \rightarrow \alpha$ can be made in the second sum, yielding

$$\frac{d\rho_S(t)}{dt} \approx \sum_{\alpha\beta\omega} \frac{\gamma_{\alpha\beta}(\omega)}{2} \left(A_\alpha(\omega)\rho_S(t)A_\beta^\dagger(\omega) - A_\beta^\dagger(\omega)A_\alpha(\omega)\rho_S(t) + A_\alpha^\dagger(\omega)\rho_S(t)A_\beta(\omega) - \rho_S(t)A_\beta^\dagger(\omega)A_\alpha(\omega) \right) \quad (\text{A.54})$$

$$- i \sum_{\alpha} \left(A_\alpha(\omega)\rho_S(t)A_\beta^\dagger(\omega) - A_\beta^\dagger(\omega)A_\alpha(\omega)\rho_S(t) + A_\alpha^\dagger(\omega)\rho_S(t)A_\beta(\omega) - \rho_S(t)A_\beta^\dagger(\omega)A_\alpha(\omega) \right) \quad (\text{A.55})$$

This expression can be finally compressed as

$$\frac{d\rho_S(t)}{dt} \approx -i[H_{LS}, \rho_S(t)] + \mathcal{D}(\rho_S(t)) \quad (\text{A.56})$$

where $H_{LS} = \sum_{\alpha\beta\omega} S_{\alpha\beta}(\omega) A_{\alpha}^{\dagger} A_{\beta}(\omega)$ and $\mathcal{D}(\rho_S) = \sum_{\alpha\beta\omega} \gamma_{\alpha\beta}(\omega) \left(A_{\beta}(\omega) \rho_S A_{\alpha}^{\dagger} - \frac{1}{2} \left\{ A_{\alpha}^{\dagger}(\omega) A_{\beta}(\omega), \rho_S \right\} \right)$. Equation (A.56) is the same Lindblad equation shown in Equation (A.31).

The formalism derived in this chapter will be used to numerically solve the dynamics and steady states of some QED systems, which will be modeled with Lindblad master equations with dissipators of the form $\mathcal{D}_{\hat{c}}(\rho_S)$.

Master equation for operators

After having derived the Lindblad equation for the master equation, we will briefly discuss the aspect of a master equation for operators. The Lindblad equation for the density matrix once again is,

$$\partial_t \rho(t) = i[\rho, H] + \frac{1}{2} \sum_k (2\hat{L}_k \rho \hat{L}_k^{\dagger} - \hat{L}_k^{\dagger} \hat{L}_k \rho - \rho \hat{L}_k^{\dagger} \hat{L}_k) = i[\rho, H] + \frac{1}{2} \sum_k \mathcal{L}_{\hat{L}_k} \rho \quad (\text{A.57})$$

Where L_k are the jump operators. This equation is written in the Schrödinger picture because the time evolution is presented for the density matrix ρ , which is a projection of states as $\rho = \sum_j p_j |\Psi_j(t)\rangle \langle \Psi_j(t)|$. Now the question is since an operator O is independent in the Schrödinger picture, is it possible to derive a master equation for its time evolution? The direct answer is yes. You can obtain a Lindblad master equation for an operator in the Schrödinger picture. We will outline this procedure next.

Since \hat{O} is time independent one could write the following property for the expected value of this operator

$$\begin{aligned} \hat{O} \partial_t \rho(t) &= \partial_t (\hat{O} \rho(t)) \\ \text{Tr}\{\partial_t (\hat{O} \rho(t))\} &= \partial_t \text{Tr}\{\hat{O} \rho(t)\} = \partial_t \langle \hat{O} \rangle(t) \\ \partial_t \langle \hat{O} \rangle(t) &= \text{Tr}\{\hat{O} \partial_t \rho(t)\} \end{aligned}$$

Now, we obtain that the time evolution of the operator O can be obtained using the Lindblad equation for the density operator as

$$\partial_t \langle \hat{O} \rangle(t) = \text{Tr} \left\{ \hat{O} \left(i[\rho, H] + \frac{1}{2} \sum_k (2\hat{L}_k \rho \hat{L}_k^{\dagger} - \hat{L}_k^{\dagger} \hat{L}_k \rho - \rho \hat{L}_k^{\dagger} \hat{L}_k) \right) \right\} \quad (\text{A.58})$$

After some straightforward calculations, on which the cyclic properties of the trace must be used, one can finally obtain the following equation for the evolution of the expectation value of $\langle \hat{O} \rangle$

$$\partial_t \langle \hat{O} \rangle(t) = i \langle [H, \hat{O}] \rangle + \frac{1}{2} \sum_k \left(2 \langle \hat{L}_k^{\dagger} \hat{O} \hat{L}_k \rangle - \langle \hat{O} \hat{L}_k^{\dagger} \hat{L}_k \rangle - \langle \hat{L}_k^{\dagger} \hat{L}_k \hat{O} \rangle \right) \quad (\text{A.59})$$

The reader can rapidly identify that the first part of the equation coincides with the Ehrenfest theorem for Heisenberg's equation of motion, and the dissipative term actually corresponds to the conjugated version of the Lindblad master equation for the density matrix, i.e., the dissipator $\mathcal{L}_{\hat{L}_k}^{\dagger}$ is the one that applies for the time evolution of an operator O . Equation (A.59) constitutes an important result that we will apply later on when we solve specific Hamiltonians.

Bibliography

- [1] A. Imamoglu, H. Schmidt, G. Woods, and M. Deutsch. Strongly Interacting Photons in a Nonlinear Cavity. *Physical Review Letters*, 79(8):1467–1470, August 1997.
- [2] I.L. Aleiner, P.W. Brouwer, and L.I. Glazman. Quantum effects in Coulomb blockade. *Physics Reports*, 358(5-6):309–440, March 2002.
- [3] K. M. Birnbaum, A. Boca, R. Miller, A. D. Boozer, T. E. Northup, and H. J. Kimble. Photon blockade in an optical cavity with one trapped atom. *Nature*, 436(7047):87–90, July 2005.
- [4] T. C. H. Liew and V. Savona. Single Photons from Coupled Quantum Modes. *Physical Review Letters*, 104(18):183601, May 2010.
- [5] Motoaki Bamba, Atac Imamoglu, Iacopo Carusotto, and Cristiano Ciuti. Origin of strong photon antibunching in weakly nonlinear photonic molecules. *Physical Review A*, 83(2):021802, February 2011.
- [6] Marc-Antoine Lemonde, Nicolas Didier, and Aashish A. Clerk. Antibunching and unconventional photon blockade with Gaussian squeezed states. *Physical Review A*, 90(6):063824, December 2014.
- [7] Marina Radulaski. A Double Take on Unconventional Photon Blockade. *Physics*, 11:74, July 2018.
- [8] H.J. Snijders, J.A. Frey, J. Norman, H. Flayac, V. Savona, A.C. Gossard, J.E. Bowers, M.P. van Exter, D. Bouwmeester, and W. Löffler. Observation of the Unconventional Photon Blockade. *Physical Review Letters*, 121(4):043601, July 2018.
- [9] Cyril Vaneph, Alexis Morvan, Gianluca Aiello, Mathieu Féchant, Marco Aprili, Julien Gabelli, and Jérôme Estève. Observation of the Unconventional Photon Blockade in the Microwave Domain. *Physical Review Letters*, 121(4):043602, July 2018.
- [10] E. Zubizarreta Casalengua, J. C. López Carreño, F. P. Laussy, and E. del Valle. Conventional and unconventional photon statistics. *Laser & Photonics Reviews*, 14(6):1900279, June 2020. arXiv: 1901.09030.
- [11] Roy J. Glauber. The Quantum Theory of Optical Coherence. *Physical Review*, 130(6):2529–2539, June 1963.
- [12] H. J. Kimble, M. Dagenais, and L. Mandel. Photon Antibunching in Resonance Fluorescence. *Physical Review Letters*, 39(11):691–695, September 1977.
- [13] R. E. Slusher, L. W. Hollberg, B. Yurke, J. C. Mertz, and J. F. Valley. Observation of Squeezed States Generated by Four-Wave Mixing in an Optical Cavity. *Physical Review Letters*, 55(22):2409–2412, November 1985.
- [14] Xiu Gu, Anton Frisk Kockum, Adam Miranowicz, Yu-xi Liu, and Franco Nori. Microwave photonics with superconducting quantum circuits. *Physics Reports*, 718-719:1–102, November 2017.

- [15] John M. Martinis, Sergio Boixo, Hartmut Neven, Frank Arute, Kunal Arya, Ryan Babbush, Dave Bacon, Joseph C. Bardin, Rami Barends, Rupak Biswas, Fernando G. S. L. Brandao, David A. Buell, Brian Burkett, Yu Chen, Zijun Chen, Ben Chiaro, Roberto Collins, William Courtney, Andrew Dunsworth, Edward Farhi, Brooks Foxen, Austin Fowler, Craig Gidney, Marissa Giustina, Rob Graff, Keith Guerin, Steve Habegger, Matthew P. Harrigan, Michael J. Hartmann, Alan Ho, Markus Hoffmann, Trent Huang, Travis S. Humble, Sergei V. Isakov, Evan Jeffrey, Zhang Jiang, Dvir Kafri, Kostyantyn Kechedzhi, Julian Kelly, Paul V. Klimov, Sergey Knysh, Alexander Korotkov, Fedor Kostritsa, David Landhuis, Mike Lindmark, Erik Lucero, Dmitry Lyakh, Salvatore Mandrà, Jarrod R. McClean, Matthew McEwen, Anthony Megrant, Xiao Mi, Kristel Michielsen, Masoud Mohseni, Josh Mutus, Ofer Naaman, Matthew Neeley, Charles Neill, Murphy Yuezhen Niu, Eric Ostby, Andre Petukhov, John C. Platt, Chris Quintana, Eleanor G. Rieffel, Pedram Roushan, Nicholas C. Rubin, Daniel Sank, Kevin J. Satzinger, Vadim Smelyanskiy, Kevin J. Sung, Matthew D. Trevithick, Amit Vainsencher, Benjamin Vallalunga, Theodore White, Z. Jamie Yao, Ping Yeh, and Adam Zalcman. Quantum supremacy using a programmable superconducting processor, 2019. Artwork Size: 13320049066 bytes Pages: 13320049066 bytes Version Number: 11 Type: dataset.
- [16] A. Kavokin, J.J. Baumberg, G. Malpuech, and F.P. Laussy. *Microcavities*. Oxford science publications. OUP Oxford, 2011.
- [17] Lu Cai, Junyao Pan, Yong Zhao, Jin Wang, and Shiyuan Xiao. Whispering Gallery Mode Optical Microresonators: Structures and Sensing Applications. *physica status solidi (a)*, 217(6):1900825, March 2020.
- [18] Yun-Qi Hu, Hong Yang, Tao Wang, Xuan Mao, Ran-Ran Xie, Jing-Yu Liang, Guo-Qing Qin, Min Wang, and Gui-Lu Long. A novel method to fabricate on-chip ultra-high-Q microtoroid resonators. *Optics Communications*, 476:126259, December 2020.
- [19] M. L. Gorodetsky, A. A. Savchenkov, and V. S. Ilchenko. Ultimate Q of optical microsphere resonators. *Optics Letters*, 21(7):453, April 1996.
- [20] Lu Cai, Junyao Pan, and Sheng Hu. Overview of the coupling methods used in whispering gallery mode resonator systems for sensing. *Optics and Lasers in Engineering*, 127:105968, April 2020.
- [21] Oliver Wright. Gallery of whispers. *Physics World*, 25(02):31–36, February 2012.
- [22] Misha Sumetsky. Lasing microbottles. *Light: Science & Applications*, 6(10):e171102–e171102, October 2017.
- [23] Kerry J. Vahala. Optical microcavities. *Nature*, 424(6950):839–846, August 2003.
- [24] N. Nawi, B. Y. Majlis, M. A. Mahdi, R. M. De La Rue, M. Lončar, and A. R. Md Zain. Enhancement and reproducibility of high quality factor, one-dimensional photonic crystal/photonic wire (1D PhC/PhW) microcavities. *Journal of the European Optical Society-Rapid Publications*, 14(1):6, December 2018.
- [25] M.A. Butt, S.N. Khonina, and N.L. Kazanskiy. Recent advances in photonic crystal optical devices: A review. *Optics & Laser Technology*, 142:107265, October 2021.
- [26] C. P. Barrera-Patiño, J. D. Vollet-Filho, R. G. Teixeira-Rosa, H. P. Quiroz, A. Dussan, N. M. Inada, V. S. Bagnato, and R. R. Rey-González. Photonic effects in natural nanostructures on *Morpho cypris* and *Greta oto* butterfly wings. *Scientific Reports*, 10(1):5786, April 2020.
- [27] C. Schneider, P. Gold, S. Reitzenstein, S. Höfling, and M. Kamp. Quantum dot micropillar cavities with quality factors exceeding 250,000. *Applied Physics B*, 122(1):19, January 2016.
- [28] D. M. Whittaker, P. S. S. Guimaraes, D. Sanvitto, H. Vinck, S. Lam, A. Daraei, J. A. Timpson, A. M. Fox, M. S. Skolnick, Y.-L. D. Ho, J. G. Rarity, M. Hopkinson, and A. Tahraoui. High Q modes in elliptical microcavity pillars. *Applied Physics Letters*, 90(16):161105, April 2007.
- [29] Koichi Yamaguchi Koichi Yamaguchi, Kunihiro Yujobo Kunihiro Yujobo, and Toshiyuki Kaizu Toshiyuki Kaizu. Stranski-Krastanov Growth of InAs Quantum Dots with Narrow Size Distribution. *Japanese Journal of Applied Physics*, 39(12A):L1245, December 2000.
- [30] Charles Santori, David Fattal, Jelena Vuckovic, Glenn S Solomon, and Yoshihisa Yamamoto. Single-photon generation with InAs quantum dots. *New Journal of Physics*, 6:89–89, July 2004.

- [31] Bingyang Zhang, Glenn S. Solomon, Matthew Pelton, Jocelyn Plant, Charles Santori, Jelena Vučković, and Yoshihisa Yamamoto. Fabrication of InAs quantum dots in AlAsGaAs DBR pillar microcavities for single photon sources. *Journal of Applied Physics*, 97(7):073507, April 2005.
- [32] Pascale Senellart, Glenn Solomon, and Andrew White. High-performance semiconductor quantum-dot single-photon sources. *Nature Nanotechnology*, 12(11):1026–1039, November 2017.
- [33] Stephan Figge, Christian Tessarek, Timo Aschenbrenner, and Detlef Hommel. InGaN quantum dot growth in the limits of Stranski-Krastanov and spinodal decomposition: InGaN quantum dots. *physica status solidi (b)*, 248(8):1765–1776, August 2011.
- [34] F. Pelayo García de Arquer, Dmitri V. Talapin, Victor I. Klimov, Yasuhiko Arakawa, Manfred Bayer, and Edward H. Sargent. Semiconductor quantum dots: Technological progress and future challenges. *Science*, 373(6555):eaaz8541, August 2021.
- [35] M. D. Eisaman, J. Fan, A. Migdall, and S. V. Polyakov. Invited Review Article: Single-photon sources and detectors. *Review of Scientific Instruments*, 82(7):071101, July 2011.
- [36] C. K. Hong, Z. Y. Ou, and L. Mandel. Measurement of subpicosecond time intervals between two photons by interference. *Physical Review Letters*, 59(18):2044–2046, November 1987.
- [37] C. Gerry and P. Knight. *Introductory Quantum Optics*. Cambridge University Press, 2004.
- [38] Guang-Cun Shan, Zhang-Qi Yin, Chan Hung Shek, and Wei Huang. Single photon sources with single semiconductor quantum dots. *Frontiers of Physics*, 9(2):170–193, April 2014.
- [39] Yasuhiko Arakawa and Mark J. Holmes. Progress in quantum-dot single photon sources for quantum information technologies: A broad spectrum overview. *Applied Physics Reviews*, 7(2):021309, June 2020.
- [40] Shunfa Liu, Yuming Wei, Rongling Su, Rongbin Su, Ben Ma, Zesheng Chen, Haiqiao Ni, Zhichuan Niu, Ying Yu, Yujia Wei, Xuehua Wang, and Siyuan Yu. A deterministic quantum dot micropillar single photon source with >65% extraction efficiency based on fluorescence imaging method. *Scientific Reports*, 7(1):13986, October 2017.
- [41] Xing Ding, Yu He, Z.-C. Duan, Niels Gregersen, M.-C. Chen, S. Unsleber, S. Maier, Christian Schneider, Martin Kamp, Sven Höfling, Chao-Yang Lu, and Jian-Wei Pan. On-Demand Single Photons with High Extraction Efficiency and Near-Unity Indistinguishability from a Resonantly Driven Quantum Dot in a Micropillar. *Physical Review Letters*, 116(2):020401, January 2016.
- [42] Santiago Bermúdez Feijóo and Herbert Vinck Posada. *Statistical and entanglement properties of Two interacting cavities*. Bachelor Thesis, Universidad Nacional de Colombia, Bogotá Colombia, July 2019.
- [43] Anatole Kenfack and Karol yczkowski. Negativity of the Wigner function as an indicator of non-classicality. *Journal of Optics B: Quantum and Semiclassical Optics*, 6(10):396–404, October 2004.
- [44] J. A. Jones and M. Mosca. Implementation of a quantum algorithm on a nuclear magnetic resonance quantum computer. *The Journal of Chemical Physics*, 109(5):1648–1653, August 1998.
- [45] A. M. Zagoskin, S. Ashhab, J. R. Johansson, and Franco Nori. Quantum Two-Level Systems in Josephson Junctions as Naturally Formed Qubits. *Physical Review Letters*, 97(7):077001, August 2006.
- [46] He-Liang Huang, Dachao Wu, Daojin Fan, and Xiaobo Zhu. Superconducting quantum computing: a review. *Science China Information Sciences*, 63(8):180501, August 2020.
- [47] Daniele Cozzolino, Beatrice Da Lio, Davide Bacco, and Leif Katsuo Oxenløwe. High-Dimensional Quantum Communication: Benefits, Progress, and Future Challenges. *Advanced Quantum Technologies*, 2(12):1900038, December 2019.
- [48] Thomas Durt, Christian Kurtsiefer, Antia Lamas-Linares, and Alexander Ling. Wigner tomography of two-qubit states and quantum cryptography. *Physical Review A*, 78(4):042338, October 2008.
- [49] N. Zettili. *Quantum Mechanics: Concepts and Applications*. Wiley, 2009.
- [50] M.O. Scully and M.S. Zubairy. *Quantum Optics*. Quantum Optics. Cambridge University Press, 1997.

- [51] E.T. Jaynes and F.W. Cummings. Comparison of quantum and semiclassical radiation theories with application to the beam maser. *Proceedings of the IEEE*, 51(1):89–109, 1963.
- [52] D. Braak. Integrability of the Rabi Model. *Physical Review Letters*, 107(10):100401, August 2011.
- [53] Surendra Singh. Antibunching, sub-poissonian photon statistics and finite bandwidth effects in resonance fluorescence. *Optics Communications*, 44(4):254–258, January 1983.
- [54] X. T. Zou and L. Mandel. Photon-antibunching and sub-Poissonian photon statistics. *Physical Review A*, 41(1):475–476, January 1990.
- [55] R. Hanbury Brown and R.Q. Twiss. LXXIV. A new type of interferometer for use in radio astronomy. *The London, Edinburgh, and Dublin Philosophical Magazine and Journal of Science*, 45(366):663–682, July 1954.
- [56] R. Hanbury Brown and R. Q. Twiss. Correlation between Photons in two Coherent Beams of Light. *Nature*, 177(4497):27–29, January 1956.
- [57] J. H. Eberly and K. Wódkiewicz. The time-dependent physical spectrum of light*. *Journal of the Optical Society of America*, 67(9):1252, September 1977.
- [58] E. del Valle, A. Gonzalez-Tudela, F. P. Laussy, C. Tejedor, and M. J. Hartmann. Theory of Frequency-Filtered and Time-Resolved N -Photon Correlations. *Physical Review Letters*, 109(18):183601, October 2012.
- [59] Alejandro Gonzalez-Tudela, Fabrice P Laussy, Carlos Tejedor, Michael J Hartmann, and Elena del Valle. Two-photon spectra of quantum emitters. *New Journal of Physics*, 15(3):033036, March 2013.
- [60] Juan Camilo Lopez Carreño. *Exciting with quantum light*. Phd Thesis, Universidad Autonoma de Madrid, Madrid, November 2019.
- [61] Juan Camilo López Carreño, Elena del Valle, and Fabrice P. Laussy. Photon Correlations from the Mollow Triplet: Photon Correlations from the Mollow Triplet. *Laser & Photonics Reviews*, 11(5):1700090, September 2017.
- [62] C. Sánchez Muñoz, E. del Valle, C. Tejedor, and F. P. Laussy. Violation of classical inequalities by photon frequency filtering. *Physical Review A*, 90(5):052111, November 2014.
- [63] M. Peiris, B. Petrak, K. Konthasinghe, Y. Yu, Z. C. Niu, and A. Muller. Two-color photon correlations of the light scattered by a quantum dot. *Physical Review B*, 91(19):195125, May 2015.
- [64] Juan Camilo López Carreño, Eduardo Zubizarreta Casalengua, Elena del Valle, and Fabrice P. Laussy. Criterion for Single Photon Sources. 2016. Publisher: arXiv Version Number: 1.
- [65] M. Avenhaus, K. Laiho, M. V. Chekhova, and C. Silberhorn. Accessing Higher Order Correlations in Quantum Optical States by Time Multiplexing. *Physical Review Letters*, 104(6):063602, February 2010.
- [66] M. J. Fitch, B. C. Jacobs, T. B. Pittman, and J. D. Franson. Photon-number resolution using time-multiplexed single-photon detectors. *Physical Review A*, 68(4):043814, October 2003.
- [67] S Ferretti, V Savona, and D Gerace. Optimal antibunching in passive photonic devices based on coupled nonlinear resonators. *New Journal of Physics*, 15(2):025012, February 2013.
- [68] Xun-Wei Xu and Yuan-Jie Li. Antibunching photons in a cavity coupled to an optomechanical system. *Journal of Physics B: Atomic, Molecular and Optical Physics*, 46(3):035502, February 2013.
- [69] Bijita Sarma and Amarendra K. Sarma. Unconventional photon blockade in three-mode optomechanics. *Physical Review A*, 98(1):013826, July 2018.
- [70] Y. H. Zhou, H. Z. Shen, and X. X. Yi. Unconventional photon blockade with second-order nonlinearity. *Physical Review A*, 92(2):023838, August 2015.
- [71] Xun-Wei Xu and Yong Li. Tunable photon statistics in weakly nonlinear photonic molecules. *Physical Review A*, 90(4):043822, October 2014.

- [72] H. Flayac and V. Savona. Unconventional photon blockade. *Physical Review A*, 96(5):053810, November 2017.
- [73] Eduardo Zubizarreta Casalengua, Juan Camilo López Carreño, Fabrice P. Laussy, and Elena del Valle. Tuning photon statistics with coherent fields. *Physical Review A*, 101(6):063824, June 2020.
- [74] Xinyun Liang, Zhenglu Duan, Qin Guo, Cunjin Liu, Shengguo Guan, and Yi Ren. Antibunching effect of photons in a two-level emitter-cavity system. *Physical Review A*, 100(6):063834, December 2019.
- [75] J. P. Reithmaier, G. Şek, A. Löffler, C. Hofmann, S. Kuhn, S. Reitzenstein, L. V. Keldysh, V. D. Kulakovskii, T. L. Reinecke, and A. Forchel. Strong coupling in a single quantum dot–semiconductor microcavity system. *Nature*, 432(7014):197–200, November 2004.
- [76] T. Yoshie, A. Scherer, J. Hendrickson, G. Khitrova, H. M. Gibbs, G. Rupper, C. Ell, O. B. Shchekin, and D. G. Deppe. Vacuum Rabi splitting with a single quantum dot in a photonic crystal nanocavity. *Nature*, 432(7014):200–203, November 2004.
- [77] E. Peter, P. Senellart, D. Martrou, A. Lemaître, J. Hours, J. M. Gérard, and J. Bloch. Exciton-Photon Strong-Coupling Regime for a Single Quantum Dot Embedded in a Microcavity. *Physical Review Letters*, 95(6):067401, August 2005.
- [78] Satoshi Kako, Charles Santori, Katsuyuki Hoshino, Stephan Götzinger, Yoshihisa Yamamoto, and Yasuhiko Arakawa. A gallium nitride single-photon source operating at 200 K. *Nature Materials*, 5(11):887–892, November 2006.
- [79] Michael Förtsch, Josef U. Fürst, Christoffer Wittmann, Dmitry Strekalov, Andrea Aiello, Maria V. Chekhova, Christine Silberhorn, Gerd Leuchs, and Christoph Marquardt. A versatile source of single photons for quantum information processing. *Nature Communications*, 4(1):1818, October 2013.
- [80] J. A. Timpson, D. Sanvitto, A. Daraei, P. S. S. Guimaraes, H. Vinck, S. Lam, D. M. Whittaker, M. S. Skolnick, A. M. Fox, C. Y. Hu, Y.-L. D. Ho, R. Gibson, J. G. Rarity, S. Pellegrini, K. J. Gordon, R. E. Warburton, A. Tahaoui, G. S. Buller, P. W. Fry, and M. Hopkinson. Single photon sources based upon single quantum dots in semiconductor microcavity pillars. *Journal of Modern Optics*, 54(2-3):453–465, January 2007.
- [81] Guido Burkard, Michael J. Gullans, Xiao Mi, and Jason R. Petta. Superconductor–semiconductor hybrid-circuit quantum electrodynamics. *Nature Reviews Physics*, 2(3):129–140, January 2020.
- [82] Alexandre Blais, Arne L. Grimsmo, S.M. Girvin, and Andreas Wallraff. Circuit quantum electrodynamics. *Reviews of Modern Physics*, 93(2):025005, May 2021.
- [83] Alexandre Blais, Ren-Shou Huang, Andreas Wallraff, S. M. Girvin, and R. J. Schoelkopf. Cavity quantum electrodynamics for superconducting electrical circuits: An architecture for quantum computation. *Physical Review A*, 69(6):062320, June 2004.
- [84] A. Wallraff, D. I. Schuster, A. Blais, L. Frunzio, R.-S. Huang, J. Majer, S. Kumar, S. M. Girvin, and R. J. Schoelkopf. Strong coupling of a single photon to a superconducting qubit using circuit quantum electrodynamics. *Nature*, 431(7005):162–167, September 2004.
- [85] Ulrich Hohenester. Cavity quantum electrodynamics with semiconductor quantum dots: Role of phonon-assisted cavity feeding. *Physical Review B*, 81(15):155303, April 2010.
- [86] Arka Majumdar, Erik D. Kim, Yiyang Gong, Michal Bajcsy, and Jelena Vučković. Phonon mediated off-resonant quantum dot–cavity coupling under resonant excitation of the quantum dot. *Physical Review B*, 84(8):085309, August 2011.
- [87] Santiago Echeverri-Arteaga, Herbert Vinck-Posada, and Edgar A. Gómez. Explanation of the quantum phenomenon of off-resonant cavity-mode emission. *Physical Review A*, 97(4):043815, April 2018.
- [88] Santiago Echeverri-Arteaga, Herbert Vinck-Posada, and Edgar A. Gómez. The strange attraction phenomenon in cQED: The intermediate quantum coupling regime. *Optik*, 183:389–394, April 2019.
- [89] Alexandre Le Boité. Theoretical Methods for Ultrastrong Light–Matter Interactions. *Advanced Quantum Technologies*, 3(7):1900140, July 2020.

- [90] P. Forn-Díaz, L. Lamata, E. Rico, J. Kono, and E. Solano. Ultrastrong coupling regimes of light-matter interaction. *Reviews of Modern Physics*, 91(2):025005, June 2019.
- [91] T. Niemczyk, F. Deppe, H. Huebl, E. P. Menzel, F. Hocke, M. J. Schwarz, J. J. Garcia-Ripoll, D. Zueco, T. Hümmer, E. Solano, A. Marx, and R. Gross. Circuit quantum electrodynamics in the ultrastrong-coupling regime. *Nature Physics*, 6(10):772–776, October 2010.
- [92] A. Ridolfo, M. Leib, S. Savasta, and M. J. Hartmann. Photon Blockade in the Ultrastrong Coupling Regime. *Physical Review Letters*, 109(19):193602, November 2012.
- [93] Alexandre Le Boité, Myung-Joong Hwang, Hyunchul Nha, and Martin B. Plenio. Fate of photon blockade in the deep strong-coupling regime. *Physical Review A*, 94(3):033827, September 2016.
- [94] C. A. Jiménez-Orjuela, H. Vinck-Posada, and José M. Villas-Bôas. Dark excitons in a quantum-dot–cavity system under a tilted magnetic field. *Physical Review B*, 96(12):125303, September 2017.
- [95] C.A. Jiménez-Orjuela, H. Vinck-Posada, and José M. Villas-Bôas. Polarization switch in an elliptical micropillar – quantum dot system induced by a magnetic field in Faraday configuration. *Physics Letters A*, 382(44):3216–3219, November 2018.
- [96] Heinz-Peter Breuer and Francesco Petruccione. *The Theory of Open Quantum Systems*. Oxford University PressOxford, 1 edition, January 2007.